Notes on EMMA III loci for VWI

Locus 1

Significance (based on data with full allele set): CORRECT

Top hit : position chr3 : 82'991'172
alleles (EMMA) # alleles 1 = 14; # alleles 2 = 8 (do alleles #2 include strain Balb/cJ ?)
condition / stat control, REMLt
p-value: **2.593×10^{-6}**
a. alleles from the Broad1 SNP set (MPD): 14 vs 7

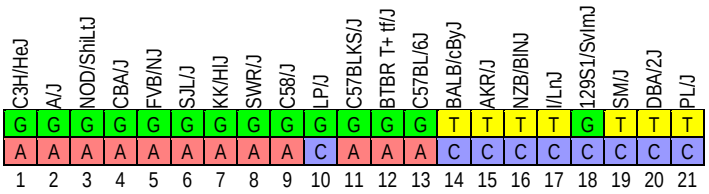

b. alleles from the CGD1 imputed SNP set (MPD): 14 vs 2. Does not bring more information than above, as several alleles are missing.

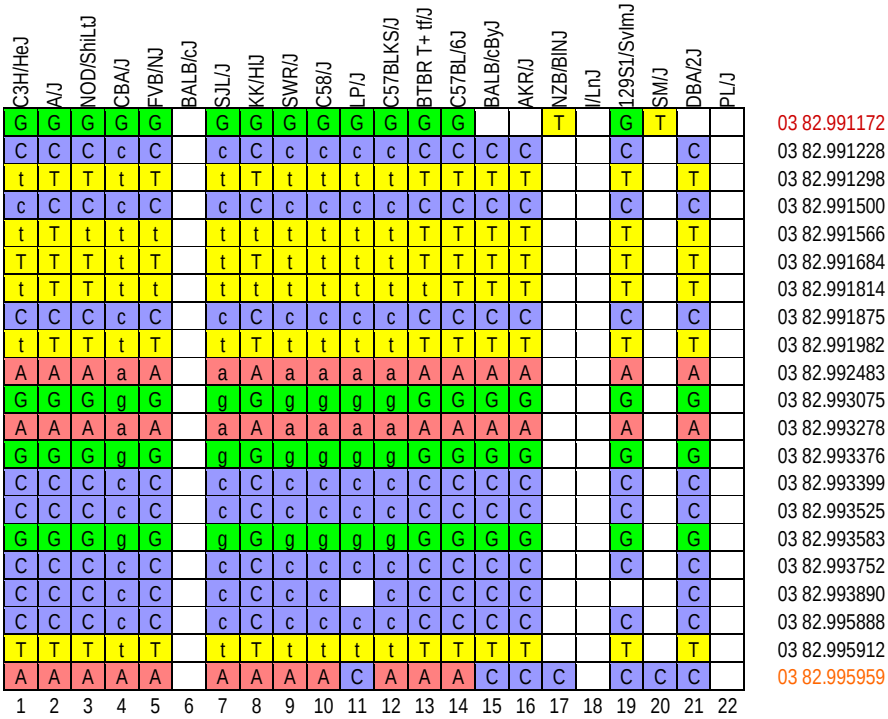

range : ca 81-85 Mb ($p<6 \times 10^{-3}$)

Candidate gene(s) : **none**. According to the MPD medium size SNP dataset (ca Broad1), top hits are located between *EG627094* (a predicted gene) and *Dchs2* (dachsous 2, isoform 1). These entries are not indicated in the UCSC genome browser. No PubMed entry on *Dchs2*.

Notes and bibliography:

In addition: region of *Npy2r* using CGD1 imputed SNPs.

Top hit : position chr3 : 82'348'468
alleles (EMMA) # alleles 1 = 15; # alleles 2 = 6 (-> 1 strain is missing; that's the only position in *Npy2r* that has been analysed in EMMA III, see next page for a matching SNP with the full allele set)
condition / stat control, REMLt
p-value: 2.305×10^{-4}
The association is not very strong (see table below; strains are sorted by increasing values of VWI in control conditions).

C3H/HeJ	A/J	NOD/ShiLtJ	CBA/J	FVB/NJ	BALB/cJ	SJL/J	KK/HlJ	SWR/J	C58/J	LP/J	C57BLKS/J	BTBR T+ tf/J	C57BL/6J	BALB/cByJ	AKR/J	NZB/BlNJ	I/LnJ	129S1/SvImJ	SM/J	DBA/2J	PL/J			
A	A	A	a	A	a	a	A	a	a	a	a	A	A	A	A	a	a	A	a	A	a	03 82.342618	Npy2r	UTR
C	C	C	c	C	c	c	C	c	c	c	c	C	C	C	C	c	c	C	c	C	c	03 82.342913	Npy2r	UTR
G	G	G	g	G	t	g	G	g	g	g	g	G	G	T	T	t	t	G	g	T	t	03 82.342948	Npy2r	UTR
T	T	T	t	t	c	t	T	t	t	t	t	T	T	C	C	c	c	T	t	C	c	03 82.343543	Npy2r	UTR
T	T	T	t	T	c	t	T	t	t	t	t	t	T	C	C	c	c	T	t	C	c	03 82.343964	Npy2r	UTR ... exon3,UTR
A	A	A	a	a	a	a	a	a	a	a	a	a	A	A	A	a	a	A	a	A	a	03 82.344194	Npy2r	UTR ... exon3,UTR
C	C	C	c	C	c	c	C	c	c	c	c	C	C	C	C	c	c	C	c	C	c	03 82.344351	Npy2r	exon2 ... exon3,UTR
T	T	T	t	T	t	t	T	t	t	t	t	T	T	T	T	t	t	T	t	T	t	03 82.345235	Npy2r	exon2 ... intron2
C	C	C	c	C	c	c	C	c	c	c	c	C	C	C	C	c	c	C	c	C	c	03 82.345417	Npy2r	intron1 agrees
T	T	T	t	T		t	T	t	t	t	t	T	T					T	t			03 82.345454	Npy2r	intron1 agrees
A	A	A	a	A	g	a	A	a	a	a	a	A	A	G	g	g	g	A	a	G	g	03 82.345482	Npy2r	intron1 agrees
C	C	C	c	C	c	c	C	c	c	c	c	C	C	C	C	c	c	C	c	C	c	03 82.345546	Npy2r	intron1 agrees
T	T	T	t	T	t	t	T	t	t	t	t	t	T	T	T	t	t	T	t	T	t	03 82.345677	Npy2r	intron1 agrees
a	A	A	a	A	a	a	a	a	a	a	a	a	A	A	A	a	a	A	a	A	a	03 82.345854	Npy2r	intron1 agrees
C	C	C	c	C	c	c	C	c	c	c	c	C	C	C	C	c	c	C	c	C	c	03 82.345923	Npy2r	intron1 agrees
G	G	G	g	G	g	g	G	g	g	g	g	G	G	G	G	g	g	G	g	G	g	03 82.346460	Npy2r	intron1 agrees
G	G	G	g	G	g	g	G	g	g	g	g	G	G	G	G	g	g	G	g	G	g	03 82.346683	Npy2r	intron1 agrees
A	A	A	a	A	a	a	A	a	a	a	a	A	A	A	A	a	a	A	a	A	a	03 82.346768	Npy2r	intron1 agrees
G	G	G	g	G	g	g	G	g	g	g	g	G	G	G	G	g	g	G	g	G	g	03 82.347933	Npy2r	intron1 agrees
C	C	C	c	C	c	c	C	c	c	c	c	c	C	C	C	c	c	C	c	C	c	03 82.348016	Npy2r	intron1 agrees
					c									C	c	c	c			C	c	03 82.348117	Npy2r	intron1 agrees
T	T	t	t	t	t	t	t	t	t	t	t	t	T	T	T	t	t	T	t	T	t	03 82.348143	Npy2r	intron1 agrees
A	A	A	A	A	G	A	A	A	A	A	A	A	A	G	G	G	G	A	A	G	G	03 82.348468	Npy2r	intron1 *p= 2.305x10⁻⁴*
A	A	A	a	A		a	A	a	a	a	a	a	A					A	a			03 82.348592	Npy2r	intron1 agrees
G	G	G	g	G	g	g	G	g	g	g	g	G	G	G	G	g	g	G	g	G	g	03 82.349079	Npy2r	intron1 agrees
A	A	A	a	A	g	a	A	a	a	a	a	A	A	g	G	g	g	A	a	g	g	03 82.349093	Npy2r	intron1 agrees
C	C	C	c	C	c	c	C	c	c	c	c	C	C	C	C	c	c	C	c	C	c	03 82.349156	Npy2r	intron1 agrees
A	A	A	a	A	g	a	a	a	a	a	a	a	A	G	G	g	g	A	a	G	g	03 82.349398	Npy2r	intron1 agrees
G	G	G	g	G	a	g	G	g	g	g	g	g	G	A	A	a	a	G	g	A	a	03 82.349444	Npy2r	intron1 agrees
T	T	T	t	T	t	t	T	t	t	t	t	t	T	T	t	t	t	T	t	T	t	03 82.349516	Npy2r	intron1 agrees
T	T	T	t	T		t	T	t	t	t	t	T	T					T	t			03 82.349524	Npy2r	intron1 agrees
T	T	t	t	t	c	t	t	t	t	t	t	T	T	C	c	c	c	T	t	C	c	03 82.349528	Npy2r	intron1 agrees
T	T	T	t	T		t	T	t	t	t	t	t	T					T	t			03 82.349619	Npy2r	intron1 agrees
T	T	T	t	T	a	t	T	t	t	t	t	t	T	A	a	a	a	T	t	A	a	03 82.349713	Npy2r	intron1 agrees
T	T	T	t	T	a	t	T	t	t	t	t	t	T	A	A	a	a	T	t	A	a	03 82.349753	Npy2r	intron1 agrees
a	A	a	a	a	a	a	a	a	a	a	a	a	A	A	A	a	a	A	a	A	a	03 82.349796	Npy2r	intron1 agrees
A	A	A	a	A	g	a	A	a	a	a	a	A	A	G	G	g	g	A	a	G	g	03 82.349870	Npy2r	intron1 agrees
t	t	T	t	t	c	t	t	t	t	t	t	t	T	C	C	c	c	T	t	C	c	03 82.349895	Npy2r	intron1 agrees
A	A	A	a	A	g	a	A	a	a	a	a	A	A	G	G	g	g	A	a	g	g	03 82.350213	Npy2r	intron1 agrees
C	C	C	c	C	t	c	C	c	c	c	c	c	C	T	t	t	t	C	c	T	t	03 82.350304	Npy2r	intron1 agrees
A	A	A	a	A	a	a	A	a	a	a	a	a	A	A	A	a	a	A	a	A	a	03 82.350497	Npy2r	intron1 agrees
A	A	A	a	A	a	a	A	a	a	a	a	a	A	A	A	a	a	A	a	A	a	03 82.350671	Npy2r	intron1 agrees
G	G	G	g	G	a	g	G	g	g	g	g	g	G	A	a	a	a	G	g	A	a	03 82.350689	Npy2r	intron1 agrees
G	G	G	g	G	g	g	G	g	g	g	g	g	G	G	G	g	g	G	g	G	g	03 82.350848	Npy2r	intron1 agrees
G	G	G	g	G	g	g	G	g	g	g	g	g	G	G	G	g	g	G	g	G	g	03 82.350876	Npy2r	intron1 agrees
T	T	T	t	T	t	t	T	t	t	t	t	T	T	T	T	t	t	T	t	T	t	03 82.350900	Npy2r	intron1 agrees
A	A	A	a	A	t	a	A	a	a	a	a	a	A	T	T	t	t	A	a	T	t	03 82.350972	Npy2r	intron1 agrees
G	G	G	g	G	g	g	G	g	g	g	g	G	G	G	G	g	g	G	g	G	g	03 82.351565	Npy2r	intron1 agrees
T	T	t	t	t	t	t	t	t	t	t	t	t	T	T	T	t	t	T	t	T	t	03 82.351836	Npy2r	UTR agrees
g	G	G	g	g	c	g	g	g	g	g	g	g	G	C	C	c	c	G	g	C	c	03 82.351938	Npy2r	UTR
1	2	3	4	5	6	7	8	9	10	11	12	13	14	15	16	17	18	19	20	21	22			

Matching hit for *Npy2r* SNP at position 82'348'468 with full SDP in EMMAIII :

position	chr3 : 82'359'090
alleles (EMMA)	# alleles 1 = 15; # alleles 2 = 7
condition / stat	control, REMLt
p-value:	**1.917×10^{-4}**

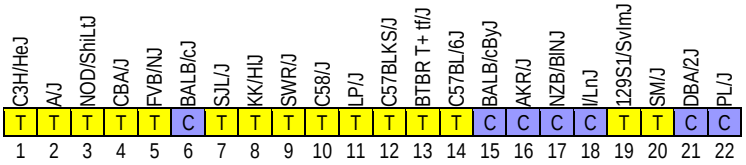

Notes and bibliography:

Kuo LE, Kitlinska JB, Tilan JU, Li L, Baker SB, Johnson MD, Lee EW, Burnett MS, Fricke ST, Kvetnansky R, Herzog H, Zukowska Z. **Neuropeptide Y acts directly in the periphery on fat tissue and mediates stress-induced obesity and metabolic syndrome.** Nat Med. 2007 Jul;13(7):803-11. URL. Comment in: Nat Med. 2007 Jul;13(7):781-3. URL

The relationship between stress and obesity remains elusive. In response to stress, some people lose weight, whereas others gain. Here we report that stress exaggerates diet-induced obesity through a peripheral mechanism in the abdominal white adipose tissue that is mediated by neuropeptide Y (NPY). Stressors such as exposure to cold or aggression lead to the release of NPY from sympathetic nerves, which in turn upregulates NPY and its Y2 receptors (NPY2R) in a glucocorticoid-dependent manner in the abdominal fat. This positive feedback response by NPY leads to the growth of abdominal fat. Release of NPY and activation of NPY2R stimulates fat angiogenesis, macrophage infiltration, and the proliferation and differentiation of new adipocytes, resulting in abdominal obesity and a metabolic syndrome-like condition. NPY, like stress, stimulates mouse and human fat growth, whereas pharmacological inhibition or fat-targeted knockdown of NPY2R is anti-angiogenic and anti-adipogenic, while reducing abdominal obesity and metabolic abnormalities. Thus, manipulations of NPY2R activity within fat tissue offer new ways to remodel fat and treat obesity and metabolic syndrome.

Campbell CD, Lyon HN, Nemesh J, Drake JA, Tuomi T, Gaudet D, Zhu X, Cooper RS, Ardlie KG, Groop LC, Hirschhorn JN. **Association studies of BMI and type 2 diabetes in the neuropeptide Y pathway: a possible role for NPY2R as a candidate gene for type 2 diabetes in men.** Diabetes. 2007 May;56(5):1460-7. URL

The neuropeptide Y (NPY) family of peptides and receptors regulate food intake. Inherited variation in this pathway could influence susceptibility to obesity and its complications, including type 2 diabetes. We genotyped a set of 71 single nucleotide polymorphisms (SNPs) that capture the most common variation in NPY, PPY, PYY, NPY1R, NPY2R, and NPY5R in 2,800 individuals of recent European ancestry drawn from the near extremes of BMI distribution. Five SNPs located upstream of NPY2R were nominally associated with BMI in men (P values = 0.001-0.009, odds ratios [ORs] 1.27-1.34). No association with BMI was observed in women, and no consistent associations were observed for other genes in this pathway. We attempted to replicate the association with BMI in 2,500 men and tested these SNPs for association with type 2 diabetes in 8,000 samples. We observed association with BMI in men in only one replication sample and saw no association in the combined replication samples (P = 0.154, OR = 1.09). Finally, a 9% haplotype was associated with type 2 diabetes in men (P = 1.73 x 10(-4), OR = 1.36) and not in women. Variation in this pathway likely does not have a major influence on BMI, although small effects cannot be ruled out; NPY2R should be considered a candidate gene for type 2 diabetes in men.

Locus 2

Significance (based on data with full allele set): INFLATED

Top hit 1 : position chr3 : 87'719'795 (*Hdgf*)
alleles (EMMA) # alleles 1 = 13; # alleles 2 = 7 (-> allele set is incomplete; this is also the case with the imputed CGD1 set of SNPs)
condition / stat control, REMLt
p-value: 4.236×10^{-6}

a. alleles from the Broad1 SNP set (MPD): 14 vs 6. Note that top hit #1 of EMMA III is given at a position with 2 missing alleles. ⇨ check which allele configuration was used in EMMA

Matching SNP with full allele set:

position chr 3: 87'720'406
alleles (EMMA) #alleles 1 =14; # alleles 2 = 8
condition / stat iso 10, REMLt
p-value: **3.219×10^{-4}**
alleles from the Broad1 SNP set (MPD): 14 vs 7

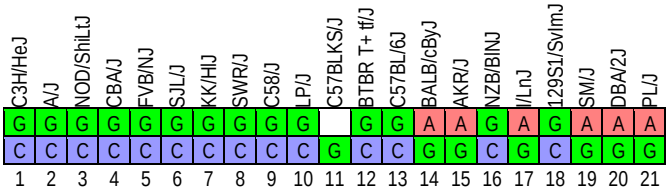

b. the same position is not given in the CGD1 imputed SNP set. The closest SNP is the following (*Hgdf*, exon 6), but this information is not really useful:

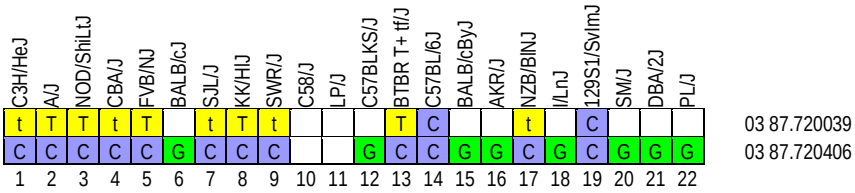

Top hit 2 : position chr3 : 87487048 (*Arhgef11*)
alleles (EMMA) #alleles 1 =10; # alleles 2 = 10 (-> allele set is incomplete; yet it is complete with the MPD medium size SNP set given below -> it is not clear which alleles are missing in the EMMA III association scan)
condition / stat control, REMLt
p-value: 1.031×10^{-5}
alleles from the Broad1 SNP set (MPD): 12 vs 9. There is no close position that matches the same SDP, so one cannot infer a « true » p-value for the full allele set.

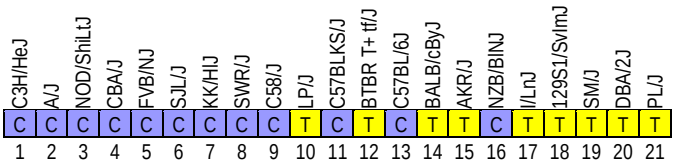

alleles from the CGD1 imputed SNP set (MPD): 14 vs 2

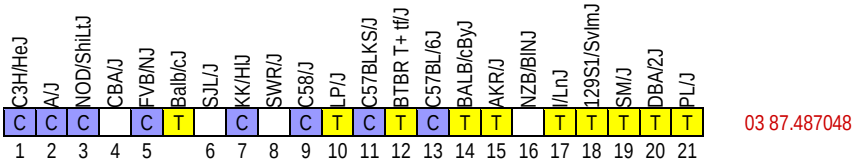

range : ca 87-88 Mb ($p<6x10^{-3}$)

Candidate gene(s) :

1. ***Hdgf*** : hepatoma-derived growth factor. According to MPD medium size SNP dataset (ca Broad1), top hit is located in exon 6 (3'UTR) of *Hdgf*. Link to UCSC gene description page.

Notes and bibliography:

Everett AD, Lobe DR, Matsumura ME, Nakamura H, McNamara CA. **Hepatoma-derived growth factor stimulates smooth muscle cell growth and is expressed in vascular development**. J Clin Invest. 2000 Mar;105(5):567-75. URL

Hepatoma-derived growth factor (HDGF) is the first member identified of a new family of secreted heparin-binding growth factors highly expressed in the fetal aorta. The biologic role of HDGF in vascular growth is unknown. Here, we demonstrate that HDGF mRNA is expressed in smooth muscle cells (SMCs), most prominently in proliferating SMCs, 8-24 hours after serum stimulation. Exogenous HDGF and endogenous overexpression of HDGF stimulated a significant increase in SMC number and DNA synthesis. Rat aortic SMCs transfected with a hemagglutinin-epitope-tagged rat HDGF cDNA contain HA-HDGF in their nuclei during S-phase. We also detected native HDGF in nuclei of cultured SMCs, of SMCs and endothelial cells from 19-day fetal (but not in the adult) rat aorta, of SMCs proximal to abdominal aortic constriction in adult rats, and of SMCs in the neointima formed after endothelial denudation of the rat common carotid artery. Moreover, HDGF colocalizes with the proliferating cell nuclear antigen (PCNA) in SMCs in human atherosclerotic carotid arteries, suggesting that HDGF helps regulate SMC growth during development and in response to vascular injury.

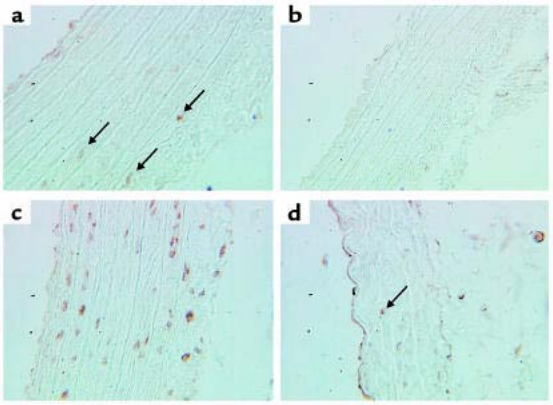

Figure 10
HDGF expression is increased in SMCs of the aorta after aortic constriction.
HDGF immunostaining is shown in sham thoracic (**a**, arrows) and abdominal aorta (**b**) and in the thoracic aorta above the constriction (**c**, brown nuclei) and in the abdominal aorta below the constriction (**d**, arrow).

Everett AD. **Identification, cloning, and developmental expression of hepatoma-derived growth factor in the developing rat heart**. Dev Dyn. 2001 Nov;222(3):450-8. URL

Hepatoma derived growth factor (HDGF) was identified as a developmentally regulated cardiac gene by mRNA differential display using 12-day rat fetal conotruncus vs. newborn aorta. The full-length rat HDGF cDNA was cloned from a rat fetal heart cDNA library and found to be 94 and 88% homologous to the mouse and human sequence, respectively. The rat sequence, like the human and mouse, contains a highly conserved amino portion and putative bipartite nuclear localization sequence. By Northern analysis, HDGF is highly expressed in the fetal conotruncus, heart, kidney, brain, and gut. By immunocytochemistry, HDGF was first detected only in atrial myocytes, hind gut epithelia, and notochord of the E10 rat with a nuclear expression pattern. By E12, expression had broadened to include the ventricular myocytes, endocardial cells, and cells of the ventricular outflow tract. HDGF is unique in that it is the first described nuclear targeted growth factor in the developing heart. The early expression of HDGF in embryonic heart and fetal gut suggests that HDGF may play a role in cardiovascular growth and differentiation.

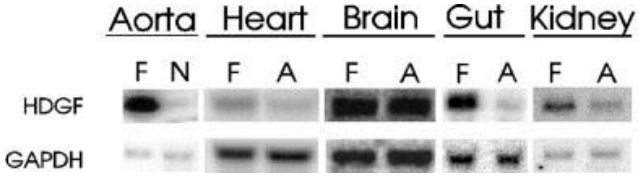

Figure 3. Developmental expression of HDGF.
Ten micrograms of total RNA from 90-day-old adult (**A**) and E14 embryonic (**F**) heart, brain, intestines (gut), and kidney or newborn aorta (4 days old, **N**) was analyzed by Northern analysis for HDGF mRNA. The blot was reprobed for the control gene GAPDH to control for loading.

2. ***Arhgef11*** : Rho guanine nucleotide exchange factor 11. According to MPD medium size SNP dataset (ca Broad1), top SNP 2 is located in intron 1 of *Argef11*. Link to UCSC gene description page.

Notes and bibliography:

Ohtsu H, Mifune M, Frank GD, Saito S, Inagami T, Kim-Mitsuyama S, Takuwa Y, Sasaki T, Rothstein JD, Suzuki H, Nakashima H, Woolfolk EA, Motley ED, Eguchi S. **Signal-crosstalk between Rho/ROCK and c-Jun NH2-terminal kinase mediates migration of vascular smooth muscle cells stimulated by angiotensin II**. Arterioscler Thromb Vasc Biol. 2005 Sep;25(9):1831-6. URL

BACKGROUND: Rho and its effector Rho-kinase/ROCK mediate cytoskeletal reorganization as well as smooth muscle contraction. Recent studies indicate that Rho and ROCK are critically involved in vascular remodeling. Here, we tested the hypothesis that Rho/ROCK are critically involved in angiotensin II (Ang II)-induced migration of vascular smooth muscle cells (VSMCs) by mediating a specific signal cross-talk. METHODS AND RESULTS: Immunoblotting demonstrated that Ang II stimulated phosphorylation of a ROCK substrate, regulatory myosin phosphatase targeting subunit (MYPT)-1. Phosphorylation of MYPT-1 as well as migration of VSMCs induced by Ang II was inhibited by dominant-negative Rho (dnRho) or ROCK inhibitor, Y27632. Ang II-induced c-Jun NH2-terminal kinase (JNK) activation, but extracellular signal-regulated kinase (ERK) activation was not mediated through Rho/ROCK. Thus, infection of adenovirus encoding dnJNK inhibited VSMC migration by Ang II. We have further demonstrated that the Rho/ROCK activation by Ang II requires protein kinase C-delta (PKCdelta) and proline-rich tyrosine kinase 2 (PYK2) activation, but not epidermal growth factor receptor transactivation. Also, VSMCs express PDZ-Rho guanine nucleotide exchange factor (GEF) and Ang II stimulated PYK2 association with tyrosine phosphorylated PDZ-RhoGEF. CONCLUSIONS: PKCdelta/PYK2-dependent Rho/ROCK activation through PDZ-RhoGEF mediates Ang II-induced VSMC migration via JNK activation in VSMCs, providing a novel mechanistic role of the Rho/ROCK cascade that is involved in vascular remodeling.

Fu M, Sabra MM, Damcott C, Pollin TI, Ma L, Ott S, Shelton JC, Shi X, Reinhart L, O'Connell J, Mitchell BD, Baier LJ, Shuldiner AR. **Evidence that Rho guanine nucleotide exchange factor 11 (ARHGEF11) on 1q21 is a type 2 diabetes susceptibility gene in the Old Order Amish**. Diabetes. 2007 May;56(5):1363-8. URL

Rho guanine nucleotide exchange factor 11 (ARHGEF11), located on chromosome 1q21, is involved in G protein signaling and is a pathway known to play a role in both insulin secretion and action. We genotyped 52 single nucleotide polymorphims (SNPs) in ARHGEF11 and compared the genotype frequencies of subjects with type 2 diabetes (n = 145) or type 2 diabetes/impaired glucose tolerance (IGT) (n = 293) with those of control subjects with normal glucose tolerance (NGT) (n = 358). Thirty SNPs, spanning the entire gene, were significantly associated with type 2 diabetes or type 2 diabetes/IGT. The most significantly associated SNP was rs6427340 (intron 2), in which the less common allele was the risk allele (odds ratio [OR] 1.82 [95% CI 1.20-2.70], P = 0.005 for type 2 diabetes vs. NGT and 1.79 [1.27-2.50], P = 0.0008 for type 2 diabetes/IGT vs. NGT). In an expanded set of nondiabetic subjects (n = 754), most of the type 2 diabetes-and IGT-associated SNPs were significantly associated with glucose levels during an oral glucose tolerance test, with the same SNP (rs6427340) showing the most significant associations (P = 0.007). All type 2 diabetes-and IGT-associated SNPs were in high linkage disequilibrium and constitute a single 133-kb haplotype block. These results, coupled with similar findings in Pima Indians, suggest that sequence variation in ARHGEF11 may influence risk of type 2 diabetes.

Several reports further suggest an association between Arhgef11 and T2D.

3. *Crabp2 ?* : cellular retinoic acid binding protein II. Link to UCSC gene information. See SDP of CGD1 SNP set (strains are sorted by increasing VWI in control condtions) below. Alleles at position 87'757'418 in EMMAIII are given as 11 vs 9:

C3H/HeJ	A/J	NOD/ShiLtJ	CBA/J	FVB/NJ	BALB/cJ	SJL/J	KK/HlJ	SWR/J	C58/J	LP/J	C57BLKS/J	BTBR T+ tf/J	C57BL/6J	BALB/cByJ	AKR/J	NZB/BINJ	I/LnJ	129S1/SvImJ	SM/J	DBA/2J	PL/J				p in EMMA III
C	C	C	c	C	c	c	C	c			c	C	C	C	C	c	c	C	c	C	c	03 87.752758	Crabp2	UTR	... exon1,UTR
G	G	G	g	G	g	g	G	g			g	G	G	G	G	g	g	G	g	G	g	03 87.753474	Crabp2	intron1	agrees
C	C	C	c	C	c	c	C	c			c	C	C	C	C	c	c	C	c	C	c	03 87.753740	Crabp2	intron1	agrees
A	A	A	A	A	G	A	A	A			G	A	G	G	G	A	G	G	G	G	G	03 87.754643	Crabp2	intron1	agrees
G	G	G	g	G	g	g	G	g			g	G	G	G	G	g	g	G	g	G	g	03 87.755063	Crabp2	intron1	agrees
C	C	C	c	C	c	c	C	c			c	C	C	C	C	c	c	C	c	C	c	03 87.756003	Crabp2	intron1	agrees
C	C	C	c	C	c	c	C	c			c	C	C	C	C	c	c	C	c	C	c	03 87.756303	Crabp2	intron2	agrees
G	G	G	g	G	g	g	G	g			g	G	G	G	G	g	g	G	g	G	g	03 87.756576	Crabp2	intron3	agrees
G	G	G	g	G	g	g	G	g			g	G	G	G	G	g	g	G	g	G	g	03 87.756948	Crabp2	exon4	agrees
T	T	T	t	T	c	t	T	t			c	T	C	C	C	t	c	C	c	C	c	03 87.756996	Crabp2	UTR	... exon4,UTR
C	C	C	c	C	t	c	C	c			t	C	C	T	T	c	t	C	t	T	t	03 87.757087	Crabp2	UTR	... exon4,UTR
c	c	c	c	C	a	c	C	c			a	C	A	A	A	c	a	A	a	A	a	03 87.757110	Crabp2	UTR	... exon4,UTR
					c						c		C	C	C		c	C	c	C	c	03 87.757183	Crabp2	UTR	... exon4,UTR
C	C	C	C	C	A	C	C	C			A	C	A	A	A	C	A	A	A	A	A	03 87.757418			*p= 0.000743*
1	2	3	4	5	6	7	8	9	10	11	12	13	14	15	16	17	18	19	20	21	22				

Comments and Description Text from UniProt (Swiss-Prot/TrEMBL) ID: RABP2_MOUSE

DESCRIPTION: Cellular retinoic acid-binding protein 2 (Cellular retinoic acid- binding protein II) (CRABP-II) (Retinoic acid-binding protein II, cellular).

FUNCTION: Transports retinoic acid to the nucleus. Regulates the access of retinoic acid to the nuclear retinoic acid receptors.

SUBUNIT: Interacts with importin alpha (By similarity). Interacts with RXR and RARA.

SUBCELLULAR LOCATION: Cytoplasm. Nucleus. Note=Upon ligand binding, a conformation change exposes a nuclear localization motif and the protein is transported into the nucleus.

TISSUE SPECIFICITY: Embryo and skin of adult mouse.

INDUCTION: By retinoic acid.

DOMAIN: Forms a beta-barrel structure that accommodates hydrophobic ligands in its interior (By similarity).
SIMILARITY: Belongs to the calycin superfamily. Fatty-acid binding protein (FABP) family.

Notes and bibliography:

Salazar J, Guardiola M, Ferré R, Coll B, Alonso-Villaverde C, Winklhofer-Roob BM, Rock E, Fernández-Ballart JD, Civeira F, Pocoví M, Masana L, Ribalta J. **Association of a polymorphism in the promoter of the cellular retinoic acid-binding protein II gene (CRABP2) with increased circulating low-density lipoprotein cholesterol.** Clin Chem Lab Med. 2007;45(5):615-20. URL
BACKGROUND: The cellular retinoic acid-binding protein II (CRABP-II), together with nuclear receptors such as the retinoid X receptor (RXR) and retinoic acid receptor (RAR), is involved in the transcriptional regulation of genes that control lipid metabolism via the retinoid signaling pathway and, as such, may be associated with disorders of lipid metabolism. Interestingly, the gene for CRABP-II is located on chromosome 1q21-23, which is a region that has been linked with disorders such as familial combined hyperlipidemia (FCHL), type 2 diabetes mellitus, and partial lipodystrophy, all of which are characterized by dyslipidemia. METHODS: We investigated the hypothesis that the CRABP2 gene is involved in the regulation of lipid metabolism. Using the promoter -394T>C polymorphism of the CRABP2 gene, we performed association studies in three different cohorts: 299 healthy males, 182 HIV-infected patients and 151 patients with familial hypercholesterolemia (FH). All cholesterol measurements were performed in the absence of any lipid-lowering agents. ANOVA was performed on data adjusted for age, body mass index (BMI), gender, and use of protease inhibitors. RESULTS: The frequency of the C allele was 0.03 in the three groups. Among healthy males, carriers of the C allele had 9% higher total plasma cholesterol (p=0.027) and 13% higher low-density lipoprotein cholesterol (LDL-C) concentrations (p=0.020). In HIV-infected patients, multivariate analysis of four measures over a 1-year period showed that carriers of the C allele had significantly higher LDL-C of between 10% and 31% (p=0.001) compared with non-carriers of the allele. FH patients who were carriers of the C allele had 16% higher LDL-C (p=0.038). The C allele was significantly over-represented among hypercholesterolemic patients (p=0.001). CONCLUSIONS: Our results show that the CRABP2 gene, a member of the retinoid signaling pathway, is associated with increased plasma LDL-C concentrations.

4. *Bcan ?* brevican (BEHAB, Brain Enriched HyAluronan Binding/brevican). Link to UCSC gene information. Some SNPs share the same SDP as position 87'757'418 above, but there is no SNP within this gene in the EMMA III scan.

   There is a lot of bibliography on the role of brevican (a brain-specific ECM protein) in spinal cord injury, axonal guidance, brain development, and so on. There might be a link between HNK-1 (see *Chst10*) and brevican, but there is no clear indication of a role for brevican in heart function or morphogenesis.

Comments and Description Text from UniProt (Swiss-Prot/TrEMBL) ID: PGCB_MOUSE
DESCRIPTION: Brevican core protein precursor.
FUNCTION: May play a role in the terminally differentiating and the adult nervous system during postnatal development. Could stabilize interactions between hyaluronan (HA) and brain proteoglycans.
SUBUNIT: Interacts with TNR (By similarity).
SUBCELLULAR LOCATION: Secreted, extracellular space, extracellular matrix (By similarity).
TISSUE SPECIFICITY: Brain (By similarity).
PTM: Contains mostly chondroitin sulfate (By similarity).
SIMILARITY: Belongs to the aggrecan/versican proteoglycan family.
SIMILARITY: Contains 1 C-type lectin domain.
SIMILARITY: Contains 1 EGF-like domain.
SIMILARITY: Contains 1 Ig-like V-type (immunoglobulin-like) domain.
SIMILARITY: Contains 2 Link domains.
SIMILARITY: Contains 1 Sushi (CCP/SCR) domain.

5. *Hapln2 ?* : hyaluronan and proteoglycan link protein 2. HAPLN2 is restricted in expression to the brain/central nervous system. Link to UCSC gene informartion. Some SNPs share the same SDP as position 87'757'418 above, but there is no SNP within this gene in the EMMA III scan.

Comments and Description Text from UniProt (Swiss-Prot/TrEMBL) ID: HPLN2_MOUSE
DESCRIPTION: Hyaluronan and proteoglycan link protein 2 precursor (Brain link protein 1).
FUNCTION: Mediates a firm binding of versican V2 to hyaluronic acid. May play a pivotal role in the formation of the hyaluronan- associated matrix in the central nervous system (CNS) which facilitates neuronal conduction and general structural stabilization. Binds to hyaluronic acid.
SUBCELLULAR LOCATION: Secreted, extracellular space, extracellular matrix.
TISSUE SPECIFICITY: Brain. Predominantly expressed by neurons. Colocalizes with versican V2 in developing and adult cerebellar white matter and at the nodes of Ranvier.
DEVELOPMENTAL STAGE: Expression starts at postnatal day 20 and increases thereafter.
SIMILARITY: Belongs to the HAPLN family.
SIMILARITY: Contains 1 Ig-like V-type (immunoglobulin-like) domain.

SIMILARITY: Contains 2 Link domains.

6. *Gpatc4 ?* G patch domain containing 4 (*Gpatch4*). Link to UCSC gene information. There are several SNPs with the SDP presented below (based on the CGD1 imputed SNP set). Alleles at position 87'854'631 in EMMAIII are given as 12 vs 9, with a p = 5.532×10^{-4}:

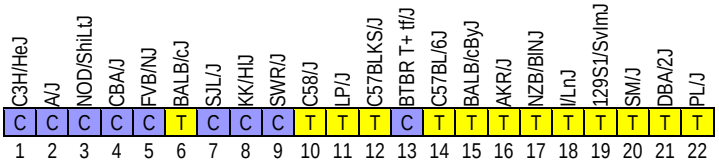

C3H/HeJ	A/J	NOD/ShiLtJ	CBA/J	FVB/NJ	BALB/cJ	SJL/J	KK/HlJ	SWR/J	C58/J	LP/J	C57BLKS/J	BTBR T+ tf/J	C57BL/6J	BALB/cByJ	AKR/J	NZB/BINJ	I/LnJ	129S1/SvImJ	SM/J	DBA/2J	PL/J				p in EMMA III
C	C	C	C	C	T	C	C	C	T	T	T	C	T	T	T	T	T	T	T	T	T	03 87.854631	Gpatc4	intron2	*p= 0.0005532*
1	2	3	4	5	6	7	8	9	10	11	12	13	14	15	16	17	18	19	20	21	22				

7. *Apoa1b ?* apolipoprotein A-I binding protein. Link to UCSC gene information. There are several SNPs with the SDP presented below (based on the CGD1 imputed SNP set). Alleles at position 87'860'731 in EMMAIII are given as 13 vs 9, with a p = **3.314×10^{-4}** :

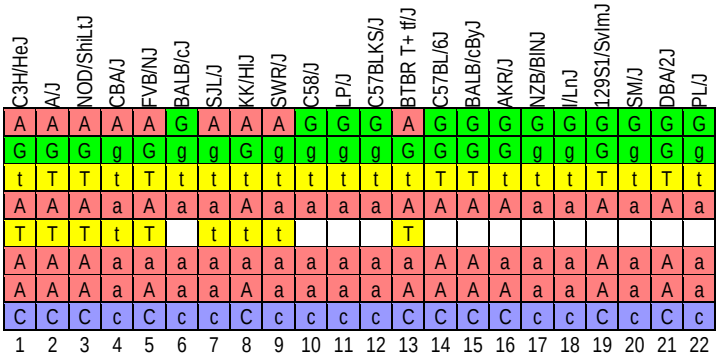

C3H/HeJ	A/J	NOD/ShiLtJ	CBA/J	FVB/NJ	BALB/cJ	SJL/J	KK/HlJ	SWR/J	C58/J	LP/J	C57BLKS/J	BTBR T+ tf/J	C57BL/6J	BALB/cByJ	AKR/J	NZB/BINJ	I/LnJ	129S1/SvImJ	SM/J	DBA/2J	PL/J				p in EMMA III
A	A	A	A	A	G	A	A	A	G	G	G	A	G	G	G	G	G	G	G	G	G	03 87.860731	Apoa1bp	intron5	p= 0.0003314
G	G	G	g	G	g	g	G	g	g	g	g	G	G	G	G	g	g	G	g	G	g	03 87.861017	Apoa1bp	exon5	agrees
t	T	T	t	T	t	t	t	t	t	t	t	t	T	T	t	t	t	T	t	T	t	03 87.861301	Apoa1bp	intron4	agrees
A	A	A	a	A	a	a	A	a	a	a	a	A	A	A	A	a	a	A	a	A	a	03 87.861475	Apoa1bp	intron4	agrees
T	T	T	t	T		t	t	t				T										03 87.861840	Apoa1bp	intron3	agrees
A	A	A	a	a	a	a	a	a	a	a	a	a	A	A	a	a	a	A	a	A	a	03 87.862061	Apoa1bp	exon2	agrees
A	A	A	a	A	a	a	A	a	a	a	a	A	A	A	A	a	a	A	a	A	a	03 87.862326	Apoa1bp	exon1	agrees
C	C	C	c	C	c	c	C	c	c	c	c	C	C	C	C	c	c	C	c	C	c	03 87.862350	Apoa1bp	exon1	agrees
1	2	3	4	5	6	7	8	9	10	11	12	13	14	15	16	17	18	19	20	21	22				

Comments and Description Text from UniProt (Swiss-Prot/TrEMBL) ID: AIBP_MOUSE
DESCRIPTION: Apolipoprotein A-I-binding protein precursor (AI-BP).
SUBUNIT: Interacts with APOA1 and APOA2 (By similarity).
SUBCELLULAR LOCATION: Secreted (By similarity).
SIMILARITY: Contains 1 YjeF N-terminal domain.

8. *Ttc24 ?* tetratricopeptide repeat domain 24. Link to UCSC gene information. Some SNPs share the same SDP as position 87'860'731 above, but there is no SNP within this gene in the EMMA III scan.

9. *Mef2d* is an unlikely candidate when considering SDP of CGD1 SNP set:

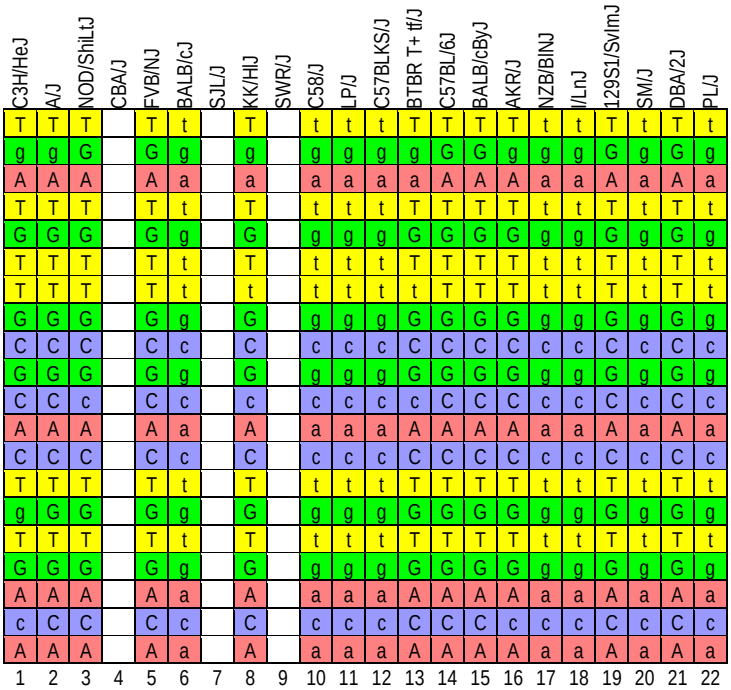

C3H/HeJ	A/J	NOD/ShiLtJ	CBA/J	FVB/NJ	BALB/cJ	SJL/J	KK/HlJ	SWR/J	C58/J	LP/J	C57BLKS/J	BTBR T+ tf/J	C57BL/6J	BALB/cByJ	AKR/J	NZB/BINJ	I/LnJ	129S1/SvImJ	SM/J	DBA/2J	PL/J				
T	T	T		T	t		T		t	t	t	T	T	T	T	t	t	T	t	T	t	03 87.954411	Mef2d	intron1	agrees
g	g	G		G	g		g		g	g	g	g	G	G	g	g	g	G	g	G	g	03 87.955810	Mef2d	intron1	agrees
A	A	A		A	a		a		a	a	a	a	A	A	A	a	a	A	a	A	a	03 87.956722	Mef2d	intron1	agrees
T	T	T		T	t		T		t	t	t	T	T	T	T	t	t	T	t	T	t	03 87.957661	Mef2d	intron1	agrees
G	G	G		G	g		G		g	g	g	G	G	G	G	g	g	G	g	G	g	03 87.959352	Mef2d	intron1	agrees
T	T	T		T	t		T		t	t	t	T	T	T	T	t	t	T	t	T	t	03 87.960573	Mef2d	intron3	agrees
T	T	T		T	t		t		t	t	t	t	T	T	T	t	t	T	t	T	t	03 87.960616	Mef2d	intron3	agrees
G	G	G		G	g		G		g	g	g	G	G	G	G	g	g	G	g	G	g	03 87.960686	Mef2d	intron3	agrees
C	C	C		C	c		C		c	c	c	C	C	C	C	c	c	C	c	C	c	03 87.962661	Mef2d	intron4	agrees
G	G	G		G	g		G		g	g	g	G	G	G	G	g	g	G	g	G	g	03 87.962720	Mef2d	intron4	agrees
C	C	c		C	c		c		c	c	c	c	C	C	C	c	c	C	c	C	c	03 87.964181	Mef2d	intron6	agrees
A	A	A		A	a		A		a	a	a	A	A	A	A	a	a	A	a	A	a	03 87.964516	Mef2d	intron6	agrees
C	C	C		C	c		C		c	c	c	C	C	C	C	c	c	C	c	C	c	03 87.965090	Mef2d	intron6	agrees
T	T	T		T	t		T		t	t	t	T	T	T	T	t	t	T	t	T	t	03 87.966096	Mef2d	intron7	... intron8
g	G	G		G	g		G		g	g	g	G	G	G	G	g	g	G	g	G	g	03 87.966623	Mef2d	intron7	... intron8
T	T	T		T	t		T		t	t	t	T	T	T	T	t	t	T	t	T	t	03 87.967934	Mef2d	intron8	... intron9
G	G	G		G	g		G		g	g	g	G	G	G	G	g	g	G	g	G	g	03 87.967958	Mef2d	intron8	... intron9
A	A	A		A	a		A		a	a	a	A	A	A	A	a	a	A	a	A	a	03 87.968291	Mef2d	intron8	... intron9
c	C	C		C	c		C		c	c	c	C	C	C	c	c	c	C	c	C	c	03 87.970136	Mef2d	intron8	... intron9
A	A	A		A	a		A		a	a	a	A	A	A	A	a	a	A	a	A	a	03 87.970511	Mef2d	intron8	... intron9
1	2	3	4	5	6	7	8	9	10	11	12	13	14	15	16	17	18	19	20	21	22				

Locus 3

Significance (based on data with full allele set): CORRECT

Top hit 1 : position chr 4 : 94'807'400 (a single strong hit)
alleles (EMMA) # alleles 1 = 17; # alleles 2 = 4
condition / stat iso1, REMLt
p-value: **3.351×10^{-6}**
alleles from the Broad1 SNP set (MPD): 16 vs 4

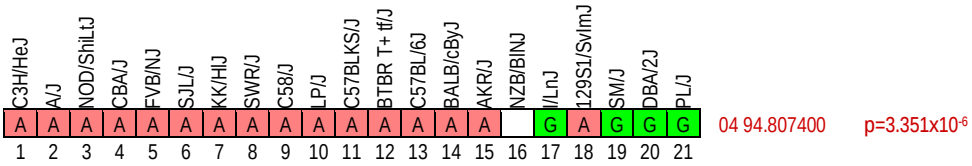

range : single position

Candidate gene(s) : **none**. The closest gene upstream of this position is *Jun*, but the CGD1 SNP strain distribution pattern around *Jun* is distinct and does not correlate with the patterns of VWI across strains for any of the drug conditions.

Locus 4

Significance (based on data with full allele set): CORRECT

Top hit 1 : position chr7 : 75'814'117
alleles (EMMA) # alleles 1 = 17; # alleles 2 = 5
condition / stat atenolol, REMLt
p-value: **3.038×10^{-6}**

Top hit 2 : position chr7 : 75'824'602
alleles (EMMA) # alleles 1 = 17; # alleles 2 = 5
condition / stat atenolol, REMLt
p-value: **3.038×10^{-6}**
alleles from the Broad1 SNP set (MPD): 16 vs 5

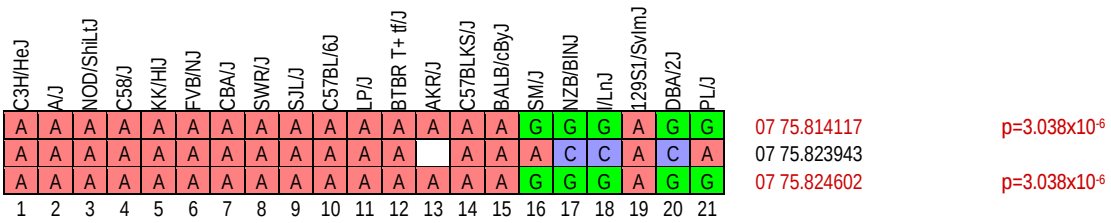

alleles from the CGD1 imputed SNP set (MPD): 17 vs 3

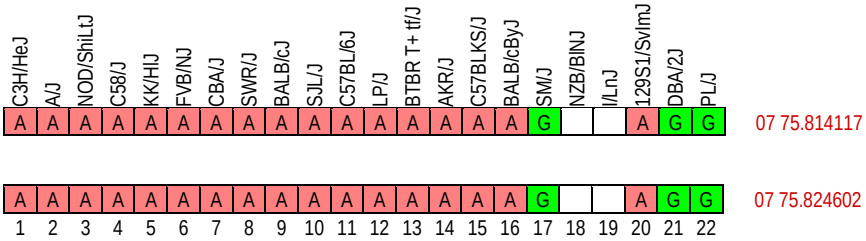

range : ca 75-77 Mb ($p<6 \times 10^{-3}$)

Candidate gene(s) :

1. ***Arrdc4*** : arrestin domain-containing 4. According to MPD medium size SNP dataset (ca Broad1), both hits are located upstream of *Arrdc4*. When investigating SNPs within *Arrdc4* in the CGD1 imputed dataset, either all positions are identical within the PGX strains, or alleles are missing (i.e alleles of strains NZB/BINJ and I/LnJ are missing for both positions). Link to UCSC gene description page.

Notes and bibliography: there are only 2 entries on *Arrdc4* in PubMed.

Knoll B, Goldammer M, Wojewoda A, Flügge J, Johne A, Mrozikiewicz PM, Roots I, Köpke K. **An anomalous haplotype distribution of the arrestin domain-containing 4 gene (ARRDC4) haplotypes in Caucasians.** Genet Test. 2008 Mar;12(1):147-52. URL

Slavotinek AM, Moshrefi A, Davis R, Leeth E, Schaeffer GB, Burchard GE, Shaw GM, James B, Ptacek L, Pennacchio LA. **Array comparative genomic hybridization in patients with congenital diaphragmatic hernia: mapping of four CDH-critical regions and sequencing of candidate genes at 15q26.1-15q26.2**. Eur J Hum Genet. 2006 Sep;14(9):999-1008. URL

2. *Igf1r* ? insulin-like growth factor I receptor. Link to UCSC gene information. Either all CGD1 imputed alleles are identical across PGX strains (except for 1 strain), or many alleles are missing and it is not possible to infer whether there is a positive association or not. Data are thus inconclusive for this gene.

Notes and bibliography: there are >3000 refs related to *Igf1r* in PubMed. There is evidence of a link between Igf1, Igf1r, and cardiac hypertrophy.

Sabatino L, Gliozheni E, Molinaro S, Bonotti A, Azzolina S, Popoff G, Carpi A, Iervasi G. **Thyroid hormone receptor and IGF1/IGFR systems: possible relations in the human heart.** Biomed Pharmacother. 2007 Sep;61(8):457-62. URL

Thyroid hormone (TH) and insulin growth factor 1 (IGF1) systems both play crucial roles in the regulation of cardiac remodeling and hypertrophy processes. The mediation of this regulation is attributed to specific thyroid hormone receptors (TRs) and to the IGF1 receptor (IGF1R). In humans, two TR genes are expressed in the heart, TRalpha and TRbeta. Each gene generates two isoforms: TRalpha1, TRalpha2 and TRbeta1, TRbeta2. The aim of the present work was to study the local thyroid hormone and IGF1 signaling in human myocardium through the evaluation of the gene expression of TRalpha1, TRalpha2, TRbeta1 and IGF1R among atrial and ventricular biopsies obtained from patients undergoing cardiac surgery. Moreover, we evaluated possible correlations between TR and IGF1/IGF1R systems. Eighteen clinically and biochemically euthyroid patients (aged 68.3+/-3.2years, mean+/-SEM) without overt heart failure (Ejection Fraction (EF), 46.4+/-2.8%; Left Ventricular End Diastolic Diameter (LVEDD), 54.3+/-1.2mm, mean+/-SEM; NYHA I-II) were enrolled in the study: 13 undergoing aorto-coronary bypass and 5 undergoing valve replacement (aortic/mitral valve). The examination of total RNA, using real time PCR (LightCycler Technology) confirmed the expression of specific mRNAs encoding TRalpha1, TRalpha2, TRbeta1 and both IGF1 and IGF1R. We found that the three TR genes are co-expressed in the human atrium and ventricle. The finding of a strong correlation among IGF1R and the three TR genes expressed in the atrium ($p<0.001$) and among the three TRs in the atrium ($p<0.001$) suggests the interesting possibility that the two systems, TRs and IGF1R could also be functionally associated.

McMullen JR, Shioi T, Huang WY, Zhang L, Tarnavski O, Bisping E, Schinke M, Kong S, Sherwood MC, Brown J, Riggi L, Kang PM, Izumo S. **The insulin-like growth factor 1 receptor induces physiological heart growth via the phosphoinositide 3-kinase(p110alpha) pathway.** J Biol Chem. 2004 Feb 6;279(6):4782-93. URL

Insulin-like growth factor 1 (IGF1) was considered a potential candidate for the treatment of heart failure. However, some animal studies and clinical trials have questioned whether elevating IGF1 chronically is beneficial. Secondary effects of increased serum IGF1 levels on other tissues may explain these unfavorable results. The aim of the current study was to examine the role of IGF1 in cardiac myocytes in the absence of secondary effects, and to elucidate downstream signaling pathways and transcriptional regulatory effects of the IGF1 receptor (IGF1R). Transgenic mice overexpressing IGF1R in the heart displayed cardiac hypertrophy, which was the result of an increase in myocyte size, and there was no evidence of histopathology. IGF1R transgenics also displayed enhanced systolic function at 3 months of age, and this was maintained at 12-16 months of age. The phosphoinositide 3-kinase (PI3K)-Akt-p70S6K1 pathway was significantly activated in hearts from IGF1R transgenics. Cardiac hypertrophy induced by overexpression of IGF1R was completely blocked by a dominant negative PI3K(p110alpha) mutant, suggesting IGF1R promotes compensated cardiac hypertrophy in a PI3K(p110alpha)-dependent manner. This study suggests that targeting the cardiac IGF1R-PI3K(p110alpha) pathway could be a potential therapeutic strategy for the treatment of heart failure.

Brink M, Chrast J, Price SR, Mitch WE, Delafontaine P. A**ngiotensin II stimulates gene expression of cardiac insulin-like growth factor I and its receptor through effects on blood pressure and food intake. Hypertension**. 1999 Nov;34(5):1053-9. URL

Angiotensin II (Ang II) is known to act as a growth factor and may be involved in cardiac remodeling. We have shown that insulin-like growth factor-I (IGF-I) is an autocrine mediator of growth responses to Ang II in vascular smooth muscle cells in vitro, and we hypothesized that IGF-I also serves as an important modulator of cardiovascular growth in vivo. To study the effect of Ang II on cardiac IGF-I, we infused rats for 3, 7, or 14 days with Ang II through osmotic minipumps. After 7 days, left ventricular mass normalized for body weight was increased by 20% ($P<0.01$) in Ang II rats compared with pair-fed control rats that were given a restricted amount of food identical to that eaten by the anorexic, Ang II-infused rats. Ang II increased left ventricular IGF-I mRNA levels by 1.5- to 1.8-fold compared with ad libitum-fed or pair-fed control rats ($P<0.05$). Cardiac IGF-I protein was increased correspondingly and was localized on the cardiomyocytes. Treatment with hydralazine abolished the induction of IGF-I mRNA, which indicates that Ang II induces cardiac IGF-I mRNA expression through a pressor-mediated mechanism. IGF-I receptor (IGF-IR) mRNA was induced 2.1-fold in Ang II rats compared with ad libitum-fed rats ($P<0.01$). However, this increase was also observed in pair-fed controls and is thus due to the anorexigenic effect of Ang II. We have recently shown that circulating IGF-I levels are reduced in response to Ang II infusion. Elevation of IGF-I levels by coinfusion of IGF-I and Ang II significantly increased left ventricular index by 16% compared with rats infused with Ang II alone ($P<0.05$). In conclusion, autocrine upregulation of cardiac IGF-I and IGF-IR mRNA by Ang II occurs through hemodynamic and nonhemodynamic mechanisms, respectively, and may modulate cardiac structural changes that occur in hypertension.

Locus 5

Significance (based on data with full allele set): INFLATED

Top hit 1 : position chr 1:11'871'998
alleles (EMMA) # alleles 1 = 13; # alleles 2 = 7 (-> allele set is not complete)
condition / stat iso10, REMLt
p-value: 2.680×10^{-6}
alleles from the Broad1 SNP set (MPD): 13 vs 8

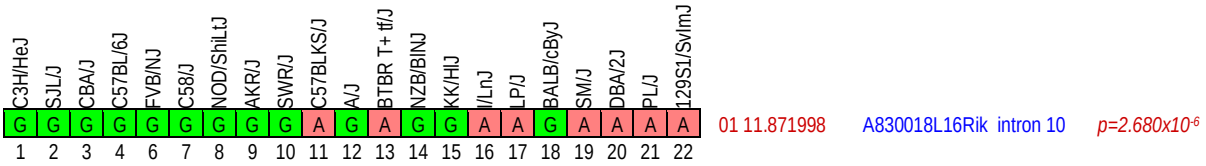

Matching SNP with full allele set:

position chr 1: 11'902'481
alleles (EMMA) #alleles 1 =14; # alleles 2 = 8
condition / stat iso 10, REMLt
p-value: **2.056×10^{-4}**
alleles from the Broad1 SNP set (MPD): 13 vs 8

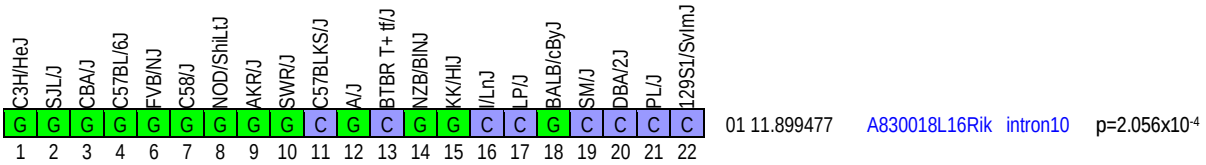

Top hit 2 : position chr 1:11'899'477
alleles (EMMA) #alleles 1 =14; # alleles 2 = 7 (1 missing allele; see matching SNP above)
condition / stat atenolol, LRT
p-value: 1.351×10^{-6}
alleles from the Broad1 SNP set (MPD): 13 vs 7

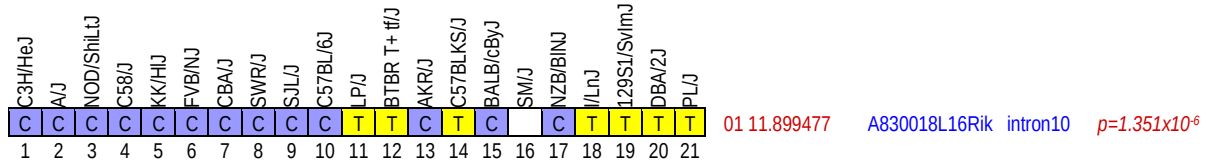

range : ca 11.8-12 Mb

Candidate gene(s) :

1. ***A830018L16Rik***: RIKEN cDNA A830018L16 gene. According to MPD SNP data, top hit is located in intron 11 of *A830018L16Rik*. Function is unknown. Link to UCSC gene description page.

Notes and bibliography:

Locus 6

Significance (based on data with full allele set): INFLATED ?

Top hit 1 : position: chr 1:38'947'935
alleles (EMMA): # alleles 1 = 14; # alleles 2 = 5 (-> allele set is not complete)
condition / stat: atenolol, LRT
p-value: 8.232×10^{-7}

a. alleles from the Broad1 SNP set (MPD): 13 vs 5. Note that top hit #1 is given at a position where some alleles are missing. There is no other position that matches the same SDP in this area, so one cannot infer a « true » p-value for the full allele set.

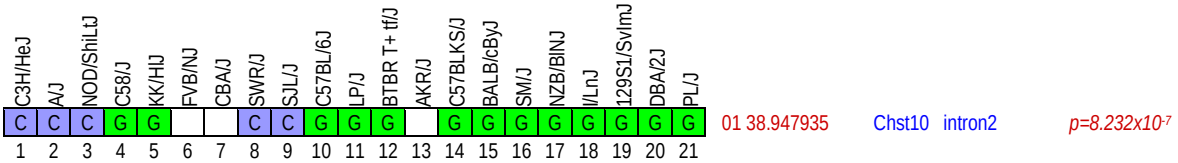

b. alleles from the CGD1 imputed SNP set (MPD): 15 vs 7. There is a discrepancy for Balb/cByJ between both sources.

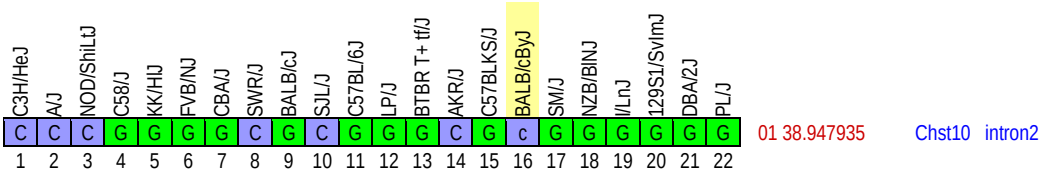

range: single position

Candidate gene(s) :

1. *Chst10* : carbohydrate sulfotransferase 10. According to MPD SNP data, top hit is located in intron 2 of *Chst10*. Link to UCSC gene description page.

Comments and Description Text from UniProt (Swiss-Prot/TrEMBL) ID: CHSTA_MOUSE

DESCRIPTION: Carbohydrate sulfotransferase 10 (EC 2.8.2.-) (HNK-1 sulfotransferase) (HNK1ST) (HNK-1ST).

FUNCTION: Catalyzes the transfer of sulfate to position 3 of terminal glucuronic acid of both protein- and lipid-linked oligosaccharides. Participates in biosynthesis of HNK-1 carbohydrate structure, a sulfated glucuronyl-lactosaminyl residue carried by many neural recognition molecules, which is involved in cell interactions during ontogenetic development and in synaptic plasticity in the adult. May be indirectly involved in synapse plasticity of the hippocampus, via its role in HNK-1 biosynthesis.

SUBCELLULAR LOCATION: Golgi apparatus membrane; Single-pass type II membrane protein (By similarity).

MISCELLANEOUS: Mice lacking Chst10 are viable, fertile and show normal cerebellar granule neuron migration. The anatomy of all major brain areas are histologically normal. However, basal synaptic transmission in pyramidal cells in the CA1 region of the hippocampus are increased and long-term potentiation evoked by theta-burst stimulation are reduced. Mice show an impaired long- term memory and a poorer spatial learning when a short inter-trial interval is used.

SIMILARITY: Belongs to the sulfotransferase 2 family.

SEQUENCE CAUTION: Sequence=AAH56956.1; Type=Miscellaneous discrepancy; Note=Intron retention;

Bibliography

Wenink AC, Symersky P, Ikeda T, DeRuiter MC, Poelmann RE, Gittenberger-de Groot AC. **HNK-1 expression patterns in the embryonic rat heart distinguish between sinuatrial tissues and atrial myocardium.** Anat Embryol (Berl). 2000 Jan;201(1):39-50. URL

HNK-1 expression was studied by immunohistochemistry in serial sections of embryonic and fetal rat hearts from 11.5 to 16.5 embryonic days. Graphic reconstructions were made to obtain detailed 3D information on the localization of immunoreactive tissues. The antibody used appeared to stain most parts of the venous sinus and the sinuatrial transitional zone as well as the atrioventricular transitional zone, but the patterns varied through the different developmental stages. At 11.5 days, positive

myocardium was found in the right atrium and on top of the ventricular septal primordium. At 13.5 days, the left venous valve and the posterior atrial wall containing the orifice of the pulmonary vein were immunoreactive, and so were the right venous valve, the septum spurium and the superior, right-lateral and inferior parts of the atrioventricular canal. From the latter, immunoreactivity continued onto the crest of the ventricular septum. At 15.5 days, HNK-1 positivity in the two venous valves had become continuous, whereas the right-lateral part of the atrioventricular canal had lost its positivity, thus making the positive areas in the superior and inferior parts of this canal discontinuous. From the venous valves immunoreaction continued into the venous sinus septum but this area remained discontinuous with the inferior part of the atrioventricular canal. It is concluded that the entirety of venous sinus and sinuatrial transitional zone expresses the HNK-1 antigen and that the orifice of the pulmonary vein belongs to this complex, rather than to the embryonic atrium proper, which is HNK-1 negative. Extrapolation of these data to the adult human atrium leads to the conclusion hat most "atrial septal structures" are of sinuatrial origin, leaving the flap valve of the oval fossa (atrial septum primum) as the only really atrial structure. It is suggested that the atrioventricular node is derived from the inferior portion of the atrioventricular canal, and that two expansions of sinuatrial tissue form the substrate for anterior and posterior atrionodal inputs which in the literature have been described as internodal tracts.

Chau MD, Tuft R, Fogarty K, Bao ZZ. **Notch signaling plays a key role in cardiac cell differentiation.** Mech Dev. 2006 Aug;123(8):626-40. URL

Results from lineage tracing studies indicate that precursor cells in the ventricles give rise to both cardiac muscle and conduction cells. Cardiac conduction cells are specialized cells responsible for orchestrating the rhythmic contractions of the heart. Here, we show that Notch signaling plays an important role in the differentiation of cardiac muscle and conduction cell lineages in the ventricles. Notch1 expression coincides with a conduction marker, HNK-1, at early stages. Misexpression of constitutively active Notch1 (NIC) in early heart tubes in chick exhibited multiple effects on cardiac cell differentiation. Cells expressing NIC had a significant decrease in expression of cardiac muscle markers, but an increase in expression of conduction cell markers, HNK-1, and SNAP-25. However, the expression of the conduction marker connexin 40 was inhibited. Loss-of-function study, using a dominant-negative form of Suppressor-of-Hairless, further supports that Notch1 signaling is important for the differentiation of these cardiac cell types. Functional studies show that the expression of constitutively active Notch1 resulted in abnormalities in ventricular conduction pathway patterns.

Locus 7

Significance (based on data with full allele set): CORRECT

Top hit 1 : position chr 2:131'352'413
alleles (EMMA) # alleles 1 = 16; # alleles 2 = 6
condition / stat atenolol, LRT
p-value: **2.584×10^{-6}**
alleles from the Broad1 SNP set (MPD): 15 vs 6; BUT note that SDP indicated by an asterisk has not been investigated in EMMA III

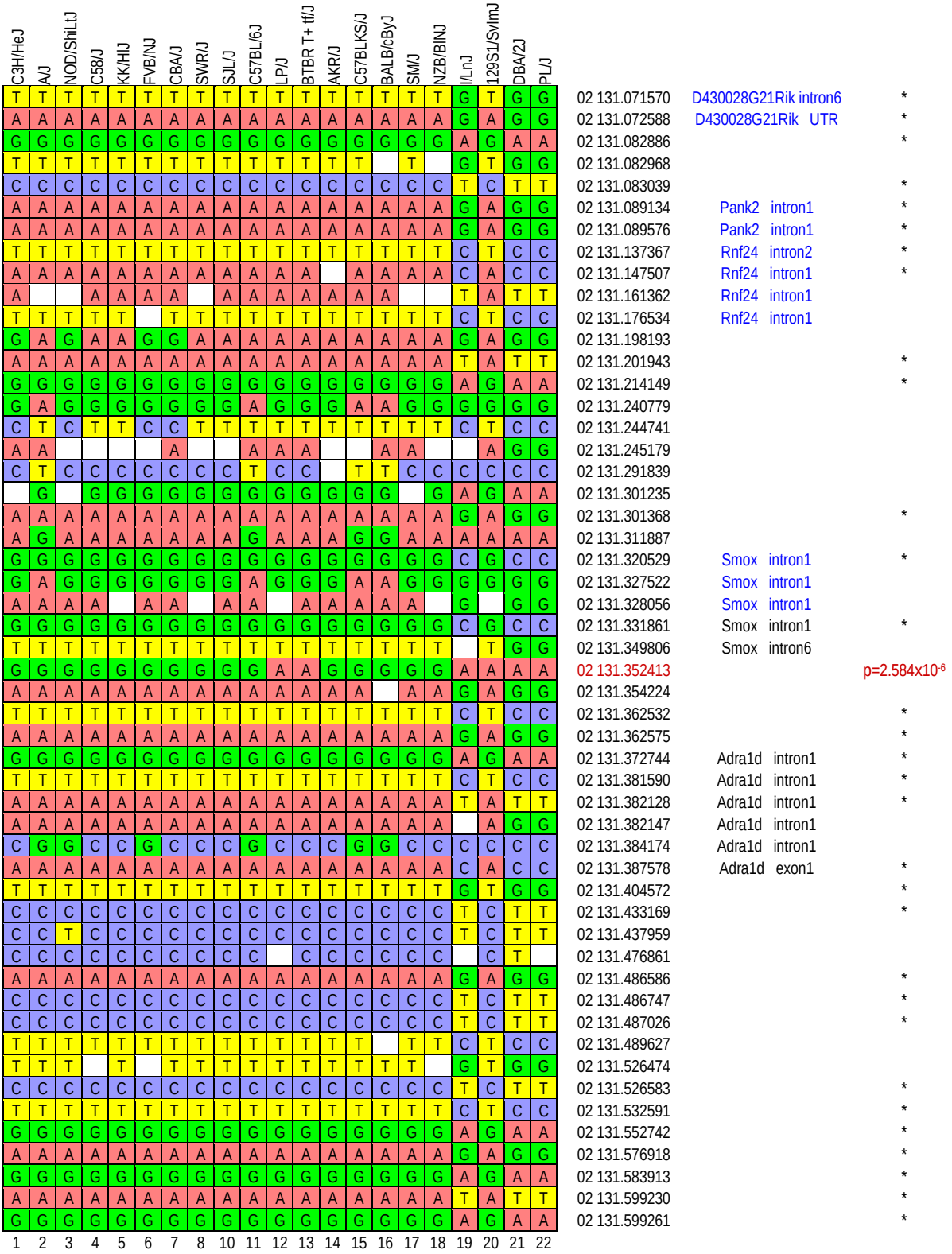

range : 131.07-131.6 Mb

Candidate gene(s), notes and bibliography :

1. ***Pank2*** : pantothenate kinase 2. Associated to neurodegeneration. Link to UCSC gene description page.

2. ***Rnf24*** : ring finger protein 24. A single report in PubMed mentions Rnf24 as a Trpc6 binding partner . The canonical transient receptor potential channels (TRPCs) are Ca^{2+}-permeable nonselective cation channels with various physiological functions. There might be a link between *Trpc* (incl. *Trpc6*) and cardiac hypertrophy. There is a lot of information on *Trpc6*. Link to UCSC gene description page.

Dyachenko V, Husse B, Rueckschloss U, Isenberg G. **Mechanical deformation of ventricular myocytes modulates both TRPC6 and Kir2.3 channels**. Cell Calcium. 2008 Jul 15. URL

Cardiomyocytes respond to mechanical stretch with an increase [Ca(2+)](i). Here, we analyzed which ion channels could mediate this effect. Murine ventricular myocytes were attached to a glass coverslip and a cell-attached glass stylus sheared the upper cell part versus the attached cell bottom. At negative clamp potentials, stretch induced inward currents that increased with the extent of stretch and reversed within 2min after relaxation from stretch. Stretch activated a nearly voltage-independent GsMTx-4-sensitive non-selective cation conductance G(ns), antibodies against TRPC6 prevented G(ns) activation. In addition, stretch deactivated a Cs(+)-sensitive inwardly rectifying potassium conductance G(K1), antibodies against Kir2.3 inhibited this effect. Immunolabeling localized TRPC6 and Kir2.3 in T-tubular membranes, and stretch-induced changes in membrane currents were absent in cells whose T-tubules had been removed. In absence of stretch, we could activate G(ns) and deactivate G(K1) by 1-oleoyl-2-acetyl-sn-glycerol (OAG) and other amphipaths. We interpret that the function of TRPC6 and Kir2.3 channels is controlled by both tension and curvature of the surrounding lipid bilayer that are changed by incorporation of amphipaths. Stretch-activation of TRPC6 channels may increase Ca(2+) influx directly and indirectly, by membrane depolarization (activation of voltage-gated Ca(2+) channels) and by elevated [Na(+)](i) (augmented Na(+),Ca(2+)-exchange).

Nishida M, Kurose H. **Roles of TRP channels in the development of cardiac hypertrophy**. Naunyn Schmiedebergs Arch Pharmacol. 2008 Oct;378(4):395-406. URL

Cardiac hypertrophy is induced by various stresses such as hypertension and myocardial infarction. It is believed that hypertrophy is adaptive in the early phase but becomes maladaptive in the late phase. Cardiac hypertrophy develops heart failure when the heart is exposed persistently to the stresses. The increase in intracellular Ca(2+) ([Ca(2+)](i)) plays an important role in the development of hypertrophy. It is generally thought that the increase in [Ca(2+)](i) for hypertrophy occurs via G(q)-stimulated production of inositol-1,4,5-trisphosphate (IP(3)) and IP(3)-mediated release of Ca(2+) from intracellular store. However, several groups recently reported that canonical transient receptor potential (TRPC) channels are responsible for the increase in [Ca(2+)](i). Among them, three TRPC subtypes (TRPC3/TRPC6/TRPC7) are activated by another G(q)-mediated second messenger, diacylglycerol. Although several groups independently demonstrated that TRPC channels mediate receptor-stimulated and pressure overload-induced hypertrophy, there is discrepancy of which subtypes of TRPC channels predominantly mediate hypertrophy. However, there is consensus that TRPC-mediated Ca(2+) influx is essential for hypertrophy. As TRPC channels participate in pathological hypertrophy, but not physiological contraction and the relaxation cycle, TPRC channels are a new target for the treatment of hypertrophy.

Dietrich A, Gudermann T. **TRPC6**. Handb Exp Pharmacol. 2007;(179):125-41. URL

TRPC6 is a Ca(2+)-permeable non-selective cation channel expressed in brain, smooth muscle containing tissues and kidney, as well as in immune and blood cells. Channel homomers heterologously expressed have a characteristic doubly rectifying current-voltage relationship and are six times more permeable for Ca2+ than for Na+. In smooth muscle tissues, however, Na+ influx and activation of voltage-gated calcium channels by membrane depolarization rather than Ca2+ elevation by TRPC6 channels is the driving force for contraction. TRPC6 channels are directly activated by the second messenger diacylglycerol (DAG) and regulated by specific tyrosine or serine phosphorylation. Extracellular Ca2+ has inhibitory effects, while Ca2+/calmodulin acting from the intracellular side has potentiator effects on channel activity. Given its specific expression, TRPC6 is likely to play a number of physiological roles. Studies with TRPC6(-/-) mice suggest a role for the channel in the regulation of vascular and pulmonary smooth muscle contraction. TRPC6 was identified as an essential component of the slit diaphragm architecture of kidney podocytes. Other functions in immune and blood cells, as well as in brain and in smooth muscle-containing tissues such as stomach, colon and myometrium, remain elusive.

Onohara N, Nishida M, Inoue R, Kobayashi H, Sumimoto H, Sato Y, Mori Y, Nagao T, Kurose H. **TRPC3 and TRPC6 are essential for angiotensin II-induced cardiac hypertrophy**. EMBO J. 2006 Nov 15;25(22):5305-16. URL

Angiotensin (Ang) II participates in the pathogenesis of heart failure through induction of cardiac hypertrophy. Ang II-induced hypertrophic growth of cardiomyocytes is mediated by nuclear factor of activated T cells (NFAT), a Ca(2+)-responsive transcriptional factor. It is believed that phospholipase C (PLC)-mediated production of inositol-1,4,5-trisphosphate (IP(3)) is responsible for Ca(2+) increase that is necessary for NFAT activation. However, we demonstrate that PLC-mediated production of diacylglycerol (DAG) but not IP(3) is essential for Ang II-induced NFAT activation in rat cardiac myocytes. NFAT activation and hypertrophic responses by Ang II stimulation required the enhanced frequency of Ca(2+) oscillation triggered by membrane depolarization through activation of DAG-sensitive TRPC channels, which leads to activation of L-type Ca(2+) channel. Patch clamp recordings from single myocytes revealed that Ang II activated DAG-sensitive TRPC-like currents. Among DAG-activating TRPC channels (TRPC3, TRPC6, and TRPC7), the activities of TRPC3 and TRPC6 channels correlated with Ang II-induced NFAT activation and hypertrophic responses. These data suggest that DAG-induced Ca(2+) signaling pathway through TRPC3 and TRPC6 is essential for Ang II-induced NFAT activation and cardiac hypertrophy.

3. ***Smox*** : spermine oxidase. Link to UCSC gene description page.

Comments and Description Text from UniProt (Swiss-Prot/TrEMBL) ID: SMOX_MOUSE

DESCRIPTION: Spermine oxidase (EC 1.5.3.-) (Polyamine oxidase 1) (PAO-1) (PAOh1).
FUNCTION: Flavoenzyme which catalyzes the oxidation of spermine to spermidine. Can also use N(1)-acetylspermine and spermidine as substrates, with different affinity depending on the isoform (isozyme) and on the experimental conditions. Plays an important role in the regulation of polyamine intracellular concentration and has the potential to act as a determinant of cellular sensitivity to the antitumor polyamine analogs. May contribute to beta-alanine production via aldehyde dehydrogenase conversion of 3-amino-propanal.
CATALYTIC ACTIVITY: Spermine + O(2) + H(2)O = Spermidine + 3- aminopropanal + H(2)O(2).
COFACTOR: FAD (By similarity).
PATHWAY: Amine and polyamine degradation; spermine degradation.
SUBCELLULAR LOCATION: Cytoplasm.
SUBCELLULAR LOCATION: Isoform 2: Cytoplasm. Nucleus.
TISSUE SPECIFICITY: Widely expressed. Isoform 1 and isoform 2 are expressed at higher level in brain and skeletal muscle. Isoform 7 is found in brain and spleen, isoform 10 is widely expressed but found at lower level in heart, kidney, liver and lung.
INDUCTION: By antitumor polyamine analogs (Probable).
SIMILARITY: Belongs to the flavin monoamine oxidase family.

4. ***Adra1d*** : adrenergic receptor, alpha 1d. Link to UCSC gene description page.

Nonen S, Okamoto H, Fujio Y, Takemoto Y, Yoshiyama M, Hamaguchi T, Matsui Y, Yoshikawa J, Kitabatake A, Azuma J. **Polymorphisms of norepinephrine transporter and adrenergic receptor alpha1D are associated with the response to beta-blockers in dilated cardiomyopathy.** Pharmacogenomics J. 2008 Feb;8(1):78-84. URL

Recent clinical trials have clearly demonstrated that the administration with beta-blockers decreases the mortality in the patients with chronic heart failure (CHF). However, significant heterogeneity exists in the effectiveness of beta-blockers among individual cases. We focused on 39 polymorphisms in 16 genes related to adrenergic system and investigated their association with the response to beta-blockers among 80 patients with CHF owing to idiopathic dilated cardiomyopathy. The polymorphisms of NET T-182C (P=0.019), ADRA1D T1848A (P=0.023) and ADRA1D A1905G (P=0.029) were associated with the improvement of left ventricular fractional shortening (LVFS) by beta-blockers. Furthermore, combined genotype analysis of NET T-182C and ADRA1D T1848A revealed a significant difference in LVFS improvement among genotype groups (P=0.011). These results suggest that NET (T-182C) and ADRA1D (T1848A and A1905G) polymorphisms are predictive markers of the response to beta-blockers. Genotyping of these polymorphisms may provide clinical insights into an individual difference in the response to the beta-blocker therapy in CHF.

Top hit 2 : position chr2:130'952'456
alleles (EMMA) # alleles 1 = 17; # alleles 2 = 4 (incomplete allele set)
condition / stat atenolol, REMLt
p-value: $1.439x10^{-5}$
alleles from the Broad1 SNP set (MPD): 17 vs 4

Matching SNP with full allele set:

position chr 2: 130'912'557
alleles (EMMA) #alleles 1 =17; # alleles 2 = 5
condition / stat atenolol, REMLt
p-value: **$9.943x10^{-5}$**
alleles from the Broad1 SNP set (MPD): 17 vs 4

C3H/HeJ	A/J	NOD/ShiLtJ	C58/J	KK/HlJ	FVB/NJ	CBA/J	SWR/J	SJL/J	C57BL/6J	LP/J	BTBR T+ tf/J	AKR/J	C57BLKS/J	BALB/cByJ	SM/J	NZB/BINJ	I/LnJ	129S1/SvImJ	DBA/2J	PL/J			
G	G	G	G	G	G	G	G	G	G	G	G	G	G	A	G	G	A	G	A	A	02 130.881869	Adam33 intron6	
A	A	A	A	A	A	A	A	A	A	A	A	A	A		A	A	G	A	G	G	02 130.884056	Adam33 intron3	
C	C	C	C	C	C	C	C	C	C	C	C	C	C		C	C	T	C	T	T	02 130.887044	Adam33 intron1	
A	A	A	A	A	A	A	A	A	A	A	A	A	A	G	A	A	G	A	G	G	02 130.888228	Adam33 intron1	
T	T	T	T	T				T	T	T	T		T	A	T	T		T	A	A	02 130.904515	Siglec1 intron8	
G	G	G	G	G	G	G	G	G	G	G	G	G	G	A	G	G	A	G	A	A	02 130.910030	Siglec1 intron3	
	T	T				T			T		T		T	C			C	T	C	C	02 130.911279	Siglec1 exon2	
A	A	A	A	A	A	A	A	A	A	A	A	A	A	G	A	A	G	A	G	G	02 130.912557		p=9.943x10-5
A	A	A	A	A	A	A	A	A	A	A	A	A	A			A	G	A	G	G	02 130.932263	LOC100043457 intron2	
T	T	T	T	T	T	T	T	T	T	T	T	T	T	G	T	T	G	T	G	G	02 130.952456		*p=1.439x10-5*
	C	C							C						C			C	G		02 130.957579	Hspa12b intron1	

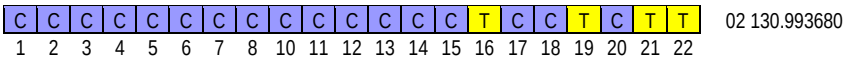

range : 130.8-131 Mb

Candidate gene(s), notes and bibliography :

5. ***Adam33*** : a disintegrin and metallopeptidase domain 33. Link to UCSC gene description page.

Comments and Description Text from UniProt (Swiss-Prot/TrEMBL) ID: ADA33_MOUSE
DESCRIPTION: ADAM 33 precursor (EC 3.4.24.-) (A disintegrin and metalloproteinase domain 33).
COFACTOR: Binds 1 zinc ion per subunit (By similarity).
SUBCELLULAR LOCATION: Membrane; Single-pass type I membrane protein.
DOMAIN: The conserved cysteine present in the cysteine-switch motif binds the catalytic zinc ion, thus inhibiting the enzyme. The dissociation of the cysteine from the zinc ion upon the activation-peptide release activates the enzyme.
PTM: The precursor is cleaved by a furin endopeptidase (By similarity).
SIMILARITY: Contains 1 disintegrin domain.
SIMILARITY: Contains 1 EGF-like domain.
SIMILARITY: Contains 1 peptidase M12B domain.

Adam33 has been associated to asthma and psioriasis (PubMed).

6. ***Siglec1*** : sialoadhesin. No further information. Link to UCSC gene description page.

7. ***Hspa12b*** : Link to UCSC gene description page.

Steagall RJ, Rusiñol AE, Truong QA, Han Z. **HSPA12B is predominantly expressed in endothelial cells and required for angiogenesis**. Arterioscler Thromb Vasc Biol. 2006 Sep;26(9):2012-8. URL
OBJECTIVE: HSPA12B is the newest member of HSP70 family of proteins and is enriched in atherosclerotic lesions. This study focused on HSPA12B expression in mice and its involvement in angiogenesis. METHODS AND RESULTS: The expression of HSPA12B in mice and cultured cells was studied by: (1) Northern blot; (2) in situ hybridization; (3) immunostaining with HSPA12B-specific antibodies; and (4) expressing Enhanced-Green-Fluorescent-Protein under the control of the HSPA12B promoter in mice. The function of HSPA12B was probed by an in vitro angiogenesis assay (Matrigel) and a migration assay. Interacting proteins were identified through a yeast two-hybrid screening. HSPA12B is predominantly expressed in vascular endothelium and induced during angiogenesis. In vitro angiogenesis and migration are inhibited in human umbilical vein endothelial cells in the presence of HSPA12B-neutralizing antibodies. HSPA12B interacts with multiple proteins in yeast 2-hybrid system. CONCLUSIONS: We provide the first evidence to our knowledge that the HSPA12B is predominantly expressed in endothelial cells, required for angiogenesis, and interacts with known angiogenesis regulators. We postulate that HSPA12B provides a new mode of angiogenesis regulation and a novel therapeutic target for angiogenesis-related diseases.

Locus 8

Significance (based on data with full allele set): INFLATED

Top hit 1 : position chr 2:117'682'002
alleles (EMMA) # alleles 1 = 15; # alleles 2 = 4 (-> allele set is not complete)
condition / stat iso 1, REMLt
p-value: $1.174x10^{-6}$
alleles from the Broad1 SNP set (MPD): 15 vs 4

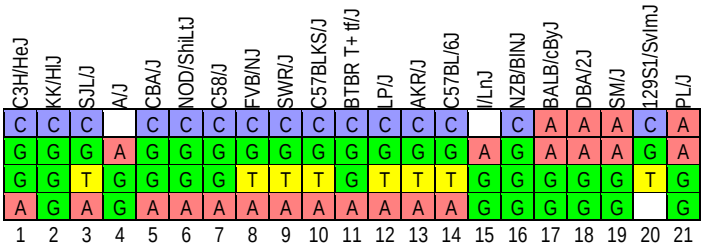

Matching SNP with full allele set (for position 117'682'202):

position chr 2: 11'7677'222
alleles (EMMA) #alleles 1 =15; # alleles 2 = 7
condition / stat iso 1 and iso 10, REMLt
p-value: $1.751x10^{-4}$ for iso 1, and **$6.703x10^{-5}$** for iso 10, REMLt

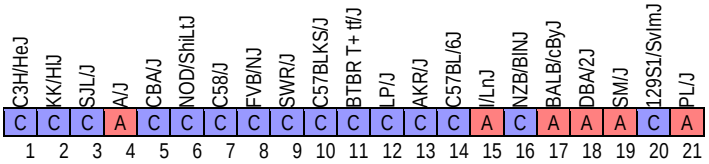

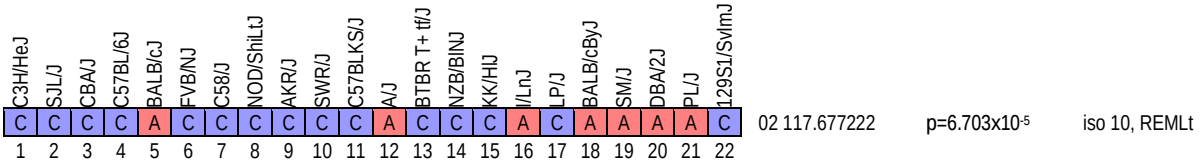

range :

Candidate gene(s) : **none**

Locus 9

Significance (based on data with full allele set): INFLATED, but p-values still below 10^{-5}

Top hit 1 : position chr 4:151'355'820
alleles (EMMA) # alleles 1 = 16; # alleles 2 = 5 (allele set is incomplete)
condition / stat iso 1, REMLt
p-value: 3.346×10^{-7}
alleles from the Broad1 SNP set (MPD): 16 vs 5

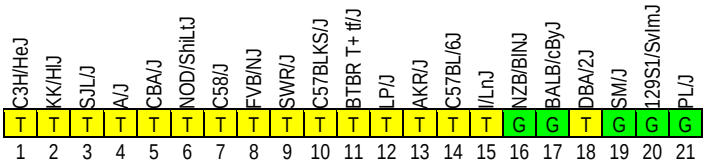

04 151.355820 *p=3.346x10-7* Dnajc11 exon16,UTR

alleles from the CGD1 imputed SNP set (MPD): 16 vs 6

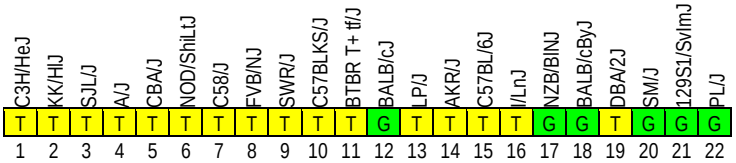

04 151.355820 Dnajc11 exon16,UTR

Matching SNP with full allele set:

position chr 4: 151'352'086
alleles (EMMA) #alleles 1 =16; # alleles 2 = 6
condition / stat iso 1, REMLt
p-value: **2.866×10^{-6}**

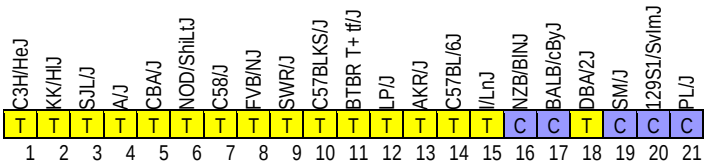

04 151.352086 p=2.866x10-6 Dnajc11 intron11

range : ca 151.35-151.4 Mb

Candidate gene(s), notes and bibliography:

1. ***Dnajc11*** : DnaJ (Hsp40) homolog, subfamily C, member 11. Only 3 refs in PubMed. Mitochondrial chaperone, maybe related to neuroblastoma. Link to UCSC gene description page.
2. ***Thap3*** ? THAP domain containing, apoptosis associated. No info in PubMed. Link to UCSC gene description page.
3. ***Phf13*** ? PHD finger protein 13. No info in PubMed. Link to UCSC gene description page.
4. ***Klhl21*** ? kelch-like 21. No info in PubMed. Link to UCSC gene description page.

Comments and Description Text from UniProt (Swiss-Prot/TrEMBL) ID: KLH21_MOUSE
DESCRIPTION: Kelch-like protein 21.
FUNCTION: Probable substrate-specific adapter of an E3 ubiquitin- protein ligase complex which mediates the ubiquitination and subsequent proteasomal degradation of target proteins (By similarity).
PATHWAY: Protein modification; protein ubiquitination.
SUBUNIT: Interacts with CUL3 (By similarity).
SIMILARITY: Contains 1 BACK (BTB/Kelch associated) domain.
SIMILARITY: Contains 1 BTB (POZ) domain.
SIMILARITY: Contains 6 Kelch repeats.

Other genes (incl. *Kcnab2*) are unlikely candidates, based on the SNP SDP in CGD1 imputed set.

Top hit 2 : position chr 4:152'394'133
alleles (EMMA) # alleles 1 = 17; # alleles 2 = 4 (incomplete allele set)
condition / stat iso 10, REMLt
p-value: $2.307x10^{-7}$
alleles from the Broad1 SNP set (MPD): 17 vs 4

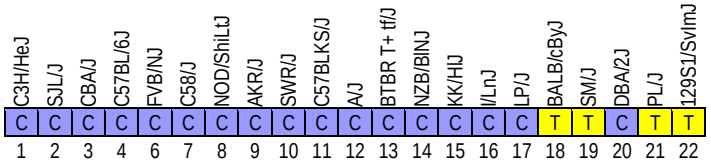

04 152.394133 *p=2.307x10-7*

alleles from the CGD1 imputed SNP set (MPD): 17 vs 5

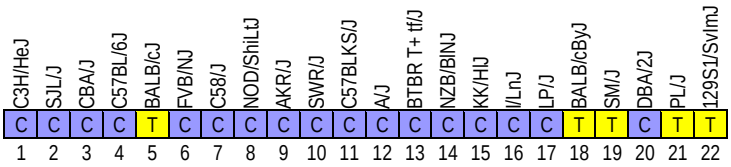

04 152.394133

Matching SNP with full allele set:

position chr 4: 152'341'831
alleles (EMMA) #alleles 1 =17; # alleles 2 = 5
condition / stat iso 1, REMLt
p-value: **$4.147x10^{-6}$**

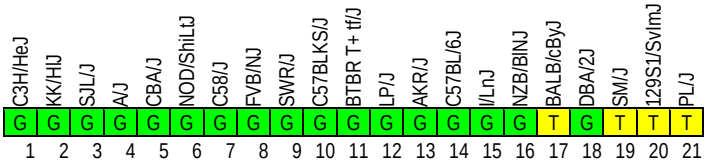

04 152.341831 p=4.147x10-6

range : ca 155.2-152.5 Mb

Candidate gene(s), notes and bibliography: **none**

Locus 10

Significance (based on data with full allele set): INFLATED

Top hit 1 : position chr 10:110'702'509
alleles (EMMA) # alleles 1 = 16; # alleles 2 = 4 (-> allele set is incomplete)
condition / stat iso 1, REMLt
p-value: $1.588x10^{-6}$
alleles from the Broad1 SNP set (MPD): 15 vs 4

Matching SNP with full allele set:

position chr 10: 110'607'856
alleles (EMMA) #alleles 1 =18; # alleles 2 = 4
condition / stat iso 1, REMLt
p-value: **$1.141x10^{-5}$**
alleles from the Broad1 SNP set (MPD): 17 vs 4

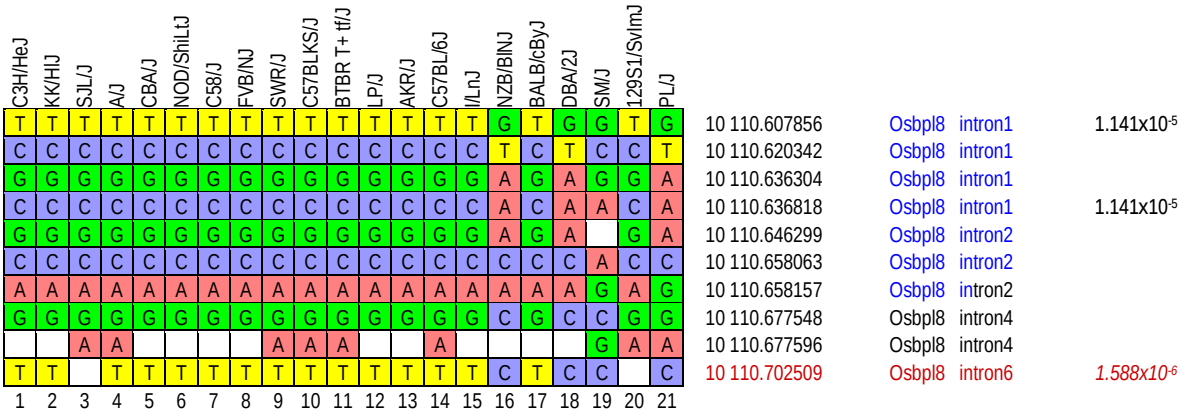

alleles from the CGD1 imputed SNP set (MPD): 18 vs 3

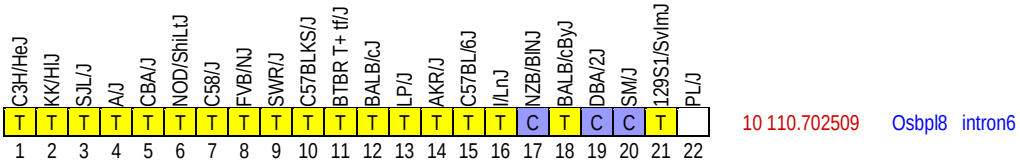

range : ca 110.6-110.8 Mb (see SDP in CGD1 imputed SNP panel)

Candidate gene(s) :

1. ***Osbpl8*** : oxysterol-binding protein-like protein 8 isoform. Protein known as Orp8. RefSeq Summary (NM_175489): This gene encodes a member of the oxysterol-binding protein (Osbp) family, a group of intracellular lipid receptors. Link to UCSC gene description.
2. ***Bbs10*** : Bardet-Biedl syndrome 10. This gene is not indicated in the UCSC genome browser but is present in the MPD entries, immediately downstream of *Osbpl8*. See entries #209900 and *610148 in OMIM

Notes and bibliography:

There are only 2 entries about *Osbpl8* in PubMed, but there are more on Osbp. Like most members of the Osbp family of proteins, the encoded protein contains an N-terminal pleckstrin homology domain and a highly conserved C-terminal Osbp-like sterol-binding domain. Two transcript variants encoding different isoforms have been found for this gene. By screening for cDNAs with the potential to encode large proteins expressed in brain, Nagase et al. (2000) identified a cDNA encoding OSBPL8, which they called KIAA1451. The deduced 488-amino acid protein was predicted to be 33% identical to mouse Osbp. RT-PCR analysis detected wide expression that was strongest in testis, ovary, liver, kidney, and brain. Within brain, expression was particularly strong in caudate nucleus. Most interestingly, key information

connecting *OSBPL8* mRNA expression with indexed left ventricular mass in humans can be found in Petretto et al. (see Table 1 below).

Petretto E, Sarwar R, Grieve I, Lu H, Kumaran MK, Muckett PJ, Mangion J, Schroen B, Benson M, Punjabi PP, Prasad SK, Pennell DJ, Kiesewetter C, Tasheva ES, Corpuz LM, Webb MD, Conrad GW, Kurtz TW, Kren V, Fischer J, Hubner N, Pinto YM, Pravenec M, Aitman TJ, Cook SA. **Integrated genomic approaches implicate osteoglycin (*Ogn*) in the regulation of left ventricular mass**. Nat Genet. 2008 May;40(5):546-52. URL

Left ventricular mass (LVM) and cardiac gene expression are complex traits regulated by factors both intrinsic and extrinsic to the heart. To dissect the major determinants of LVM, we combined expression quantitative trait locus1 and quantitative trait transcript (QTT) analyses of the cardiac transcriptome in the rat. Using these methods and in vitro functional assays, we identified osteoglycin (*Ogn*) as a major candidate regulator of rat LVM, with increased Ogn protein expression associated with elevated LVM. We also applied genome-wide QTT analysis to the human heart and observed that, out of 22,000 transcripts, *OGN* transcript abundance had the highest correlation with LVM. We further confirmed a role for *Ogn* in the in vivo regulation of LVM in *Ogn* knockout mice. Taken together, these data implicate *Ogn* as a key regulator of LVM in rats, mice and humans, and suggest that *Ogn* modifies the hypertrophic response to extrinsic factors such as hypertension and aortic stenosis.

Table 1 Differentially expressed genes in human cardiac hypertrophy and associated with indexed left ventricular mass

Probe identifier	Gene symbol	Gene name	Relative change[a]	FDR[b] (%)	Correlation with LVM[c]	*P* value[d]
218730_s_at	*OGN*	Osteoglycin	2.2	2.7	0.62	1.2×10^{-3}
202766_s_at	*FBN1*	Fibrillin 1	2.0	2.7	0.55	4.5×10^{-3}
209621_s_at	*PDLIM3*	PDZ and LIM domain 3	1.6	5.0	0.52	6.5×10^{-3}
219087_at	*ASPN*	Asporin	1.9	5.0	0.52	7.5×10^{-3}
213646_x_at	*TUBA1B*	Tubulin, alpha 1b	1.5	2.7	0.52	5.7×10^{-3}
213765_at	*MFAP5*	Microfibrillar associated protein 5	1.8	5.0	0.51	6.8×10^{-3}
203570_at	*LOXL1*	Lysyl oxidase-like 1	1.5	5.0	0.51	8.1×10^{-3}
208782_at	*FSTL1*	Follistatin-like 1	1.5	2.7	0.51	1.1×10^{-2}
213867_x_at	*ACTB*	Actin, beta	1.5	2.7	0.49	1.1×10^{-2}
212614_at	*ARID5B*	AT rich interactive domain 5B	1.6	2.7	0.49	9.9×10^{-3}
216442_x_at	*FN1*	Fibronectin 1	1.9	5.0	0.49	1.1×10^{-2}
211750_x_at	*TUBA1C*	Tubulin, alpha 1c	1.6	2.7	0.48	1.3×10^{-2}
212582_at	*OSBPL8*	Oxysterol binding protein-like 8	1.6	2.7	0.48	1.1×10^{-2}
221729_at	*COL5A2*	Collagen, type V, alpha 2	1.9	5.0	0.48	1.3×10^{-2}
201843_s_at	*EFEMP1*	EGF- fibulin-like extracellular matrix protein 1	1.8	5.0	0.48	1.2×10^{-2}
202007_at	*NID1*	Nidogen 1	1.6	2.7	0.47	1.6×10^{-2}
203548_s_at	*LPL*	Lipoprotein lipase	1.8	2.7	0.47	1.7×10^{-2}
205547_s_at	*TAGLN*	Transgelin	2.1	2.7	0.46	1.7×10^{-2}
202552_s_at	*CRIM1*	Cysteine rich transmembrane BMP regulator 1	1.6	3.9	0.46	1.9×10^{-2}
201012_at	*ANXA1*	Annexin A1	1.6	2.7	0.46	1.7×10^{-2}
209460_at	*ABAT*	4-aminobutyrate aminotransferase	1.6	2.7	0.45	2.0×10^{-2}
201302_at	*ANXA4*	Annexin A4	1.5	3.9	0.44	2.1×10^{-2}
219260_s_at	*C17orf81*	Chromosome 17 open reading frame 81	1.5	2.7	0.44	2.4×10^{-2}
209130_at	*SNAP23*	Synaptosomal-associated protein, 23kda	1.5	5.0	0.44	2.6×10^{-2}
209392_at	*ENPP2*	Ectonucleotide pyrophosphatase/phosphodiesterase 2	1.6	2.7	0.43	2.7×10^{-2}
200974_at	*ACTA2*	Actin, alpha 2, smooth muscle, aorta	1.6	2.7	0.43	2.8×10^{-2}
210942_s_at	*ST3GAL6*	ST3 beta-galactoside alpha-2,3-sialyltransferase 6	1.5	5.0	0.42	3.3×10^{-2}
212063_at	*CD44*	CD44 molecule	1.9	3.9	0.42	3.0×10^{-2}
212515_s_at	*DDX3X*	DEAD (Asp-Glu-Ala-Asp) box polypeptide 3, X-linked	1.5	5.0	0.41	3.6×10^{-2}
211509_s_at	*RTN4*	Reticulon 4	1.6	3.9	0.41	3.7×10^{-2}
209387_s_at	*TM4SF1*	Transmembrane 4 L six family member 1	1.8	2.7	0.40	4.0×10^{-2}
219922_s_at	*LTBP3*	Latent transforming growth factor beta binding protein 3	1.5	5.0	0.40	4.3×10^{-2}
202119_s_at	*CPNE3*	Copine III	1.5	3.9	0.40	4.8×10^{-2}
210095_s_at	*IGFBP3*	Insulin-like growth factor binding protein 3	1.7	2.7	0.39	5.0×10^{-2}

[a]Relative change in expression between subjects with low ($\leq$93 g/m^2) and high ($\geq$142 g/m^2) LVM in the study population. [b]False discovery rate for differential expression, estimated by SAM analysis. [c]Data are ranked according to decreasing values of the Pearson correlation with LVM (determined noninvasively by echocardiography). [d]Empirical *P* values for the correlations were calculated by 10,000 permutations.

Yan D, Mäyränpää MI, Wong J, Perttilä J, Lehto M, Jauhiainen M, Kovanen PT, Ehnholm C, Brown AJ, Olkkonen VM. **OSBP-related protein 8 (ORP8) suppresses ABCA1 expression and cholesterol efflux from macrophages.** J Biol Chem. 2008 Jan 4;283(1):332-40. URL

ORP8 is a previously unexplored member of the family of oxysterol-binding protein-related proteins (ORP). We now report the expression pattern, the subcellular distribution, and data on the ligand binding properties and the physiological function of ORP8. ORP8 is localized in the endoplasmic reticulum (ER) via its C-terminal transmembrane span and binds 25-hydroxycholesterol, identifying it as a new ER oxysterol-binding protein. ORP8 is expressed at highest levels in macrophages, liver, spleen, kidney, and brain. Immunohistochemical analysis revealed ORP8 in the shoulder regions of human coronary atherosclerotic lesions, where it is present in CD68(+) macrophages. In advanced lesions the ORP8 mRNA was up-regulated 2.7-fold as compared with healthy coronary artery wall. Silencing of ORP8 by RNA interference in THP-1 macrophages increased the expression of ATP binding cassette transporter A1 (ABCA1) and concomitantly cholesterol efflux to lipid-free apolipoprotein A-I but had no significant effect on ABCG1 expression or cholesterol efflux to spherical high density lipoprotein HDL(2). Experiments employing an ABCA1 promoter-luciferase reporter confirmed that ORP8 silencing enhances ABCA1 transcription. The silencing effect was partially attenuated by mutation of the DR4 element in the ABCA1 promoter and synergized with that of the liver X receptor agonist

T0901317. Furthermore, inactivation of the E-box in the promoter synergized with ORP8 silencing, suggesting that the suppressive effect of ORP8 involves both the liver X receptor and the E-box functions. Our data identify ORP8 as a negative regulator of ABCA1 expression and macrophage cholesterol efflux. ORP8 may, thus, modulate the development of atherosclerosis.

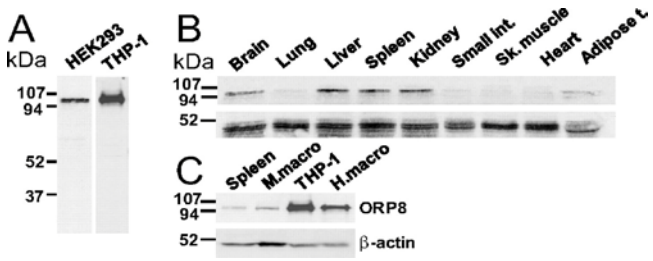

FIGURE 1. **Western analysis of ORP8 in cultured cells and mouse tissues**. **A**, characterization of the rabbit antibodies against ORP8. Total protein specimens from HEK293 cells and THP-1 macrophages (20 µg/lane) were resolved on SDS-PAGE and Western blotted using the affinity-purified anti-ORP8 antiserum. Adipose t., adipose tissue. **B**, distribution of ORP8 protein in mouse tissues. Equal amounts of total protein (20 µg/lane) from mouse tissues identified on the top were resolved by SDS-PAGE and Western blotted using affinity-purified anti-ORP8 (top panel) or monoclonal anti-β-actin (bottom panel). **C**, ORP8 protein levels in mouse peritoneal (M.macro), THP-1, and human monocyte-derived (H.macro) macrophages (20 µg/lane). A mouse spleen protein specimen is included for a comparison.

Yang H. **Nonvesicular sterol transport: two protein families and a sterol sensor?** Trends Cell Biol. 2006 Sep;16(9):427-32. URL

Sterols, essential components of eukaryotic membranes, are actively transported between cellular membranes. Although it is known that both vesicular and non-vesicular means are used to move sterols, the molecules and molecular mechanisms involved have yet to be identified. Recent studies point to a key role for oxysterol binding protein (OSBP) and its related proteins (ORPs) in nonvesicular sterol transport. Here, evidence that OSBP and ORPs are bona fide sterol carriers is discussed. In addition, I hypothesize that ATPases associated with various cellular activities regulate the recycling of soluble lipid carriers and that the Niemann Pick C1 protein facilitates the delivery of sterols from endosomal membranes to ORPs and/or the ensuing membrane dissociation of ORPs.

Im YJ, Raychaudhuri S, Prinz WA, Hurley JH. **Structural mechanism for sterol sensing and transport by OSBP-related proteins**. Nature. 2005 Sep 1;437(7055):154-8. Comment in: Mol Cell. 2005 Sep 16;19(6):722-3. URL1 and URL2

The oxysterol-binding-protein (OSBP)-related proteins (ORPs) are conserved from yeast to humans, and are implicated in the regulation of sterol homeostasis and in signal transduction pathways. Here we report the structure of the full-length yeast ORP Osh4 (also known as Kes1) at 1.5-1.9 A resolution in complexes with ergosterol, cholesterol, and 7-, 20- and 25-hydroxycholesterol. We find that a single sterol molecule binds within a hydrophobic tunnel in a manner consistent with a transport function for ORPs. The entrance is blocked by a flexible amino-terminal lid and surrounded by basic residues that are critical for Osh4 function. The structure of the open state of a lid-truncated form of Osh4 was determined at 2.5 A resolution. Structural analysis and limited proteolysis show that sterol binding closes the lid and stabilizes a conformation favouring transport across aqueous barriers and signal transmission. The structure of Osh4 in the absence of ligand exposes potential phospholipid-binding sites that are positioned for membrane docking and sterol exchange. On the basis of these observations, we propose a model in which sterol and membrane binding promote reciprocal conformational changes that facilitate a sterol transfer and signalling cycle.

Wang PY, Weng J, Anderson RG. **OSBP is a cholesterol-regulated scaffolding protein in control of ERK 1/2 activation**. Science. 2005 Mar 4;307(5714):1472-6. URL

Oxysterol-binding protein (OSBP) is the founding member of a family of sterol-binding proteins implicated in vesicle transport, lipid metabolism, and signal transduction. Here, OSBP was found to function as a cholesterol-binding scaffolding protein coordinating the activity of two phosphatases to control the extracellular signal-regulated kinase (ERK) signaling pathway. Cytosolic OSBP formed a approximately 440-kilodalton oligomer with a member of the PTPPBS family of tyrosine phosphatases, the serine/threonine phosphatase PP2A, and cholesterol. This oligomer had dual specific phosphatase activity for phosphorylated ERK (pERK). When cell cholesterol was lowered, the oligomer disassembled and the level of pERK rose. The oligomer also disassembled when exposed to oxysterols. Increasing the amount of OSBP oligomer rendered cells resistant to the effects of cholesterol depletion and decreased the basal level of pERK. Thus, cholesterol functions through its interaction with OSBP outside of membranes to regulate the assembly of an oligomeric phosphatase that controls a key signaling pathway in the cell.

Lehto M, Olkkonen VM. **The OSBP-related proteins: a novel protein family involved in vesicle transport, cellular lipid metabolism, and cell signalling**. Biochim Biophys Acta. 2003 Feb 20;1631(1):1-11. Erratum in: Biochim Biophys Acta. 2003 Apr 8;1631(3):275. URL

Proteins/genes showing high sequence homology to the mammalian oxysterol binding protein (OSBP) have been identified in a variety of eukaryotic organisms from yeast to man. The unifying feature of the gene products denoted as OSBP-related proteins (ORPs) is the presence of an OSBP-type ligand binding (LB) domain. The LB domains of OSBP and its closest homologue bind oxysterols, while data on certain other family members suggest interaction with phospholipids. Many ORPs also have a pleckstrin homology (PH) domain in the amino-terminal region. The PH domains of the family members studied in detail are known to interact with membrane phosphoinositides and play an important role in the intracellular targeting of the proteins. It is plausible that the ORPs constitute a regulatory apparatus that senses the status of specific lipid ligands in membranes, using the PH and/or LB domains, and mediates information to yet poorly known downstream machineries. Functional studies carried out on the ORP proteins in different organisms indicate roles of the gene family in diverse cellular processes including control of lipid metabolism, regulation of vesicle transport, and cell signalling events.

Anniss AM, Apostolopoulos J, Dworkin S, Purton LE, Sparrow RL. **An oxysterol-binding protein family identified in the mouse**. DNA Cell Biol. 2002 Aug;21(8):571-80. URL

Oxysterols are oxygenated derivatives of cholesterol. They have been shown to influence a variety of biological functions including sterol metabolism, lipid trafficking, and apoptosis. Recently, 12 human OSBP-related genes have been identified. In this study, we have identified a family of 12 oxysterol-binding protein (OSBP)-related proteins (ORPs) in the mouse. A high level of amino acid identity (88-97%) was determined between mouse and human ORPs, indicating a very high degree of evolutionary conservation. All proteins identified contained the conserved OSBP amino acid sequence signature motif "EQVSHHPP," and most contained a pleckstrin homology (PH) domain. Using RT-PCR, each mouse ORP gene was found to exhibit a unique tissue distribution with many showing high expression in testicular, brain, and heart tissues. Interestingly, the tissue distribution of ORP-4 and ORP-10 were the most selective within the family. Expression of the various ORP genes was also investigated, specifically in highly purified populations of hemopoietic precursor cells defined by the lin(-) c-kit(+) Sca-1(+) (LKS(+)) and lin(-) c-kit(+) Sca-1(-) (LKS(-)) immunophenotype. Most ORP genes were expressed in both LKS(+) and LKS(-) populations, although ORP-4 appeared to be more highly expressed in the primitive, stem-cell enriched LKS(+) population, whereas ORP-10 was more highly expressed by maturing LKS(-) cells. The identification of a family of ORP proteins in the mouse, the frequently preferred animal model for in vivo studies, should further our understanding of the function of these proteins and their interactions with each other.

Locus 11

Significance (based on data with full allele set): INFLATED

Top hit 1 : position chr 1:94'914'398
alleles (EMMA) # alleles 1 = 10; # alleles 2 = 5 (-> allele set is incomplete)
condition / stat iso 10, REMLt
p-value: $6.643x10^{-7}$
alleles from the Broad1 SNP set (MPD): 9 vs 5

Matching SNP with full allele set:

position chr 1: 94'893'324
alleles (EMMA) #alleles 1 =16; # alleles 2 = 6
condition / stat iso 1, REMLt
p-value: **$4.684x10^{-5}$**
alleles from the Broad1 SNP set (MPD): 15 vs 6

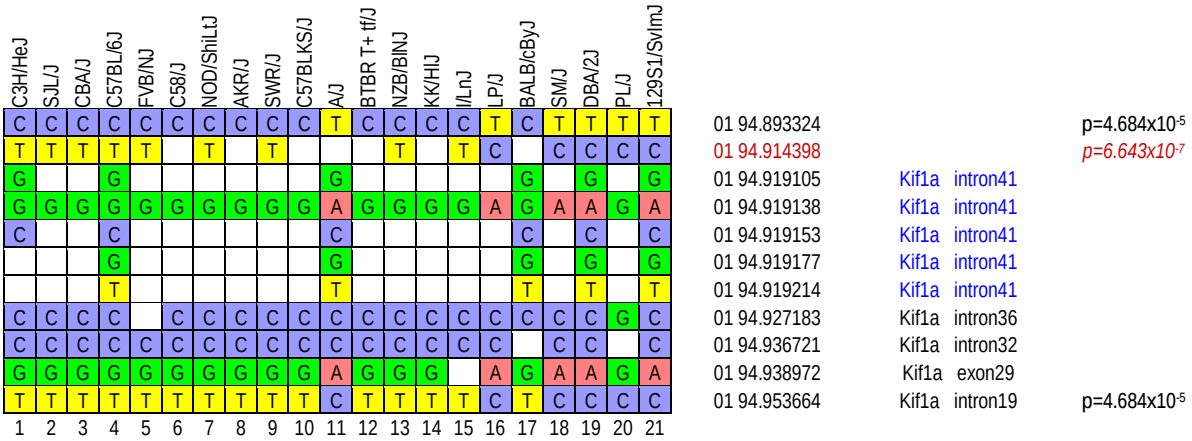

alleles from the CGD1 imputed SNP set (MPD): 16 vs 6

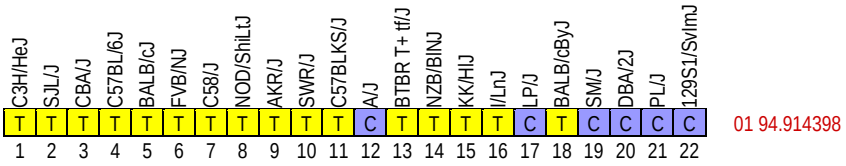

range :

Candidate gene(s), notes and bibliography:

1. ***Kif1A*** : kinesin family member 1A. Link to UCSC gene information page. Expressed mostly in the brain, mammary gland, and small intestine. Involved in axonal/synaptic vesicle transport. No indication of a link with cardiac function or localisation.

Niwa S., Tanaka Y. and Hirokawa N. **KIF1B-β and KIF1A-mediated axonal transport of presynaptic regulator Rab3 occurs in a GTP-dependent manner through DENN/MADD**. Nature Cell Biology 10, 1269 - 1279 (2008). URL

Synaptic proteins are synthesized in the cell body and transported down the axon by microtubule-dependent motors. We previously reported that KIF1B and KIF1A motors are essential for transporting synaptic vesicle precursors; however the mechanisms that regulate transport, as well as cargo recognition and control of cargo loading and unloading remain largely unknown. Here, we show that DENN/MADD (Rab3-GEP) is an essential part of the regulation mechanism through direct interaction with the stalk domain of KIF1B and KIF1A. We also show that DENN/MADD binds preferentially to GTP–Rab3 and acts as a Rab3 effector. These molecular interactions are fundamental as sequential genetic perturbations revealed that KIF1B and KIF1A are essential for the transport of DENN/MADD and Rab3, whereas DENN/MADD is essential for the transport of Rab3. GTP–Rab3 was more effectively transported than GDP–Rab3, suggesting that the nucleotide state of Rab3 regulates axonal transport of Rab3-carrying vesicles through preferential interaction with DENN/MADD.

2. ***Aqp12*** ?: aquaporin 12. Link to UCSC gene information page. Poor information on PubMed. Apparently expressed in pancreatic acinar cells (although experimental evidence does not appear so convincing, see Itoh et al. BBRC 2005).

Locus 12

Significance (based on data with full allele set): INFLATED ?

Top hit 1 : position chr 2:119'637'990
alleles (EMMA) # alleles 1 = 12; # alleles 2 = 8 (incomplete allele set)
condition / stat iso 10, REMLt
p-value: 3.255×10^{-7}
alleles from the Broad1 SNP set (MPD): 12 vs 8; there is no matching SNP with a full allele set in the vicinity

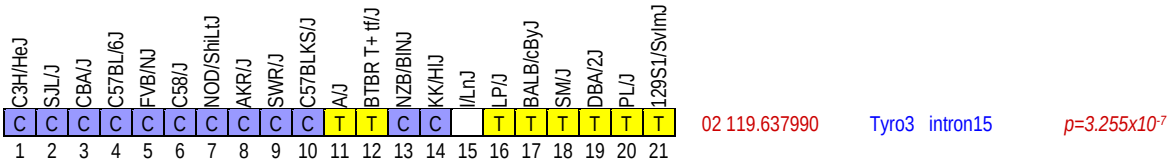

alleles from the CGD1 imputed SNP set (MPD): 12 vs 10

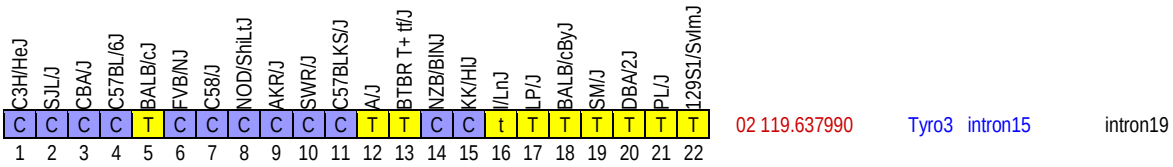

range : ca 119-121 Mb

Top hit 2 : position chr 2:120'869'441
alleles (EMMA) #alleles 1 = 13; # alleles 2 = 7 (incomplete allele set)
condition / stat iso 10, REMLt
p-value: 1.921×10^{-6}
alleles from the Broad1 SNP set (MPD): 13 vs 6; there is no matching SNP with full allele set in the vicinity

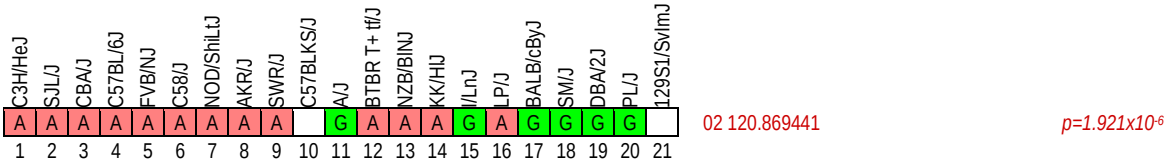

alleles from the CGD1 imputed SNP set (MPD): 15 vs 7

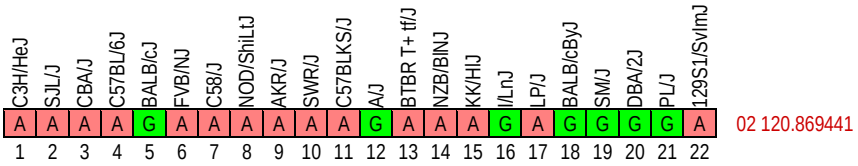

range : ca 119-121 Mb

Candidate gene(s) : there are many genes in this interval, yet the SNP SDP is complex and does not often correlate with the VWI pattern across strains (at least when considering iso 10 panels).

1. ***Tyro3*** : protein tyrosine kinase 3. Link to UCSC gene information page. There is a lot of bibliography on *Tyro3.*

Notes and bibliography:

Lemke G, Rothlin CV. **Immunobiology of the TAM receptors**. Nat Rev Immunol. 2008 May;8(5):327-36. URL

Recent studies have revealed that the TAM receptor protein tyrosine kinases--TYRO3, AXL and MER--have pivotal roles in innate immunity. They inhibit inflammation in dendritic cells and macrophages, promote the phagocytosis of apoptotic cells and membranous organelles, and stimulate the maturation of natural killer cells. Each of these phenomena may depend on a cooperative interaction between TAM receptor and cytokine receptor signalling systems. Although its importance was previously unrecognized, TAM signalling promises to have an increasingly prominent role in studies of innate immune regulation.

Rothlin CV, Ghosh S, Zuniga EI, Oldstone MB, Lemke G. **TAM receptors are pleiotropic inhibitors of the innate immune response.** Cell. 2007 Dec 14;131(6):1124-36. Comment in: Cell. 2007 Dec 14;131(6):1039-41. URL1 and URL2

The activation of Toll-like receptors (TLRs) in dendritic cells (DCs) triggers a rapid inflammatory response to pathogens. However, this response must be tightly regulated because unrestrained TLR signaling generates a chronic inflammatory milieu that often leads to autoimmunity. We have found that the TAM receptor tyrosine kinases-Tyro3, Axl, and Mer-broadly inhibit both TLR and TLR-induced cytokine-receptor cascades. Remarkably, TAM inhibition of inflammation is transduced through an essential stimulator of inflammation-the type I interferon receptor (IFNAR)-and its associated transcription factor STAT1. TLR induction of IFNAR-STAT1 signaling upregulates the TAM system, which in turn usurps the IFNAR-STAT1 cassette to induce the cytokine and TLR suppressors SOCS1 and SOCS3. These results illuminate a self-regulating cycle of inflammation, in which the obligatory, cytokine-dependent activation of TAM signaling hijacks a proinflammatory pathway to provide an intrinsic feedback inhibitor of both TLR- and cytokine-driven immune responses.

Prieto AL, O'Dell S, Varnum B, Lai C. **Localization and signaling of the receptor protein tyrosine kinase Tyro3 in cortical and hippocampal neurons**. Neuroscience. 2007 Dec 5;150(2):319-34. URL

Protein phosphorylation serves as a critical biochemical regulator of short-term and long-term synaptic plasticity. Receptor protein tyrosine kinases (RPTKs) including members of the trk, eph and erbB subfamilies have been shown to modulate signaling cascades that influence synaptic function in the central nervous system (CNS). Tyro3 is one of three RPTKs belonging to the "TAM" receptor family, which also includes Axl and Mer. Tyro3 is the most widely expressed of these receptors in the CNS. Despite recent advances suggesting roles for members of this receptor family in the reproductive and immune systems, their functions in the CNS remain largely unexplored. In an effort to elucidate the roles of Tyro3 and its ligand, the protein growth arrest-specific gene6 (Gas6) in the hippocampus and cortex, we performed a detailed study of the localization and signaling of Tyro3 polypeptides in rat hippocampal and cortical neurons. Tyro3 was readily detected in dendrites and in the soma where it was distributed in a punctate pattern. Tyro3 exhibited only a limited level of co-localization with postsynaptic density protein-95 (PSD-95), suggesting that while located within dendrites, it was not confined to the postsynaptic compartment. In addition, Tyro3 was also identified in the axons and growth cones of immature neurons. The prominent expression of Tyro3 in dendrites suggested that it may be capable of modulating signaling pathways triggered by synaptic transmission. We have provided evidence in support of this role by demonstrating that Gas6 induced the phosphorylation of Tyro3 in cortical neurons in vitro, resulting in the recruitment of the mitogen-activated protein kinase (MAPK) and the phosphoinositide-3 kinase (PI(3)K) signaling pathways. As these pathways play critical roles in the induction of hippocampal long-term potentiation (LTP), these findings suggest that Tyro3 signaling may influence synaptic plasticity in the dendritic compartment of hippocampal and cortical neurons.

Seems to be implicated in coagulation, but not clear evidence for a link with heart function, cardiac muscle, or hypertrophy.

There are several genes sharing SNP with the same SDP as at top hit position 2 (or that may share such SNPs, as full alleles sets are missing for genes with ?):

2. ***Pla2g4e*** : cytosolic phospholipase A2 epsilon. Link to UCSC gene information page. Seems to be highly expressed in skeletal muscle (in other tissues as well). There are many *pla2g4* genes... and they are not all located within the same chromosomal segment. There is a lot of bibliography on these enzymes.

   Comments and Description Text from UniProt (Swiss-Prot/TrEMBL) ID: PA24E_MOUSE
   DESCRIPTION: Cytosolic phospholipase A2 epsilon (EC 3.1.1.4) (cPLA2-epsilon) (Phospholipase A2 group IVE).
   FUNCTION: Calcium-dependent phospholipase A2 that selectively hydrolyzes glycerophospholipids in the sn-2 position.
   CATALYTIC ACTIVITY: Phosphatidylcholine + H(2)O = 1- acylglycerophosphocholine + a carboxylate.
   ENZYME REGULATION: Stimulated by cytosolic Ca(2+) (By similarity).
   SUBCELLULAR LOCATION: Cytoplasm, cytosol. Lysosome membrane; Peripheral membrane protein; Cytoplasmic side (Potential). Note=Translocates to lysosomal membranes in a calcium-dependent fashion.
   TISSUE SPECIFICITY: Predominantly expressed in heart, skeletal muscle, testis and thyroid. Expressed at lower level in brain and stomach.
   DOMAIN: The N-terminal C2 domain associates with lipid membranes and mediates its regulation by presenting the active site to its substrate in response to elevations of cytosolic Ca^{2+} (By similarity).
   SIMILARITY: Contains 1 C2 domain.
   SIMILARITY: Contains 1 PLA2c domain.

3. ***Pla2g4d*** and ***Pla2g4f*** ? phospholipase A2, group IVD (UCSC gene information) and phospholipase A2, group IVF (UCSC gene information)

Haq S, Kilter H, Michael A, Tao J, O'Leary E, Sun XM, Walters B, Bhattacharya K, Chen X, Cui L, Andreucci M, Rosenzweig A, Guerrero JL, Patten R, Liao R, Molkentin J, Picard M, Bonventre JV, Force T. **Deletion of cytosolic phospholipase A2 promotes striated muscle growth**. Nat Med. 2003 Jul;9(7):944-51. Erratum in: Nat Med. 2003 Sep;9(9):1221. URL

Generation of arachidonic acid by the ubiquitously expressed cytosolic phospholipase A2 (PLA2) has a fundamental role in the regulation of cellular homeostasis, inflammation and tumorigenesis. Here we report that cytosolic PLA2 is a negative regulator of growth, specifically of striated muscle. We find that normal growth of skeletal muscle, as well as normal and pathologic stress-induced hypertrophic growth of the heart, are exaggerated in Pla2g4a-/- mice, which lack the gene encoding cytosolic PLA2. The mechanism underlying this phenotype is that cytosolic PLA2 negatively regulates insulin-like growth factor (IGF)-1 signaling. Absence of cytosolic PLA2 leads to sustained activation of the IGF-1 pathway, which results from the failure of 3-phosphoinositide-dependent protein kinase (PDK)-1 to recruit and phosphorylate protein kinase C (PKC)-zeta, a negative regulator of IGF-1 signaling. Arachidonic acid restores activation of PKC-zeta, correcting the exaggerated IGF-1 signaling. These results indicate that cytosolic PLA2 and arachidonic acid regulate striated muscle growth by modulating multiple growth-regulatory pathways.

Ghosh M, Tucker DE, Burchett SA, Leslie CC. **Properties of the Group IV phospholipase A2 family**. Prog Lipid Res. 2006 Nov;45(6):487-510. URL

The Group IV phospholipase A2 family is comprised of six intracellular enzymes commonly called cytosolic phospholipase A2 (cPLA2) alpha, cPLA2beta, cPLA2gamma, cPLA2delta, cPLA2epsilon and cPLA2zeta. They are most homologous to phospholipase A and phospholipase B/lysophospholipases of filamentous fungi particularly in regions containing conserved residues involved in catalysis. However, a number of other serine acylhydrolases (patatin, Group VI PLA2s, Pseudomonas aeruginosa ExoU and NTE) contain the Ser/Asp catalytic dyad characteristic of Group IV PLA2s, and recent structural analysis of patatin has confirmed its structural similarity to cPLA2alpha. A characteristic of all these serine acylhydrolases is their ability to carry out multiple reactions to varying degrees (PLA2, PLA1, lysophospholipase and transacylase activities). cPLA2alpha, the most extensively studied Group IV PLA2, is widely expressed in mammalian cells and mediates the production of functionally diverse lipid products in response to extracellular stimuli. It has PLA2 and lysophospholipase activities and is the only PLA2 that has specificity for phospholipid substrates containing arachidonic acid. Because of its role in initiating agonist-induced release of arachidonic acid for the production of eicosanoids, cPLA2alpha activation is important in regulating normal and pathological processes in a variety of tissues. Current information available about the biochemical properties and tissue distribution of other Group IV PLA2s suggests they may have distinct mechanisms of regulation and functional roles.

4. ***Vps39*** ? vacuolar protein sorting 39 isoform 1. Link to UCSC gene information.

5. ***Tmem87a*** ? hypothetical protein

6. ***Ganc*** ? glucosidase, alpha; neutral C. Link to UCSC gene information.

Hirschhorn R, Huie ML, Kasper JS. Computer assisted cloning of human neutral alpha-glucosidase C (GANC): a new paralog in the glycosyl hydrolase gene family 31. Proc Natl Acad Sci U S A. 2002 Oct 15;99(21):13642-6. URL

The exponential expansion of the publicly available human DNA sequence database has increasingly facilitated cloning by homology of genes for biochemically defined, functionally similar proteins. We hypothesized that an as-yet uncloned human alpha-glucosidase (human neutral alpha-glucosidase C or GANC) is a previously uncharacterized member of a paralogous human glycosyl hydrolase gene family 31, sharing sequence homology and related, but not identical, functions with other cloned human alpha-glucosidases. We now report both the in silico and physical cloning of two alleles of human neutral alpha-glucosidase (designated GANC on the human gene map). This cloning and correct identification and annotation as GANC was successful only because of the application of the biochemical and genetic information we had previously developed regarding this gene to the results of the in silico method. Of note, this glucosidase, a member of family 31 glycosyl hydrolases, has multiple alleles, including a "null" allele and is potentially significant because it is involved in glycogen metabolism and localizes to a chromosomal region (15q15) reported to confer susceptibility to diabetes.

7. ***Capn3*** : calpain 3. Link to UCSC gene information. Highly and specifically expressed in skeletal muscle. Mutations in *Capn3* cause Limb-girdle muscular dystrophy. There is no obvious link with cardiac function / muscle. Ask Jacqui who is a specialist of this protein!

Comments and Description Text from UniProt (Swiss-Prot/TrEMBL) ID: CAN3_MOUSE
DESCRIPTION: Calpain-3 (EC 3.4.22.54) (Calpain L3) (Calpain p94) (Calcium-activated neutral proteinase 3) (CANP 3) (Muscle-specific calcium-activated neutral protease 3).
FUNCTION: Calcium-regulated non-lysosomal thiol-protease.
CATALYTIC ACTIVITY: Broad endopeptidase activity.
ENZYME REGULATION: Activated by micromolar concentrations of calcium and inhibited by calpastatin.
SUBUNIT: Interacts with TTN/titin (By similarity).
SUBCELLULAR LOCATION: Cytoplasm.
SIMILARITY: Belongs to the peptidase C2 family.
SIMILARITY: Contains 1 calpain catalytic domain.
SIMILARITY: Contains 4 EF-hand domains.

Spencer MJ, Guyon JR, Sorimachi H, Potts A, Richard I, Herasse M, Chamberlain J, Dalkilic I, Kunkel LM, Beckmann JS. **Stable expression of calpain 3 from a muscle transgene in vivo: immature muscle in transgenic mice suggests a role for calpain 3 in muscle maturation**. Proc Natl Acad Sci U S A. 2002 Jun 25;99(13):8874-9. URL

Limb-girdle muscular dystrophy, type 2A (LGMD 2A), is an autosomal recessive disorder that causes late-onset muscle-wasting, and is due to mutations in the muscle-specific protease calpain 3 (C3). Although LGMD 2A would be a feasible candidate for gene therapy, the reported instability of C3 in vitro raised questions about the potential of obtaining a stable, high-level expression of C3 from a transgene in vivo. We have generated transgenic (Tg) mice with muscle-specific overexpression of full-length C3 or C3 isoforms, which arise from alternative splicing, to test whether stable expression of C3 transgenes could occur in vivo. Unexpectedly, we found that full-length C3 can be overexpressed at high levels in vivo, without toxicity. In addition, we found that Tg expressing C3 lacking exon 6, an isoform expressed embryonically, have muscles that resemble regenerating or developing muscle. Tg expressing C3 lacking exon 15 shared this morphology in the soleus, but not other muscles. Assays of inflammation or muscle membrane damage indicated that the Tg muscles were not degenerative, suggesting that the immature muscle resulted from a developmental block rather than degeneration and regeneration. These studies show that C3 can be expressed stably in vivo from a transgene, and indicate that alternatively spliced C3 isoforms should not be used in gene-therapy applications because they impair proper muscle development.

Richard I, Roudaut C, Marchand S, Baghdiguian S, Herasse M, Stockholm D, Ono Y, Suel L, Bourg N, Sorimachi H, Lefranc G, Fardeau M, Sébille A, Beckmann JS. **Loss of calpain 3 proteolytic activity leads to muscular dystrophy and to apoptosis-associated IkappaBalpha/nuclear factor kappaB pathway perturbation in mice**. J Cell Biol. 2000 Dec 25;151(7):1583-90. URL

Calpain 3 is known as the skeletal muscle-specific member of the calpains, a family of intracellular nonlysosomal cysteine proteases. It was previously shown that defects in the human calpain 3 gene are responsible for limb girdle muscular dystrophy type 2A (LGMD2A), an inherited disease affecting predominantly the proximal limb muscles. To better understand the function of calpain 3 and the pathophysiological mechanisms of LGMD2A and also to develop an adequate model for therapy research, we generated capn3-deficient mice by gene targeting. capn3-deficient mice are fully fertile and viable. Allele transmission in intercross progeny demonstrated a statistically significant departure from Mendel's law. capn3-deficient mice show a mild progressive muscular dystrophy that affects a specific group of muscles. The age of appearance of myopathic features varies with the genetic background, suggesting the involvement of modifier genes. Affected muscles manifest a similar apoptosis-associated perturbation of the IkappaBalpha/nuclear factor kappaB pathway as seen in LGMD2A patients. In addition, Evans blue staining of muscle fibers reveals that the pathological process due to calpain 3 deficiency is associated with membrane alterations.

Richard I, Broux O, Allamand V, Fougerousse F, Chiannilkulchai N, Bourg N, Brenguier L, Devaud C, Pasturaud P, Roudaut C, et al. **Mutations in the proteolytic enzyme calpain 3 cause limb-girdle muscular dystrophy type 2A**. Cell. 1995 Apr 7;81(1):27-40. URL

Limb-girdle muscular dystrophies (LGMDs) are a group of inherited diseases whose genetic etiology has yet to be elucidated. The autosomal recessive forms (LGMD2) constitute a genetically heterogeneous group with LGMD2A mapping to chromosome 15q15.1-q21.1. The gene encoding the muscle-specific calcium-activated neutral protease 3 (CANP3) large subunit is located in this region. This cysteine protease belongs to the family of intracellular calpains. Fifteen nonsense, splice site, frameshift, or missense calpain mutations cosegregate with the disease in LGMD2A families, six of which were found within La Réunion island patients. A digenic inheritance model is proposed to account for the unexpected presence of multiple independent mutations in this small inbred population. Finally, these results demonstrate an enzymatic rather than a structural protein defect causing a muscular dystrophy, a defect that may have regulatory consequences, perhaps in signal transduction.

8. ***Zfp106*** : SH3-domain binding protein 3. Link to UCSC gene information.

Comments and Description Text from UniProt (Swiss-Prot/TrEMBL) ID: ZF106_MOUSE
DESCRIPTION: Zinc finger protein 106 (Zfp-106) (Zinc finger protein 474) (H3a minor histocompatibility antigen) (Son of insulin receptor mutant).
FUNCTION: May play a role in modulating tissue specificity to insulin (isoform 3).
SUBUNIT: Interacts with TSG118. Isoform 3 interacts with the SH3 domains of FYN and GRB2.
SUBCELLULAR LOCATION: Nucleus, nucleolus.
SUBCELLULAR LOCATION: Isoform 3: Cytoplasm.
TISSUE SPECIFICITY: Widely expressed, including lymphocytes. Isoform 3 is most abundant in insulin-sensitive tissues such as skeletal muscle, heart, fat, kidney and liver.
INDUCTION: Expression is regulated by insulin (isoform 3).
PTM: Phosphorylated upon DNA damage, probably by ATM or ATR (By similarity).
SIMILARITY: Contains 3 C2H2-type zinc fingers.
SIMILARITY: Contains 6 WD repeats.
SEQUENCE CAUTION: Sequence=AAB96870.1; Type=Frameshift; Positions=805, 816

Zuberi AR, Christianson GJ, Mendoza LM, Shastri N, Roopenian DC. **Positional cloning and molecular characterization of an immunodominant cytotoxic determinant of the mouse H3 minor histocompatibility complex**. Immunity. 1998 Nov;9(5):687-98. URL

Immune responses to minor histocompatibility antigens are poorly understood and present substantial barriers to successful solid tissue and bone marrow transplantation among MHC-matched individuals. We exploited a unique positional cloning approach relying on the potent negative selection capability of cytotoxic T cells to identify the H3a gene responsible for immunodominant H2-Db-restricted determinants of the classically defined mouse autosomal H3 complex. The allelic basis for reciprocal H3a

antigens is two amino acid changes within a single nonamer H2-Db-binding peptide. The H3a gene, now called Zfp106, encodes a 1888-amino acid protein with three zinc fingers and a beta-transducin domain consistent with DNA/protein binding. A region of ZFP106 is identical to a 600-amino acid sequence implicated in the insulin receptor signaling pathway.

9. ***Snap23*** : synaptosomal-associated protein 23. Link to UCSC gene information. Expressed in non-neuronal tissues.

Boström P, Andersson L, Rutberg M, Perman J, Lidberg U, Johansson BR, Fernandez-Rodriguez J, Ericson J, Nilsson T, Borén J, Olofsson SO. SNARE proteins mediate fusion between cytosolic lipid droplets and are implicated in insulin sensitivity. Nat Cell Biol. 2007 Nov;9(11):1286-93. Comment in: Nat Cell Biol. 2007 Nov;9(11):1219-20. URL1 and URL2

The accumulation of cytosolic lipid droplets in muscle and liver cells has been linked to the development of insulin resistance and type 2 diabetes. Such droplets are formed as small structures that increase in size through fusion, a process that is dependent on intact microtubules and the motor protein dynein. Approximately 15% of all droplets are involved in fusion processes at a given time. Here, we show that lipid droplets are associated with proteins involved in fusion processes in the cell: NSF (N-ethylmaleimide-sensitive-factor), alpha-SNAP (soluble NSF attachment protein) and the SNAREs (SNAP receptors), SNAP23 (synaptosomal-associated protein of 23 kDa), syntaxin-5 and VAMP4 (vesicle-associated membrane protein 4). Knockdown of the genes for SNAP23, syntaxin-5 or VAMP4, or microinjection of a dominant-negative mutant of alpha-SNAP, decreases the rate of fusion and the size of the lipid droplets. Thus, the SNARE system seems to have an important role in lipid droplet fusion. We also show that oleic acid treatment decreases the insulin sensitivity of heart muscle cells, and this sensitivity is completely restored by transfection with SNAP23. Thus, SNAP23 might be a link between insulin sensitivity and the inflow of fatty acids to the cell.

10. ***Cep27*** : centrosomal protein 27. Link to UCSC gene information. No entry in PubMed

11. ***Lrrc57*** : leucine rich repeat containing 57. Link to UCSC gene information. No entry in PubMed

12. ***Stard9*** : motor domain of KIF16A (fragment). Link to UCSC gene information.

13. ***Ubr1*** : ubiquitin protein ligase E3 component n-recognin. Link to UCSC gene information.

An JY, Seo JW, Tasaki T, Lee MJ, Varshavsky A, Kwon YT. **Impaired neurogenesis and cardiovascular development in mice lacking the E3 ubiquitin ligases UBR1 and UBR2 of the N-end rule pathway**. Proc Natl Acad Sci U S A. 2006 Apr 18;103(16):6212-7. URL

The N-end rule relates the in vivo half-life of a protein to the identity of its N-terminal residue. A subset of degradation signals recognized by the N-end rule pathway comprises the signals, called N-degrons, whose determinants include destabilizing N-terminal residues. Our previous work identified a family of at least four mammalian E3 ubiquitin ligases, including UBR1 and UBR2, that share the UBR box and recognize N-degrons. These E3 enzymes mediate the multifunctional N-end rule pathway, but their individual roles are just beginning to emerge. Mutations of UBR1 in humans are the cause of Johanson-Blizzard syndrome. UBR1 and UBR2 are 46% identical and appear to be indistinguishable in their recognition of N-degrons. UBR1-/- mice are viable but have defects that include pancreatic insufficiency, similarly to UBR1-/- human patients with Johanson-Blizzard syndrome. UBR2-/- mice are inviable in some strain backgrounds and are defective in male meiosis. To examine functional relationships between UBR1 and UBR2, we constructed mouse strains lacking both of these E3s. We report here that UBR1-/-UBR2-/- embryos die at midgestation, with defects in neurogenesis and cardiovascular development. These defects included reduced proliferation as well as precocious migration and differentiation of neural progenitor cells. The expression of regulators such as D-type cyclins and Notch1 was also altered in UBR1-/-UBR2-/- embryos. We conclude that the functions of UBR1 and UBR2 are significantly divergent, in part because of differences in their expression patterns and possibly also because of differences in their recognition of protein substrates that contain degradation signals other than N-degrons.

Zenker M, Mayerle J, Lerch MM, Tagariello A, Zerres K, Durie PR, Beier M, Hülskamp G, Guzman C, Rehder H, Beemer FA, Hamel B, Vanlieferinghen P, Gershoni-Baruch R, Vieira MW, Dumic M, Auslender R, Gil-da-Silva-Lopes VL, Steinlicht S, Rauh M, Shalev SA, Thiel C, Ekici AB, Winterpacht A, Kwon YT, Varshavsky A, Reis A. **Deficiency of UBR1, a ubiquitin ligase of the N-end rule pathway, causes pancreatic dysfunction, malformations and mental retardation (Johanson-Blizzard syndrome).** Nat Genet. 2005 Dec;37(12):1345-50. URL

Johanson-Blizzard syndrome (OMIM 243800) is an autosomal recessive disorder that includes congenital exocrine pancreatic insufficiency, multiple malformations such as nasal wing aplasia, and frequent mental retardation. We mapped the disease-associated locus to chromosome 15q14-21.1 and identified mutations, mostly truncating ones, in the gene UBR1 in 12 unrelated families with Johanson-Blizzard syndrome. UBR1 encodes one of at least four functionally overlapping E3 ubiquitin ligases of the N-end rule pathway, a conserved proteolytic system whose substrates include proteins with destabilizing N-terminal residues. Pancreas of individuals with Johanson-Blizzard syndrome did not express UBR1 and had intrauterine-onset destructive pancreatitis. In addition, we found that Ubr1(-/-) mice, whose previously reported phenotypes include reduced weight and behavioral abnormalities, had an exocrine pancreatic insufficiency, with impaired stimulus-secretion coupling and increased susceptibility to pancreatic injury. Our findings indicate that deficiency of UBR1 perturbs the pancreas' acinar cells and other organs, presumably owing to metabolic stabilization of specific substrates of the N-end rule pathway.

14. ***Tmem62*** : transmembrane protein 62. Link to UCSC gene information. No entry in PubMed

15. ***Ccndbp1*** : cyclin D-type binding-protein 1. Link to UCSC gene information.

Comments and Description Text from UniProt (Swiss-Prot/TrEMBL) ID: CCDB1_MOUSE

DESCRIPTION: Cyclin-D1-binding protein 1 (Grap2 and cyclin-D-interacting protein) (Maternal Id-like protein) (Stage specific embryonic cDNA-8 protein) (SSEC-8).
FUNCTION: May negatively regulate cell cycle progression. May act at least in part via inhibition of the cyclin-D1/CDK4 complex, thereby preventing phosphorylation of RB1 and blocking E2F- dependent transcription (By similarity). May be required for hepatocyte proliferation.
SUBUNIT: Interacts with CCND1 and GRAP2 (By similarity). May also interact with COPS5, RPLP0, SIRT6, SYF2 and TCF3 (By similarity).
SUBCELLULAR LOCATION: Cytoplasm (By similarity). Nucleus (By similarity).
TISSUE SPECIFICITY: Expressed at high levels in brain, intestine, muscle and ovary and at lower levels in heart, kidney, liver, lung, spleen and testis.
DEVELOPMENTAL STAGE: Highly expressed in the unfertilized egg. Expression is reduced at the two cell and blastocyst stages. Expressed in the liver, CNS and dorsal root ganglia throughout organogenesis. Also expressed in the intestine, kidney, lung, nasal cavities and thymus from E13.
INDUCTION: Expression is induced by partial hepatectomy.
PTM: Phosphorylated (By similarity).
SIMILARITY: Belongs to the CCNDBP1 family.
SEQUENCE CAUTION: Sequence=AAB58118.1; Type=Frameshift; Positions=275, 278, 286

16. ***Epb4.2*** : erythrocyte protein band 4.2. Link to UCSC gene information. Highly expressed in bone and bone marrow.

17. ***Tgm5*** : transglutaminase 5. Link to UCSC gene information.

Locus 13

Significance (based on data with full allele set): INFLATED ?

Top hit 1 : position chr 5:104'572'764
alleles (EMMA) # alleles 1 = 15; # alleles 2 = 5 (-> allele set is not complete)
condition / stat iso 10, REMLt
p-value: $8.03x10^{-7}$
alleles from the Broad1 SNP set (MPD): 16 vs 5; this SNP is absent from the CGD1 imputed set. Moreover, there are lots of missing alleles around this region in the CGD1 set.

Top hit 2 : position chr 5:104'515'280
alleles (EMMA) #alleles 1 = 17; # alleles 2 = 4
condition / stat iso 10, REMLt
p-value: $5.597x10^{-6}$
alleles from the Broad1 SNP set (MPD): 16 vs 4; there is no matching SNP with a full allele set in the vicinity

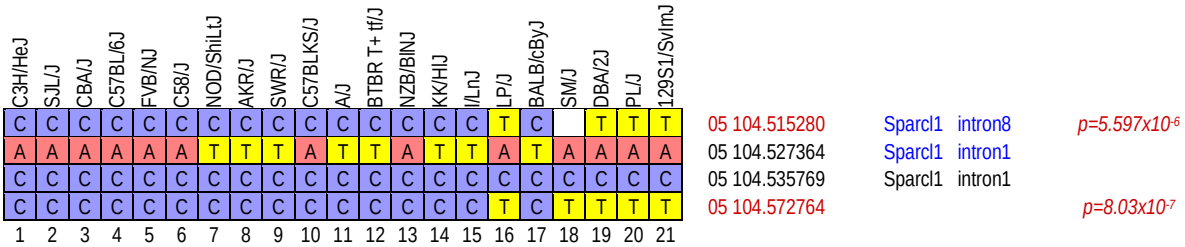

alleles from the CGD1 imputed SNP set (MPD): 15 vs 5

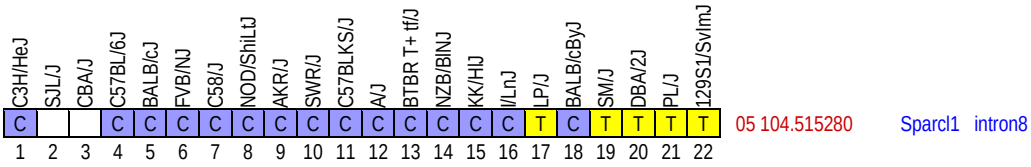

range : ca 104-105 Mb

Candidate gene(s) :

1. ***Sparcl1*** : SPARC-like 1 (mast9, hevin). Link to UCSC gene information. Protein of the ECM. SPARC-like protein 1 (SPARCL1), a member of the SPARC family, is downregulated in various tumors. Of note, the analogue *Sparc* (osteonectin) was identified as a *cis*-eQTL associated with indexed cardiac mass in the rat by Petretto et al (see Table and ref below). There is experimental evidence for a link between Sparc and cardiac hypertrophy. KO-mice exist (see below)

Petretto E, Sarwar R, Grieve I, Lu H, Kumaran MK, Muckett PJ, Mangion J, Schroen B, Benson M, Punjabi PP, Prasad SK, Pennell DJ, Kiesewetter C, Tasheva ES, Corpuz LM, Webb MD, Conrad GW, Kurtz TW, Kren V, Fischer J, Hubner N, Pinto YM, Pravenec M, Aitman TJ, Cook SA. **Integrated genomic approaches implicate osteoglycin (*Ogn*) in the regulation of left ventricular mass**. Nat Genet. 2008 May;40(5):546-52. URL

Left ventricular mass (LVM) and cardiac gene expression are complex traits regulated by factors both intrinsic and extrinsic to the heart. To dissect the major determinants of LVM, we combined expression quantitative trait locus1 and quantitative trait transcript (QTT) analyses of the cardiac transcriptome in the rat. Using these methods and in vitro functional assays, we identified osteoglycin (*Ogn*) as a major candidate regulator of rat LVM, with increased Ogn protein expression associated with elevated LVM. We also applied genome-wide QTT analysis to the human heart and observed that, out of 22,000 transcripts, *OGN* transcript abundance had the highest correlation with LVM. We further confirmed a role for *Ogn* in the in vivo regulation of LVM in *Ogn* knockout mice. Taken together, these data implicate *Ogn* as a key regulator of LVM in rats, mice and humans, and suggest that *Ogn* modifies the hypertrophic response to extrinsic factors such as hypertension and aortic stenosis.

Probeset Id	Gene Symbol[1]	Chr	P_{GW}	FDR (%)	LOD score	Fold change[2]	Cardiac mass QTLs[3]
1376780_at	*Fam103a1**	1	1.9E-04	0.9%	9.2	1.7	Cm16 / Cm23
1393508_at	*Nox4*	1	7.0E-06	0.4%	7.8	1.8	Cm16 / Cm23
1371615_at	*Dgat2*	1	1.1E-03	3.0%	5.6	1.6	Cm23
1370334_at	*Plekhb1*	1	3.2E-04	1.2%	6.7	1.7	Cm23
1373541_at	*Arhgef17_predicted*	1	1.4E-05	0.4%	8.6	-1.5	Cm23
1394160_at	*Tmem2_predicted*	1	5.5E-05	0.5%	9.7	-1.6	Siegel et al (2003)
1392972_at	*Trio*	2	1.0E-06	0.4%	17.8	3.9	Cm22
1389580_at	*Smarca3_predicted*	2	7.7E-04	2.4%	7.0	-2.0	Cm22
1395073_at	*Evi1*	2	5.2E-05	0.5%	9.4	-1.7	Cm22
1398471_at	*Cog6*	2	2.5E-05	0.4%	11.0	-1.7	Cm22
1368637_at	*Card9*	3	1.9E-05	0.4%	11.4	12.1	Cm10 / Garrett et al (2003)
1388912_at	*Rexo4*	3	1.0E-06	0.4%	13.1	-1.8	Cm10 / Garrett et al (2003)
1389816_at	*Endog*	3	3.0E-06	0.4%	19.5	-3.9	Cm10 / Garrett et al (2003)
1382984_at	*Tor1b*	3	1.0E-06	0.4%	18.6	1.9	Cm10 / Garrett et al (2003)
1390236_at	*Hmcn2**	3	5.4E-05	0.5%	6.5	1.9	Cm10 / Garrett et al (2003)
1385314_at	*Rab14*	3	1.0E-06	0.4%	17.0	3.0	Cm10 / Garrett et al (2003)
1376796_at	*Rab14*	3	1.7E-05	0.4%	10.3	1.8	Cm10 / Garrett et al (2003)
1393795_at	*Zfhx1b*	3	1.0E-06	0.4%	11.0	-1.9	Cm10 / Garrett et al (2003)
1393689_at	*Ndufaf1_predicted*	3	3.4E-05	0.4%	9.9	-2.0	Cm28
1389142_at	*Sqrdl**	3	9.2E-05	0.6%	8.5	-1.8	Cm28
1387170_at	*Csnk2a1*	3	6.7E-04	2.1%	7.2	1.6	Bp81
1369415_at	*Bhlhb2*	4	5.9E-04	2.0%	7.1	1.8	Cm18 / Cm54
1383474_at	*Irak2*	4	4.4E-04	1.6%	7.8	-2.2	Cm18 / Cm54
1373510_at	*Vamp1*	4	1.1E-04	0.7%	7.3	1.7	Cm18
1388687_at	*Dhdds*	5	5.3E-05	0.5%	7.7	1.8	Cm24
1380813_at	*Sdhb_predicted*	5	3.9E-05	0.4%	11.6	3.0	Cm24
1373567_at	*Tle6**	7	1.2E-03	3.2%	5.8	1.5	Cm6
1382763_at	*LOC691921*	7	2.0E-03	4.3%	6.6	2.0	Cm6
1386941_at	*Plec1*	7	2.0E-03	4.3%	6.3	1.7	Cm27
1398844_at	*Txn2*	7	6.6E-05	0.5%	7.6	-1.6	Cm27
1370881_at	*Tst*	7	2.0E-05	0.4%	7.7	1.7	Cm27
1390185_at	*Dcps*	8	3.0E-04	1.2%	8.3	-1.8	Kren et al (1997) / Cm3
1390185_at	*Dcps*	8	3.0E-04	1.2%	8.3	-1.8	Kren et al (1997) / Cm3
1372370_at	*Rpusd4*	8	1.6E-04	0.8%	8.3	1.6	Kren et al (1997) / Cm3
1372370_at	*Rpusd4*	8	1.6E-04	0.8%	8.3	1.6	Kren et al (1997) / Cm3
1371442_at	*Hyou1*	8	5.3E-05	0.5%	6.7	-1.7	Kren et al (1997) / Cm3
1389229_at	*Acpl2**	8	9.2E-04	2.7%	6.1	1.6	Cm2 / Cm19
1373887_at	*Sf3b1*	9	8.0E-05	0.5%	9.3	1.6	Cm28 / Cm11
1370176_at	*Trak2*	9	2.0E-06	0.4%	18.5	2.5	Cm28 / Cm11
1374196_at	*Lancl1*	9	2.9E-05	0.4%	11.4	-1.9	Cm28 / Cm11
1395354_at	*Lancl1*	9	1.7E-04	0.8%	8.5	-1.9	Cm28 / Cm11
1368127_at	*Neu2*	9	6.1E-04	2.0%	6.8	-1.5	Cm21
1368574_at	*Adra1b*	10	1.0E-06	0.4%	10.2	1.8	Cm50
1380407_at	*Kct2**	10	2.0E-06	0.4%	13.1	1.8	Cm50
1383894_at	*Fnip1*	10	6.0E-06	0.4%	9.0	1.8	Cm50
1367562_at	*Sparc*	10	8.5E-05	0.6%	7.0	1.6	Cm50
1391743_at	*Elavl1_predicted*	12	2.0E-06	0.4%	15.6	-2.3	Hamet et al (1996)
1391072_at	*Fcer2a*	12	8.3E-05	0.6%	8.2	1.8	Hamet et al (1996)
1380651_at	*Rnf6_predicted*	12	1.8E-04	0.8%	8.4	1.9	Hamet et al (1996) / Cm56
1378150_at	*Card11*	12	1.7E-03	4.1%	6.5	-1.5	Hamet et al (1996)
1376688_a_at	*Pilra**	12	1.6E-04	0.8%	6.0	1.8	Hamet et al (1996)
1383371_at	*Srcrb4d_predicted*	12	6.3E-04	2.0%	8.3	-1.9	Hamet et al (1996)
1383481_at	*Auts2_predicted*	12	8.8E-05	0.6%	8.0	1.6	Hamet et al (1996)
1390701_at	*MGC94190*	12	1.0E-04	0.6%	9.0	1.5	Hamet et al (1996)
1395393_at	*RGD1563482_predicted*	12	5.9E-04	2.0%	7.5	-1.5	Hamet et al (1996) / Cm5
1381386_at	*Pop5_predicted*	12	8.6E-05	0.6%	9.1	-2.0	Cm5
1392590_at	*Arhgap24*	14	2.6E-04	1.0%	7.6	-1.6	Clark et al (1996)
1368248_at	*Cds1*	14	6.0E-05	0.5%	9.2	-2.0	Clark et al (1996)
1388603_a_at	*Hbld2*	17	8.5E-04	2.5%	7.6	-3.1	Pravenec et al (1995) / this report
1376749_at	*Ogn*	17	1.7E-03	4.1%	6.0	2.7	Pravenec et al (1995) / this report
1383263_at	*Ogn*	17	1.3E-03	3.2%	6.3	2.5	Pravenec et al (1995) / this report
1388617_at	*Bphl*	17	2.0E-06	0.4%	14.9	1.9	Cm55
1375003_at	*Serpinb6a*	17	1.0E-06	0.4%	14.8	-1.7	Cm55
1380833_at	*Gpld1*	17	5.0E-06	0.4%	7.9	1.5	Cm55
1372000_at	*Net1*	17	1.6E-04	0.8%	7.2	1.7	Cm26
1391256_at	*Rpp38*	17	1.7E-03	4.1%	6.4	-1.8	Cm26
1371985_a_at	*Bat5*	20	1.0E-04	0.6%	9.0	2.3	Kunes et al (1990)
1381593_x_at	*RT1-Ba*	20	2.2E-05	0.4%	10.8	-9.4	Kunes et al (1990)
1392334_at	*RT1-Ba*	20	2.2E-05	0.4%	10.3	-6.6	Kunes et al (1990)
1371033_at	*RT1-Bb*	20	5.3E-05	0.5%	7.5	-3.7	Kunes et al (1990)
1370428_x_at	*RT1-A3*	20	7.0E-05	0.5%	9.8	-16.3	Kunes et al (1990)
1369667_at	*Vps52*	20	1.4E-04	0.8%	8.1	1.7	Kunes et al (1990)
1368597_at	*Snf1lk*	20	7.8E-05	0.5%	8.5	-1.9	Kunes et al (1990)
1374916_at	*Pwp2*	20	2.1E-04	1.0%	8.8	-1.8	Kunes et al (1990)
1371988_at	*Man1a_predicted*	20	2.2E-03	4.8%	5.0	1.6	Kunes et al (1990)
1369640_at	*Gja1*	20	1.0E-03	2.7%	6.8	-2.1	Kunes et al (1990)

Supplementary Table 2. **Cis -eQTLs detected with FDR≤ 5%, an absolute fold change > 1.5 at the peak of linkage by parental genotype, and that co-localize with cardiac mass QTLs** (i.e., between genetic markers at the extremes of the QTL region as defined in the Rat Genome Database, http://rgd.mcw.edu/) that have been mapped in the SHR or BN strain crosses (Supplementary Table 3).

Nie J, Sage EH. **SPARC inhibits adipogenesis by its enhancement of beta-catenin signaling**. J. Biol. Chem, 10.1074/jbc.M808285200, 2008. URL

SPARC (Secreted Protein Acidic and Rich in Cysteine) modulates interactions between cells and extracellular matrix and is enriched in white adipose tissue. We have reported that SPARC-null mice accumulate significantly more fat than wild-type mice and maintain relatively high levels of serum leptin. We now show that SPARC inhibits adipogenesis in vitro. Specifically, recombinant SPARC inhibited a) adipocyte differentiation of stromal-vascular cells isolated from murine white adipose tissue, and b) the expression of adipogenic transcription factors and adipocyte-specific genes. SPARC induced the accumulation and nuclear translocation of -catenin, and subsequently enhanced the interaction of -catenin and T cell/lymphoid enhancer factor 1. The activity of integrin-linked kinase was required for the effect of SPARC on -catenin accumulation, as well as ECM remodeling. During adipogenesis, fusiform preadipocytes change into sphere-shaped adipocytes and convert the extracellular matrix from a fibronectin-rich stroma to a laminin-rich basal lamina. SPARC retarded the morphological changes exhibited by preadipocytes during differentiation. In the presence of SPARC, the deposition of fibronectin was enhanced and that of laminin was inhibited; in parallel, the expression of 5 integrin was enhanced and that of 6 integrin was inhibited. Lithium chloride, which enhances the accumulation of -catenin, also inhibited the expression of 6 integrin. These findings demonstrate a role for SPARC in adipocyte morphogenesis and in signaling processes leading to terminal differentiation.

Sullivan MM, Sage EH. **Hevin/SC1, a matricellular glycoprotein and potential tumor-suppressor of the SPARC/BM-40/Osteonectin family**. Int J Biochem Cell Biol. 2004 Jun;36(6):991-6. URL

Hevin is an extracellular matrix-associated, secreted glycoprotein belonging to the secreted protein acidic and rich in cysteine (SPARC) family of matricellular proteins. It contains three conserved structural domains that are implicated in the regulation of cell adhesion, migration, and proliferation. Hevin is expressed during embryogenesis and tissue remodeling and is especially prominent in brain and vasculature. Its down-regulation in a number of cancers and the possibility of its functional compensation by SPARC has led to recent interest in hevin as a tumor suppressor and regulator of angiogenesis

Stary M, Pasteiner W, Summer A, Hrdina A, Eger A, Weitzer G. **Parietal endoderm secreted SPARC promotes early cardiomyogenesis in vitro**. Exp Cell Res. 2005 Nov 1;310(2):331-43. URL

Cardiomyogenesis proceeds in the presence of signals emanating from extra-embryonic lineages emerging before and during early eutherian gastrulation. In embryonic stem cell derived embryoid bodies, primitive endoderm gives rise to visceral and parietal endoderm. Parietal endoderm undergoes an epithelial to mesenchymal transition shortly before first cardiomyocytes start to contract rhythmically. Here, we demonstrate that Secreted Protein, Acidic, Rich in Cysteine, SPARC, predominantly secreted by mesenchymal parietal endoderm specifically promotes early myocardial cell differentiation in embryoid bodies. SPARC enhanced the expression of bmp2 and nkx2.5 in embryoid bodies and fetal cardiomyocytes. Inhibition of either SPARC or Bmp2 attenuated in both cases cardiomyogenesis and downregulated nkx2.5 expression. Thus, SPARC directly affects cardiomyogenesis, modulates Bmp2 signaling, and contributes to a positive autoregulatory loop of Bmp2 and Nkx2.5 in cardiomyocytes.

Chen H, Huang XN, Stewart AF, Sepulveda JL. **Gene expression changes associated with fibronectin-induced cardiac myocyte hypertrophy.** Physiol Genomics. 2004 Aug 11;18(3):273-83. URL

Fibronectin (FN) is an extracellular matrix protein that binds to integrin receptors and couples cardiac myocytes to the basal lamina. Cardiac FN expression is elevated in models of pressure overload, and FN causes cultured cardiac myocytes to hypertrophy by a mechanism that has not been characterized in detail. In this study, we analyzed the gene expression changes induced by FN in purified rat neonatal ventricular myocytes using the Affymetrix RAE230A microarray, to understand how FN affects gene expression in cardiac myocytes and to separate the effects contributed by cardiac nonmyocytes in vivo. Pathway analysis using z-score statistics and comparison with a mouse model of cardiac hypertrophy revealed several pathways stimulated by FN in cardiac myocytes. In addition to the known cardiac myocyte hypertrophy markers, FN significantly induced metabolic pathways including virtually all of the enzymes of cholesterol biosynthesis, fatty acid biosynthesis, and the mitochondrial electron transport chain. FN also increased the expression of genes coding for ribosomal proteins, translation factors, and the ubiquitin-proteasome pathway. Interestingly, cardiac myocytes plated on FN showed elevated expression of the fibrosis-promoting peptides connective tissue growth factor (CTGF), WNT1 inducible signaling pathway protein 2 (WISP2), and secreted acidic cysteine-rich glycoprotein (SPARC). Our data complement in vivo studies and reveal several novel genes and pathways stimulated by FN, pointing to cardiac myocyte-specific mechanisms that lead to development of the hypertrophic phenotype.

Bradshaw AD, Graves DC, Motamed K, Sage EH. **SPARC-null mice exhibit increased adiposity without significant differences in overall body weight.** Proc Natl Acad Sci U S A. 2003 May 13;100(10):6045-50. URL

Secreted protein acidic and rich in cysteine/osteonectin/BM-40 (SPARC) is a matrix-associated protein that elicits changes in cell shape, inhibits cell-cycle progression, and influences the synthesis of extracellular matrix (ECM). The absence of SPARC in mice gives rise to aberrations in the structure and composition of the ECM that result in generation of cataracts, development of severe osteopenia, and accelerated closure of dermal wounds. In this report we show that SPARC-null mice have greater deposits of s.c. fat and larger epididymal fat pads in comparison with wild-type mice. Similar to earlier studies of SPARC-null dermis, we observed a reduction in collagen I in SPARC-null fat pads in comparison with wild-type. Although elevated levels of serum leptin were observed in SPARC-null mice, their overall body weights were not significantly different from those of wild-type counterparts. The diameters of adipocytes from SPARC-null versus wild-type epididymal fat pads were 252 +/- 61 and 161 +/- 33 microm (means +/- SD), respectively, and there was an increase in adipocyte number within SPARC-null fat pads in comparison with wild-type pads. Thus the absence of SPARC appears to result in an increase in the size of individual adipocytes as well as an increase in the number of adipocytes per fat pad. In fat pads isolated from wild-type mice, SPARC mRNA was associated with both the stromal/vascular and adipocyte fractions. We propose that SPARC limits the accumulation of adipose tissue in mice in part through its demonstrated effects on the regulation of cell shape and production of ECM.

Ihara Y, Suzuki YJ, Kitta K, Jones LR, Ikeda T. **Modulation of gene expression in transgenic mouse hearts overexpressing calsequestrin. Cell Calcium**. 2002 Jul;32(1):21-9. URL

Calsequestrin (CSQ) is the major Ca2+ binding protein of the cardiac sarcoplasmic reticulum (SR). Transgenic mice overexpressing CSQ at the age of 7 weeks exhibit concentric cardiac hypertrophy, and by 13 weeks the condition progresses to

dilated cardiomyopathy. The present study used a differential display analysis to identify genes whose expressions are modulated in the CSQ-overexpressing mouse hearts to provide information on the mechanism of transition from concentric cardiac hypertrophy to failure. Cardiac ankyrin repeat protein (CARP), glutathione peroxidase (Gpx1), and genes which participate in the formation of extracellular matrix including decorin, TSC-36, Magp2, Osf2, and SPARC are upregulated in CSQ mouse hearts at 7 and 13 weeks of age compared to those of non-transgenic littermates. In addition, two novel genes without sequence similarities to any known genes are upregulated in CSQ-overexpressing mouse hearts. Several genes are downregulated at 13 weeks, including SR Ca2+-ATPase (SERCA2) and adenine nucleotide translocase 1 (Ant1) genes. Further, a functionally yet unknown gene (NM_026586) previously identified in the mouse wolffian duct is dramatically downregulated in CSQ mice with dilated hearts. Thus, CARP, Gpx1, and genes encoding extracellular matrix proteins may participate in the development of cardiac hypertrophy and fibrosis, and changes in SERCA2, Ant1, and NM_026586 mRNA expression may be involved in transition from concentric to dilated cardiac hypertrophy.

McKinnon PJ, McLaughlin SK, Kapsetaki M, Margolskee RF. **Extracellular Matrix-Associated Protein Sc1 Is Not Essential for Mouse Development**. Mol Cell Biol. 2000 January; 20 (2): 656-660. URL

Sc1 is an extracellular matrix-associated protein whose function is unknown. During early embryonic development, Sc1 is widely expressed, and from embryonic day 12 (E12), Sc1 is expressed primarily in the developing nervous system. This switch in Sc1 expression at E12 suggests an importance for nervous-system development. To gain insight into Sc1 function, we used gene targeting to inactivate mouse Sc1. The Sc1-null mice showed no obvious deficits in any organs. These mice were born at the expected ratios, were fertile, and had no obvious histological abnormalities, and their long-term survival did not differ from littermate controls. Therefore, the function of Sc1 during development is not critical or, in its absence, is subserved by another protein.

Masson S, Arosio B, Luvarà G, Gagliano N, Fiordaliso F, Santambrogio D, Vergani C, Latini R, Annoni G. **Remodelling of cardiac extracellular matrix during beta-adrenergic stimulation: upregulation of SPARC in the myocardium of adult rats**. J Mol Cell Cardiol. 1998 Aug;30(8):1505-14. URL

Our objectives were (i) to evaluate the expression of several genes involved in the remodelling of cardiac extracellular matrix (ECM), with a special interest on SPARC (secreted protein acidic and rich in cysteine) a glycoprotein with anti-adhesive properties, and (ii) to characterise structural changes in the left (LV) and right (RV) ventricles of rats subjected to continuous beta-adrenergic stimulation. The rats were infused for 3 or 7 days with isoproterenol (ISO, 4 mg/kg/day) or vehicle. Hybridisation analysis was done for SPARC, atrial natriuretic peptide (ANP),alpha2 (I) [COL-I] and alpha1 (III) [COL-III] procollagens, TGF-beta1 and TGF-beta3 mRNA content. Interstitial and perivascular collagen deposition in both ventricles was measured after specific staining. The mean cross-sectional area of LV cardiomyocytes was evaluated by quantitative histomorphometry. ISO provoked an increase of LV mass, and a progressive enlargement of cardiomyocytes: their cross-sectional area raised from 205+/-8 micrometer2 in vehicle-treated animals to 247+/-4 and 296+/-9 micrometer2 after 3 or 7 days of ISO infusion, respectively (P<0.001). SPARC messenger abundance increased by more than 50% in LV and RV, a first evidence of its expression in the myocardium of adult rats. Transcripts of ANP, COL-III, TGF-beta1 and TGF-beta3 increased in both ventricles. COL-I transcript increased in LV (75 and 116% on days 3 and 7), but not in RV. In LV, collagen accumulated in the interstitium (2.69+/-0.20v 9. 23+/-0.50% of tissue area for vehicle and ISO 7 days groups, P<0.05) and around coronary arteries (1.04+/-0.11v 4.47+/-0.48% of lumen area for vehicle and ISO 7 days,P<0.05). Cardiac fibrosis was less marked in RV. In conclusion, early expression of SPARC, an anti-adhesive protein, and preferential expression of COL-III, a distensible form of collagen, should increase ECM plasticity and facilitate ventricular remodelling.

Engelmann GL. **Coordinate gene expression during neonatal rat heart development. A possible role for the myocyte in extracellular matrix biogenesis and capillary angiogenesis**. Cardiovasc Res. 1993 Sep;27(9):1598-605.

OBJECTIVE: Neonatal heart development is a period of active extracellular matrix deposition and capillary angiogenesis which follows the cessation of ventricular myocyte proliferation. The aim was to determine whether coordinate expression of growth factors by the ventricular myocyte could function to inhibit myocyte proliferation directly as well as indirectly by paracrine stimulation of non-myocyte extracellular matrix deposition and capillary angiogenesis. METHODS: Immunohistochemistry and northern blot hybridisations were performed on ventricular samples from fetal to mature animals of the spontaneously hypertensive (SHR) and normotensive control Wistar Kyoto (WKY) strains. RESULTS: Ventricular expression of types I, III, and IV collagen genes reached their "maximum" within the first 2-3 postnatal weeks and then rapidly declined. Expression of TGF beta 3 and SPARC were found to precede and accompany the changes in extracellular matrix gene expression during this same developmental period. TGF beta 3 was immunolocalised to fetal cardiomyocytes with very limited expression in neonatal/adult non-myocytes. Associated with the neonatal expression of TGF beta variants, transcripts for the type 2 IGF receptor gradually declined over the first three postnatal weeks. Myocyte TGF beta gene expression, latent TGF beta release, and paracrine mechanisms of action could be facilitated by residual type 2 IGF receptor expression to help mediate stimulation of non-myocyte extracellular matrix synthesis and deposition. CONCLUSIONS: Expression of select growth factors, growth factor receptors, and components of the extracellular matrix appear to be highly coordinated during ventricular remodelling which occurs during neonatal heart development. A paradigm is presented which integrates the expression patterns of various myocyte derived stimuli and their postulated impact on formation of the structural components of the neonatal heart by modulation of myocyte and non-myocyte cell types.

Locus 14

Significance (based on data with full allele set): CORRECT

Top hit 1 : position chr 6:76'524'788
alleles (EMMA) # alleles 1 = 12; # alleles 2 = 10
condition / stat iso 10, LRT
p-value: **1.463×10^{-6}**
alleles from the Broad1 SNP set (MPD): 12 vs 9

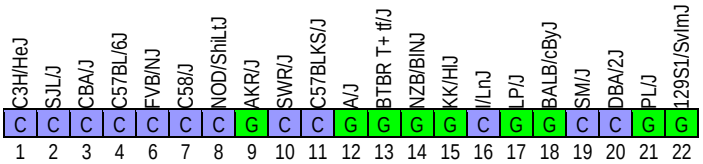

range : ca 76-77 Mb

Candidate gene(s) : **none**

Locus 15

Significance (based on data with full allele set): CORRECT

Top hit 1 : position chr 5:128'006'028
alleles (EMMA) # alleles 1 = 18; # alleles 2 = 4
condition / stat atenolol, REMLt
p-value: **8.338×10^{-6}**
alleles from the Broad1 SNP set (MPD): 17 vs 4

Top hit 2 : position chr 5:128'006'079
alleles (EMMA) #alleles 1 = 18; # alleles 2 = 4
condition / stat atenolol, REMLt
p-value: **8.338×10^{-6}**
alleles from the Broad1 SNP set (MPD): 17 vs 4

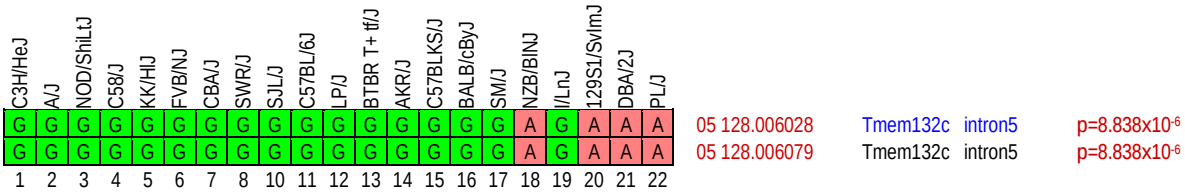

range : ca 127-129 Mb

Candidate gene(s) :

1. ***4632425D07Rik (Tmem132c)*** : 14, 17 days embryo head cDNA, RIKEN full-length enriched library, clone:3230401P16 product:RIKEN cDNA 2810482M11 (Fragment). Link to UCSC gene information. No information in PubMed.

Locus 16

Significance (based on data with full allele set): CORRECT

Top hit 1 : position chr 9:65'899'904
alleles (EMMA) # alleles 1 = 18; # alleles 2 = 4
condition / stat atenolol, REMLt
p-value: **8.396×10^{-6}**
alleles from the Broad1 SNP set (MPD):17 vs 4

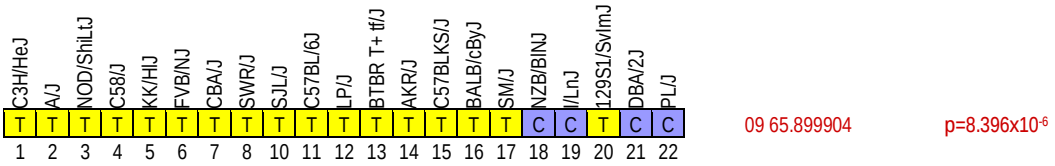

alleles from the CGD1 imputed SNP set (MPD): 17 vs 3

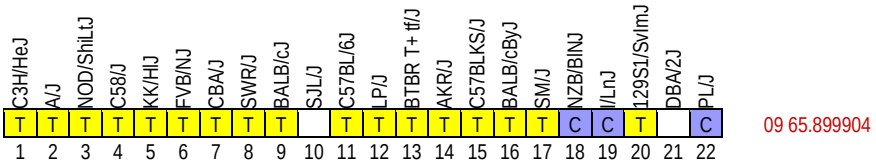

Top hit 2 : position chr 9:64'463'047
alleles (EMMA) #alleles 1 = 13; # alleles 2 = 7
condition / stat iso 10, REMLt
p-value: 1.743×10^{-5}
alleles from the Broad1 SNP set (MPD): vs

alleles from the CGD1 imputed SNP set (MPD): 14 vs 8

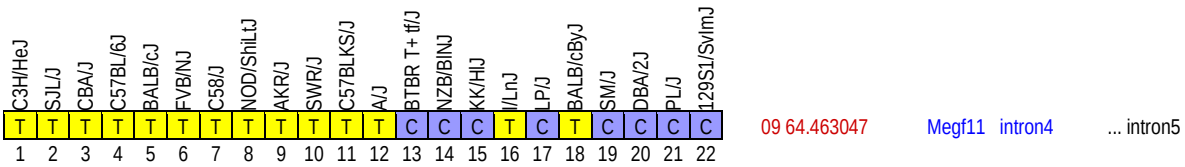

range : ca 64-67 Mb

Candidate gene(s) :

1. ***Snx22*** : sorting nexin 22. Link to UCSC gene information. Little information about that protein in PubMed. But the family of sorting nexin looks pretty large. Snx proteins are involved in trafficking.

Song J, Zhao KQ, Newman CL, Vinarov DA, Markley JL. **Solution structure of human sorting nexin 22.** Protein Sci. 2007 May;16(5):807-14. URL

The sorting nexins (SNXs) constitute a large group of PX domain-containing proteins that play critical roles in protein trafficking. We report here the solution structure of human sorting nexin 22 (SNX22). Although SNX22 has <30% sequence identity with any PX domain protein of known structure, it was found to contain the alpha/beta fold and compact structural core characteristic of PX domains. Analysis of the backbone dynamics of SNX22 by NMR relaxation measurements revealed that the two walls of the ligand binding cleft undergo internal motions: on the picosecond timescale for the beta1/beta2 loop and on the micro- to millisecond timescale for the loop between the polyproline motif and helix alpha2. Regions of the SNX22 structure that differ from those of other PX domains include the loop connecting strands beta1 and beta2 and the loop connecting helices alpha1 and alpha2, which appear to be more mobile than corresponding loops in other known structures. The interaction of dibutanoyl-phosphatidylinositol-3-phosphate (dibutanoyl-PtdIns(3)P) with SNX22 was investigated by an NMR titration experiment, which identified the binding site in a basic cleft and indicated that ligand binding leads only to a local structural rearrangement as has been found with other PX domains. Because motions in the loops are damped out when dibutanoyl-PtdIns(3)P binds, entropic effects could contribute to the lower affinity of SNX22 for this ligand compared to other PX domains.

2. ***Ppib*** ? : peptidylprolyl isomerase B. Link to UCSC gene information.
3. ***Megf11*** : multiple epidermal growth factor-like domains 11 precursor. Link to UCSC gene information.

Locus 17

Significance (based on data with full allele set): INFLATED ?

Top hit 1 : position chr 7:16'488'107
alleles (EMMA) # alleles 1 = 14; # alleles 2 = 5 (-> allele set is not complete)
condition / stat iso 1, REMLt
p-value: $3.162x10^{-6}$
alleles from the Broad1 SNP set (MPD):15 vs 5; there is no matching SNP with a full allele set in the vicinity

Top hit 2 : position chr 7:15'194'001
alleles (EMMA) #alleles 1 = 13; # alleles 2 = 5
condition / stat iso 10, REMLt
p-value: $6.614x10^{-6}$
alleles from the Broad1 SNP set (MPD): 13 vs 4; there is no matching SNP with a full allele set in the vicinity

a. sorted by iso 1 increasing strain means for VWI (hit 1):

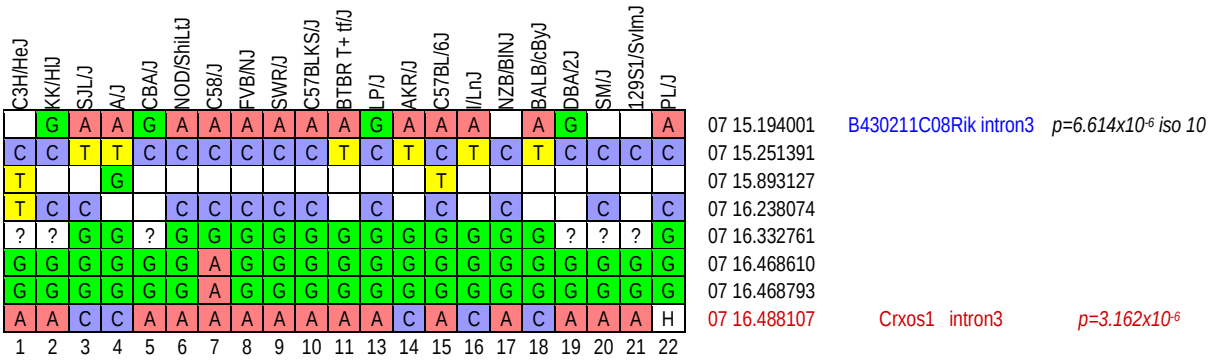

b. sorted by iso 10 increasing strain means for VWI (hit 2):

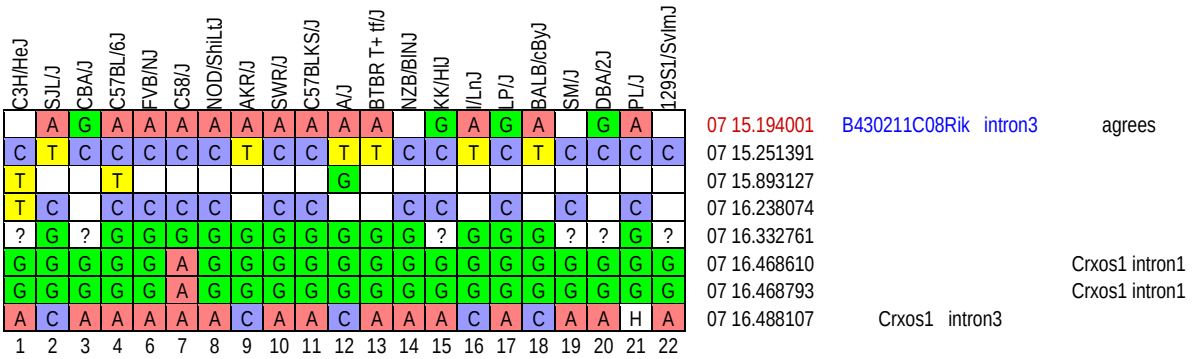

c. hit 1 alleles from the CGD1 imputed SNP set (MPD): 11 vs 6
sorted by iso 1 increasing strain means for VWI:

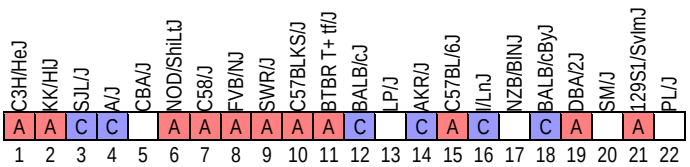

d. hit 2 alleles from the CGD1 imputed SNP set (MPD): 14 vs 6
sorted by iso 10 increasing strain means for VWI:

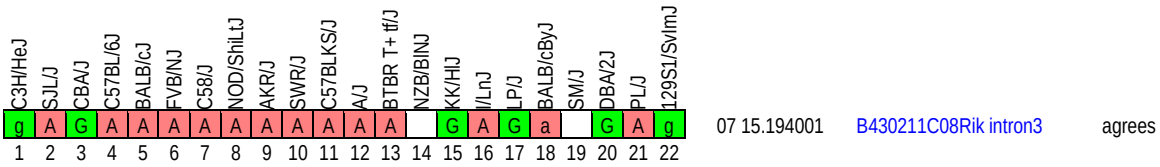

How come that there is an association with such SDPs ??

range : ca 15-17 Mb

Candidate gene(s) :

1. ***Crxos1*** : Crx (cone-rod homeobox containing) opposite strand transcript 1.

Locus 18

Significance (based on data with full allele set): CORRECT

Top hit 1 : position chr 6:125'528'422
alleles (EMMA) # alleles 1 = 17; # alleles 2 = 5
condition / stat iso 1, REMLT
p-value: **$4.072x10^{-6}$**
alleles from the Broad1 SNP set (MPD): 16 vs 5

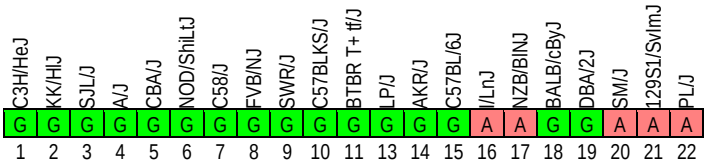

06 125.528422 Vwf intron6 p=4.072x10-6

alleles from the CGD1 imputed SNP set (MPD): 16 vs 4

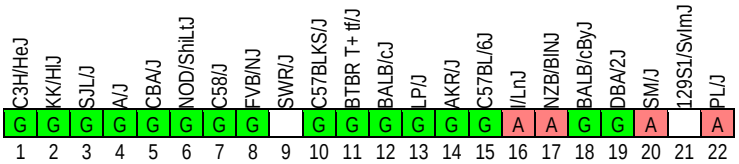

06 125.528422 Vwf intron6

range : ca 124-126 Mb

Candidate gene(s) :

1. ***vWf*** : von Willebrand factor. Link to UCSC gene information.

Notes and bibliography: there is of course a lot about vWf...

von Kanel R, Dimsdale JE, Adler KA, Dillon E, Perez CJ, Mills PJ. **Effects of nonspecific beta-adrenergic stimulation and blockade on blood coagulation in hypertension**. J Appl Physiol. 2003 Apr;94(4):1455-9. URL

A hypercoagulable state might contribute to increased atherothrombotic risk in hypertension. The sympathetic nervous system is hyperactive in hypertension, and it regulates hemostatic function. We investigated the effect of nonspecific beta-adrenergic stimulation (isoproterenol) and blockade (propranolol) on clotting diathesis in hypertension. Fifteen hypertensive and 21 normotensive subjects underwent isoproterenol infusion in two sequential, fixed-order doses of 20 and then 40 ng. kg(-1). min(-1) for 15 min/dose. Thirteen subjects were double-blind studied after receiving placebo or propranolol (100 mg/day) for 5 days each. In hypertensive subjects, isoproterenol elicited a dose-dependent increase in plasma von Willebrand factor (vWF) antigen [F(2,34) = 5.02; P = 0.032] and a decrease in D-dimer [F(2,34) = 4.57; P = 0.040], whereas soluble tissue factor remained unchanged. Propranolol completely abolished the increase in vWF elicited by isoproterenol [F(1,12) = 10.25; P = 0.008] but had no significant effect on tissue factor and D-dimer. In hypertension, vWF is readily released from endothelial cells by beta-adrenergic stimulation, which might contribute to increased cardiovascular risk. However, beta-adrenergic stimulation alone may not be sufficient to trigger fibrin formation in vivo.

Wannamethee SG, Shaper AG, Lowe GD, Lennon L, Rumley A, Whincup PH. **Renal function and cardiovascular mortality in elderly men: the role of inflammatory, procoagulant, and endothelial biomarkers**. Eur Heart J. 2006 Dec;27(24):2975-81. URL

AIMS: To assess the extent to which inflammatory, procoagulant, and endothelial biomarkers modify the relationship between diminished renal function and cardiovascular mortality. METHODS AND RESULTS: Prospective study of 4029 men aged 60-79 years followed up for a mean period of 6 years, during which 304 cardiovascular deaths occurred. Predicted estimated glomerular filtration rate (eGFR) was used as a measure of renal function. Reduced eGFR was associated with increased prevalence of established cardiovascular risk factors [cardiovascular disease, diabetes, hypertension, left ventricular (LV) hypertrophy, and dyslipidaemia] and higher levels of inflammatory markers [interleukin 6 (IL-6), C-reactive protein], endothelial markers [von Willebrand factor (vWF) and tissue plasminogen activator], activated coagulation markers (fibrin D-dimer), and blood viscosity. Cardiovascular mortality risk increased with decreasing levels of eGFR, particularly among men with eGFR <60 mL/min per 1.73 m(2) even after adjustment for established risk factors (adjusted RR 1.49, 95% CI 1.10, 2.03; <60 vs. > or =70 mL/min per 1.73 m(2)). The association was attenuated after further adjustment for vWF, D-dimer, and IL-6 (adjusted RR 1.34, 95% CI 0.98-1.82). CONCLUSION: Mild-to-moderate renal insufficiency is associated with significantly increased cardiovascular mortality in elderly men, which is partly explained by the increased prevalence of established risk factors, markers of coagulation, endothelium, and inflammation.

Spencer CG, Gurney D, Blann AD, Beevers DG, Lip GY; ASCOT Steering Committee, Anglo-Scandinavian Cardiac Outcomes Trial. **Von Willebrand factor, soluble P-selectin, and target organ damage in**

hypertension: a substudy of the Anglo-Scandinavian Cardiac Outcomes Trial (ASCOT). Hypertension. 2002 Jul;40(1):61-6. URL

To investigate the relationship between soluble markers of platelet, endothelial and rheological function, and target organ damage and their response to intensified management in a population of middle-age hypertensive patients at high risk of cardiovascular complications, we studied 382 consecutive patients (308 men; mean age, 63 years, SD 8) along with 60 normotensive controls free of cardiovascular disease. Patients were divided into those with target organ damage (TOD; n=107) and those free of end-organ damage. Plasma levels of soluble P-selectin (sP-sel), a marker of platelet activation, and von Willebrand factor (vWF), an index of endothelial damage/dysfunction (both enzyme-linked immunosorbent assay), and the rheological indices fibrinogen, plasma viscosity, hematocrit, platelet, and white cell count were measured. In 53 patients, variables were further measured after 6 months of intensified cardiovascular risk management. Patients with TOD had significantly higher vWF, 137 (SD 33) versus 125 (SD 33) IU/dL (P=0.002,) and a greater proportion of smokers, 31% versus 16% (P=0.002). There were no statistically significant differences in plasma viscosity, fibrinogen, hematocrit, white blood cell count, platelet count, or sP-sel between the 2 subgroups. In multivariate analysis, vWF was a significant independent predictor for TOD. After 6 months of intensified management in 53 patients who entered the trial, there were significant reductions in systolic blood pressure, total cholesterol, hematocrit, plasma viscosity, sP-sel, and vWF (all P<0.01) but no significant change in fibrinogen. In conclusion, there is a relationship between TOD and endothelial damage/dysfunction in hypertension. Intensified management results in improvements in hemorheology, endothelial and platelet function.

Locus 19

Significance (based on data with full allele set): CORRECT

Top hit 1 : position chr 7:25'140'278
alleles (EMMA) # alleles 1 = 18; # alleles 2 = 4
condition / stat iso 1, REMLt
p-value: **8.226×10^{-6}**
alleles from the Broad1 SNP set (MPD): 17 vs 4

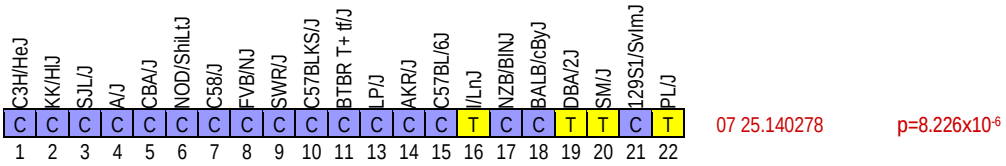

alleles from the CGD1 imputed SNP set (MPD): 18 vs 4

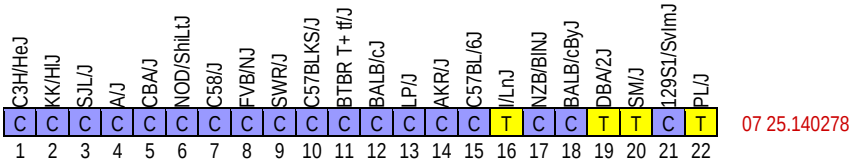

range : single position

Candidate gene(s) : **none**, even when looking at patterns of CGD1 imputed SNPs.

Locus 20

Significance (based on data with full allele set): INFLATED but p-value still below 10^{-5} (provided that alleles are correct)

Top hits 1/2: position chr 4:73'016'585 and chr 4:73'202'146
alleles (EMMA) # alleles 1 = 13; # alleles 2 = 7 (-> allele set is not complete)
condition / stat iso 10, REMLt
p-value: 2.659×10^{-6}
alleles from the Broad1 SNP set (MPD): 14 vs 7 and 12 vs 8

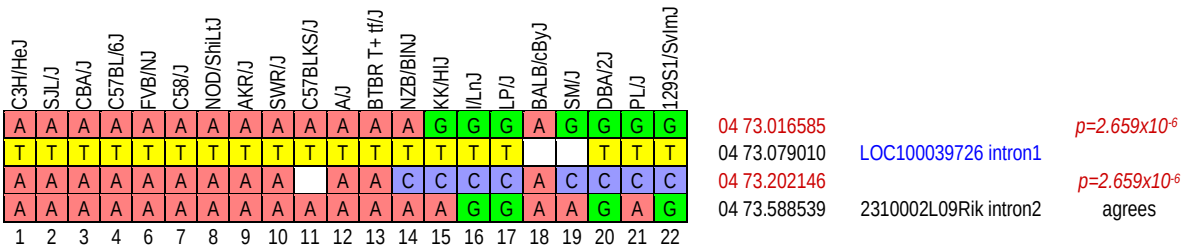

alleles from the CGD1 imputed SNP set (MPD): 15 vs 4 for hit #1; the second position is absent from the CGD1 set, but surrounding SNPs are all identical in the PGX strains.

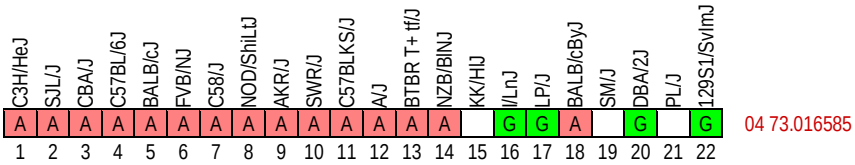

Matching SNP with full allele set: the SNP below matches top hit #1. Note that in the MPD medium size SNP database, both positions have distinct SDPs. In EMMAIII, both hits are given with equivalent p-values -> (presumably) with equivalent SDPs.

Top hit 3 : position chr 4:72'313'856
alleles (EMMA) #alleles 1 = 15; # alleles 2 = 7
condition / stat iso 10, REMLt
p-value: **2.840×10^{-6}**
alleles from the Broad1 SNP set (MPD): 14 vs 7

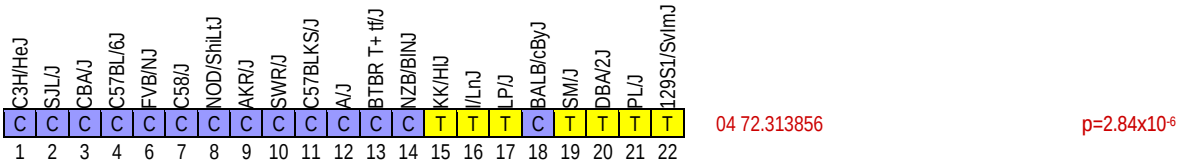

this SNP is absent from the CGD1 set, yet the surrounding SNPs seem to have a different pattern of alleles:

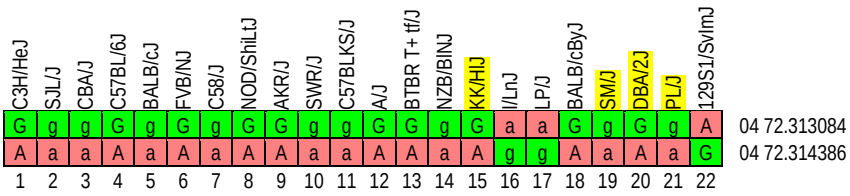

range : ca 72-73.5 Mb

Candidate gene(s) : **none**, even when looking at patterns of CGD1 imputed SNPs.

Locus 21

Significance (based on data with full allele set): INFLATED ?

Top hit 1 : position chr 4:82'834'365
alleles (EMMA) # alleles 1 = 9; # alleles 2 = 11 (-> allele set is not complete)
condition / stat iso 10, REMLt
p-value: $3.179x10^{-6}$
alleles from the Broad1 SNP set (MPD): 11 vs 10; there is no matching SNP with a full allele set in the vicinity

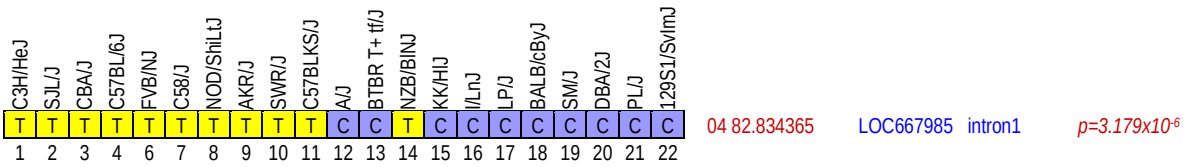

alleles from the CGD1 imputed SNP set (MPD): this position is absent from the CGD1 imputed set. There are lots of missing alleles at the surrounding positions.

Top hit 2 : position chr 4:83'326'905
alleles (EMMA) #alleles 1 = 10; # alleles 2 = 11
condition / stat iso 10, REMLt
p-value: $1.239x10^{-5}$
alleles from the Broad1 SNP set (MPD): 10 vs 10; there is no matching SNP with a full allele set in the vicinity

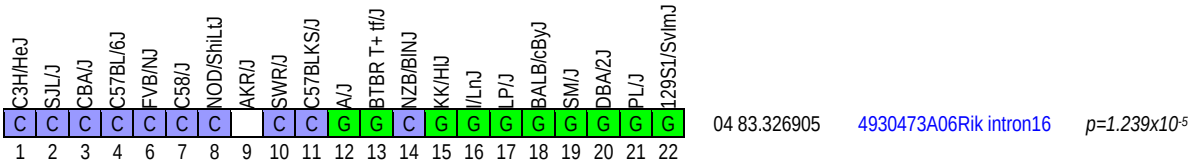

alleles from the CGD1 imputed SNP set (MPD): 11 vs 11

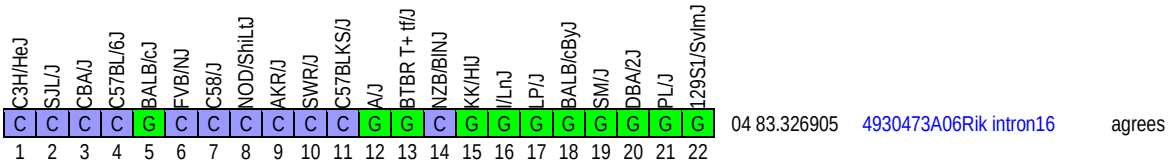

range : ca 82.5-83.5 Mb

Candidate gene(s) :

1. ***1810054D07Rik***: hypothetical protein LOC69863. Link to UCSC gene information page.
2. ***4930473A06Rik***: hypothetical protein LOC320226. Link to UCSC gene information page. Expressed in heart, spleen, pancreas and testis.

Locus 22

Significance (based on data with full allele set): CORRECT

Top hit 1 : position chr 6:145'091'729
alleles (EMMA) # alleles 1 = 16; # alleles 2 = 6
condition / stat iso 10, REMLt
p-value: **$4.025x10^{-6}$**
alleles from the Broad1 SNP set (MPD): 16 vs 5

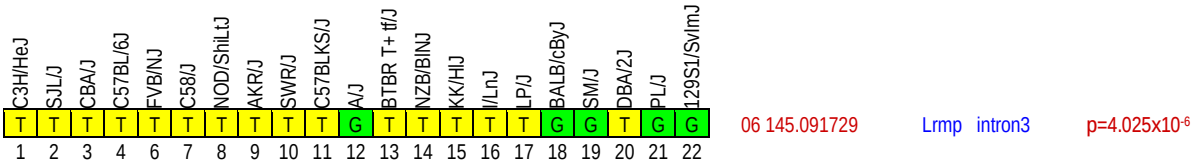

alleles from the CGD1 imputed SNP set (MPD): 15 vs 3

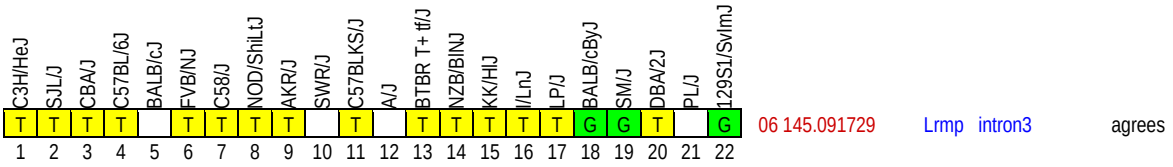

range : ca 144.5-146.5 Mb

Candidate gene(s) :

1. ***Lrmp*** : lymphoid-restricted membrane protein. Link to UCSC gene information page. No indication that *Lrmp* is expressed in cardiac tissues.

Notes and bibliography: this SNP overlaps with the *Pas1* locus.

Duarte N, Lundholm M, Holmberg D. **The *Idd6.2* diabetes susceptibility region controls defective expression of the *Lrmp* gene in nonobese diabetic (NOD) mice**. Immunogenetics. 2007 May;59(5):407-16. URL

The identification of genes mediating susceptibility to type 1 diabetes (T1D) remains a challenging task. Using a positional cloning approach based on the analysis of nonobese diabetic (NOD) mice congenic over the Idd6 diabetes susceptibility region, we found that the NOD allele at this locus mediates lower mRNA expression levels of the lymphoid restricted membrane protein gene (Lrmp/Jaw1). Analysis of thymic populations indicates that Lrmp is expressed mainly in immature thymocytes. The Lrmp gene encodes a type 1 transmembrane protein that localizes to the ER membrane and has homology to the inositol 1,4,5-triphosphate receptor-associated cGMP kinase substrate gene, which negatively regulates intracellular calcium levels. We hypothesize that the observed decrease in expression of the Lrmp gene in NOD mice may constitute a T1D susceptibility factor in the Idd6 region.

Manenti G, Galbiati F, Giannì-Barrera R, Pettinicchio A, Acevedo A, Dragani TA. **Haplotype sharing suggests that a genomic segment containing six genes accounts for the pulmonary adenoma susceptibility 1 (*Pas1*) locus activity in mice**. Oncogene. 2004 May 27;23(25):4495-504. URL

The pulmonary adenoma susceptibility 1 (Pas1) locus affects inherited predisposition and resistance to chemically induced lung tumorigenesis in mice. The A/J and C57BL/6J mouse strains carry the susceptibility and resistance allele, respectively. We identified and genotyped 65 polymorphisms in the Pas1 locus region in 29 mouse inbred strains, and delimited the Pas1 locus to a minimal region of 468 kb containing six genes. That region defined a core Pas1 haplotype with 42 tightly linked markers, including intragenic polymorphisms in five genes (Bcat1, Lrmp, Las1, Ghiso, and Kras2) and amino-acid changes in three genes (Lrmp, Las1, Lmna-rs1). In (A/J x C57BL/6J)F1 mouse lung tumors, the Lmna-rs1 gene was completely downregulated, whereas allele-specific downregulation of the C57BL/6J-derived allele was observed at the Las1 gene, suggesting the potential role of these genes in tumor suppression. These results indicate a complex multigenic nature of the Pas1 locus, and point to a functional role for both intronic and exonic polymorphisms of the six genes of the Pas1 haplotype in lung tumor susceptibility.

But then:

Liu P, Wang Y, Vikis H, Maciag A, Wang D, Lu Y, Liu Y, You M. **Candidate lung tumor susceptibility genes identified through whole-genome association analyses in inbred mice**. Nat Genet. 2006 Aug;38(8):888-95. URL

We performed a whole-genome association analysis of lung tumor susceptibility using dense SNP maps (approximately 1 SNP per 20 kb) in inbred mice. We reproduced the pulmonary adenoma susceptibility 1 (*Pas1*) locus identified in previous linkage studies and further narrowed this quantitative trait locus (QTL) to a region of less than 0.5 Mb in which at least two genes, Kras2 (Kirsten rat sarcoma oncogene 2) and Casc1 (cancer susceptibility candidate 1; also known as Las1), are strong candidates. *Casc1*

knockout mouse tumor bioassays showed that *Casc1*-deficient mice were susceptible to chemical induction of lung tumors. We also found three more genetic loci for lung adenoma development. Analysis of one of these candidate loci identified a previously uncharacterized gene Lasc1, bearing a nonsynonymous substitution (D102E). We found that the *Lasc1* Glu102 allele preferentially promotes lung tumor cell growth. Our findings demonstrate the prospects for using dense SNP maps in laboratory mice to refine previous QTL regions and identify genetic determinants of complex traits.

Tsuda H, Birrer MJ, Ito YM, Ohashi Y, Lin M, Lee C, Wong WH, Rao PH, Lau CC, Berkowitz RS, Wong KK, Mok SC. **Identification of DNA copy number changes in microdissected serous ovarian cancer tissue using a cDNA microarray platform**. Cancer Genet Cytogenet. 2004 Dec;155(2):97-107. URL

We have established a method for using a cDNA array platform in combination with degenerate oligonucleotide primer polymerase chain reaction (DOP-PCR) and taramide signal amplification (TSA) to identify DNA copy number abnormalities (CNA) in cancer cell lines and cancer cells procured with laser-based microdissection. To determine the sensitivity and specificity for detecting single-copy gain and loss, receiver-operator curve analysis was performed on hybridization signal ratios generated from non-DOP and DOP amplified female and male DNA using a 10,816-element cDNA microarray. A cutoff value of 1.12 and 1.07 average signal ratio for X-chromosomal genes versus autosomal genes provided a sensitivity and specificity of 50 and 79%, respectively, for non-DOP amplified DNA and a sensitivity and specificity of 50 and 72%, respectively, for DOP amplified DNA. We used this approach to identify DNA copy number abnormalities in the ovarian cancer cell line OVCA633, which has previously been shown to have 12p amplification. Transcription profiling of OVCA633 was also performed. Two amplified and overexpressed genes located on 12p11, KRAS2 and LRMP, were identified; these were validated with quantitative real-time PCR. Subsequently, the same approach was used to identify CNAs and gene expression alterations in 11 microdissected serous ovarian adenocarcinoma cases. Validated data revealed amplification and overexpression of ERBB3 and FOS and deletion and underexpression of KRT6 and APXL in more than 50% of the tissue samples. These results show the feasibility of using the cDNA array platform to identify changes in DNA and mRNA copy number simultaneously in microdissected tumor tissues.

Locus 23

Significance (based on data with full allele set): INFLATED

Top hit 1 : position chr 6:5'476'010
alleles (EMMA) # alleles 1 = 13; # alleles 2 = 5 (-> allele set is not complete)
condition / stat iso 10, REMLt
p-value: $4.607x10^{-6}$
alleles from the Broad1 SNP set (MPD): 12 vs 5

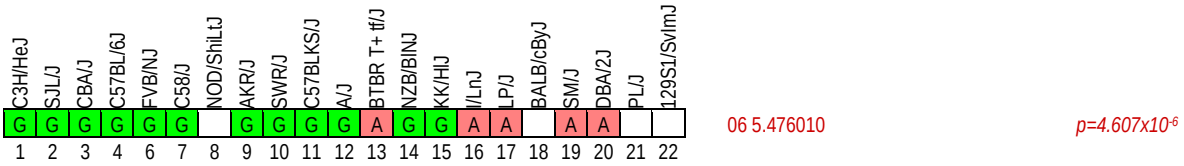

Matching SNP with full allele set in EMMAIII:

position chr 6: 5'519'967
alleles (EMMA) #alleles 1 =16; # alleles 2 = 6
condition / stat iso 10, REMLt
p-value: **$7.487x10^{-1}$**
alleles from the Broad1 SNP set (MPD): 15 vs 6; note that in the CGD1 imputed SNP set, all alleles are given as identical at this position -> there are discrepancies between databases !

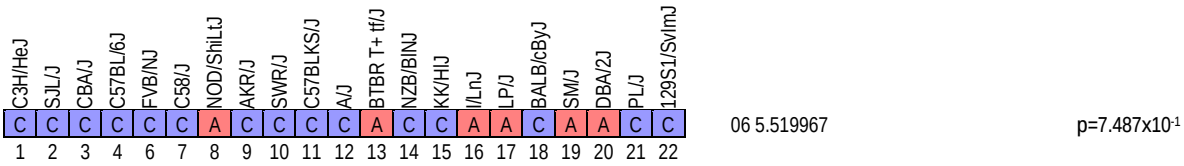

alleles from the CGD1 imputed SNP set (MPD) for top hit #1: 16 vs 6

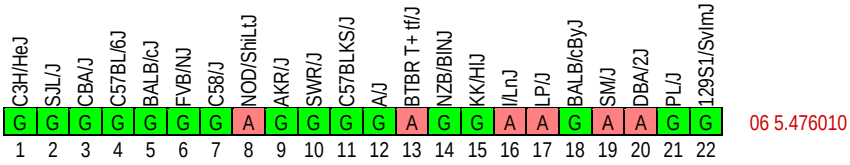

range : ca 5-6 Mb

Candidate gene(s) : there are at least 2 genes sharing SNPs with identical CGD1-based SDPs. Yet, the p-value of association is likely to stand lower than indicated here when considering the full set of strains and alleles.

1. ***Dync1i1***: dynein cytoplasmic 1 intermediate chain 1. Link to UCSC gene information page. Mostly expressed in neuronal (brain) tissues.
2. ***Slc25a13*** : solute carrier family 25 (mitochondrial carrier). Link to UCSC gene information page. Seems to be highly expressed in heart, liver and kidney.

   Comments and Description Text from UniProt (Swiss-Prot/TrEMBL) ID: CMC2_MOUSE
   DESCRIPTION: Calcium-binding mitochondrial carrier protein Aralar2 (Mitochondrial aspartate glutamate carrier 2) (Solute carrier family 25 member 13) (Citrin).
   FUNCTION: Calcium-dependent mitochondrial aspartate and glutamate carrier. May have a function in the urea cycle.
   SUBCELLULAR LOCATION: Mitochondrion inner membrane; Multi-pass membrane protein (By similarity).
   TISSUE SPECIFICITY: At E10.45, expressed in branchial arches and Irfimb and tail buds. At E13.5 expression is predominant in epithelial structures and the forebrain, kidney and liver. Expression in liver is maintained into adulthood.

SIMILARITY: Belongs to the mitochondrial carrier family.
SIMILARITY: Contains 4 EF-hand domains.
SIMILARITY: Contains 3 Solcar repeats.

Notes and bibliography:

Sinasac DS, Moriyama M, Jalil MA, Begum L, Li MX, Iijima M, Horiuchi M, Robinson BH, Kobayashi K, Saheki T, Tsui LC. ***Slc25a13*-knockout mice harbor metabolic deficits but fail to display hallmarks of adult-onset type II citrullinemia**. Mol Cell Biol. 2004 Jan;24(2):527-36. URL

Adult-onset type II citrullinemia (CTLN2) is an autosomal recessive disease caused by mutations in SLC25A13, the gene encoding the mitochondrial aspartate/glutamate carrier citrin. The absence of citrin leads to a liver-specific, quantitative decrease of argininosuccinate synthetase (ASS), causing hyperammonemia and citrullinemia. To investigate the physiological role of citrin and the development of CTLN2, an Slc25a13-knockout (also known as Ctrn-deficient) mouse model was created. The resulting Ctrn-/- mice were devoid of Slc25a13 mRNA and citrin protein. Liver mitochondrial assays revealed markedly decreased activities in aspartate transport and the malate-aspartate shuttle. Liver perfusion also demonstrated deficits in ureogenesis from ammonia, gluconeogenesis from lactate, and an increase in the lactate-to-pyruvate ratio within hepatocytes. Surprisingly, Ctrn-/- mice up to 1 year of age failed to show CTLN2-like symptoms due to normal hepatic ASS activity. Serological measures of glucose, amino acid, and ammonia metabolism also showed no significant alterations. Nitrogen-loading treatments produced only minor changes in the hepatic ammonia and amino acid levels. These results suggest that citrin deficiency alone may not be sufficient to produce a CTLN2-like phenotype in mice. These observations are compatible, however, with the variable age of onset, incomplete penetrance, and strong ethnic bias seen in CTLN2 where additional environmental and/or genetic triggers are now suspected.

Kobayashi K, Sinasac DS, Iijima M, Boright AP, Begum L, Lee JR, Yasuda T, Ikeda S, Hirano R, Terazono H, Crackower MA, Kondo I, Tsui LC, Scherer SW, Saheki T. **The gene mutated in adult-onset type II citrullinaemia encodes a putative mitochondrial carrier protein**. Nat Genet. 1999 Jun;22(2):159-63. URL

Citrullinaemia (CTLN) is an autosomal recessive disease caused by deficiency of argininosuccinate synthetase (ASS). Adult-onset type II citrullinaemia (CTLN2) is characterized by a liver-specific ASS deficiency with no abnormalities in hepatic ASS mRNA or the gene ASS (refs 1-17). CTLN2 patients (1/100,000 in Japan) suffer from a disturbance of consciousness and coma, and most die with cerebral edema within a few years of onset. CTLN2 differs from classical citrullinaemia (CTLN1, OMIM 215700) in that CTLN1 is neonatal or infantile in onset, with ASS enzyme defects (in all tissues) arising due to mutations in ASS on chromosome 9q34 (refs 18-21). We collected 118 CTLN2 families, and localized the CTLN2 locus to chromosome 7q21.3 by homozygosity mapping analysis of individuals from 18 consanguineous unions. Using positional cloning we identified a novel gene, SLC25A13, and found five different DNA sequence alterations that account for mutations in all consanguineous patients examined. SLC25A13 encodes a 3.4-kb transcript expressed most abundantly in liver. The protein encoded by SLC25A13, named citrin, is bipartite in structure, containing a mitochondrial carrier motif and four EF-hand domains, suggesting it is a calcium-dependent mitochondrial solute transporter with a role in urea cycle function

Locus 24

Significance (based on data with full allele set): INFLATED ?

Top hit 1 : position chr 18:60'889'758
alleles (EMMA) # alleles 1 = 12; # alleles 2 = 7 (-> the allele set is incomplete)
condition / stat iso 10, LRT
p-value: $2.488x10^{-6}$
alleles from the Broad1 SNP set (MPD): 12 vs 6; there is no matching SNP with a full allele set in the vicinity

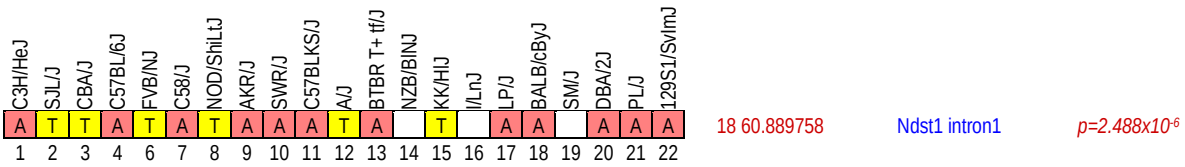

alleles from the CGD1 imputed SNP set (MPD): 12 vs 3

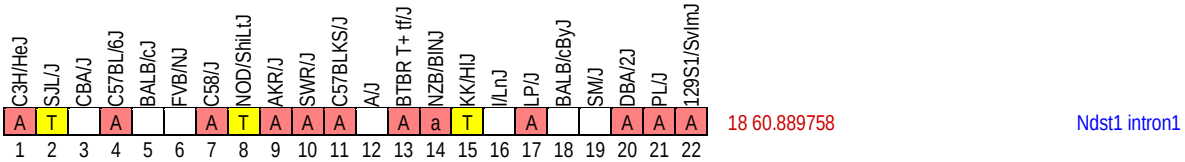

range : ca 60.5-61.5 Mb

Candidate gene(s) :

1. ***Ndst1 ?*** : heparan sulfate N-deacetylase/N-sulfotransferase 1. Link to UCSC gene information page.

Notes and bibliography:

It is not clear whether this SNP is indeed associated with PGX VWI. Several alleles are missing and may give misleading p-values of association. There are several *Ndst1* KO (full and conditional mutants) mouse models. See examples below, and more bibliography in PubMed. There is no obvious link with any cardiac phenotype.

Comments and Description Text from UniProt (Swiss-Prot/TrEMBL) ID: NDST1_MOUSE

DESCRIPTION: Bifunctional heparan sulfate N-deacetylase/N-sulfotransferase 1 (EC 2.8.2.8) (Glucosaminyl N-deacetylase/N-sulfotransferase 1) (NDST- 1) ([Heparan sulfate]-glucosamine N-sulfotransferase 1) (HSNST 1) (N- heparan sulfate sulfotransferase 1) (N-HSST 1) [Includes: Heparan sulfate N-deacetylase 1 (EC 3.-.-.-); Heparan sulfate N- sulfotransferase 1 (EC 2.8.2.-)].
FUNCTION: Essential bifunctional enzyme that catalyzes both the N- deacetylation and the N-sulfation of glucosamine (GlcNAc) of the glycosaminoglycan in heparan sulfate. Modifies the GlcNAc-GlcA dissacharide repeating sugar backbone to make N-sulfated heparosan, a prerequisite substrate for later modifications in heparin biosynthesis. Plays a role in determining the extent and pattern of sulfation of heparan sulfate. Compared to other NDST enzymes, its presence is absolutely required. Participates in biosynthesis of heparan sulfate that can ultimately serve as L- selectin ligands, thereby playing a role in inflammatory response.
CATALYTIC ACTIVITY: 3'-phosphoadenylyl sulfate + [heparan sulfate]-glucosamine = adenosine 3',5'-bisphosphate + [heparan sulfate]-N-sulfoglucosamine.
PATHWAY: Glycan metabolism; heparan sulfate biosynthesis.
PATHWAY: Glycan metabolism; heparin biosynthesis.
SUBUNIT: Monomer (By similarity).
SUBCELLULAR LOCATION: Golgi apparatus membrane; Single-pass type II membrane protein (By similarity).
TISSUE SPECIFICITY: Widely expressed in adult and throughout development.
MISCELLANEOUS: The presence of 4 different NDST enzymes in mammals, as well as differences in their enzyme activity suggest that some initiate heparan sulfate modification/sulfation reactions, whereas other later on fill in or extend already modified heparan sulfate sequences.

MISCELLANEOUS: Mice lacking Ndst1 survive until birth but are cyanotic and die neonatally in a condition resembling respiratory distress syndrome. In addition, a minor proportion of mice embryos die during the embryonic period. Mutant mice display cerebral hypoplasia and craniofacial defects, disturbed Ca(2+) kinetics in myotubes. They also display deficiencies L-selectin- and chemokine-mediated neutrophil trafficking during inflammatory responses.
SIMILARITY: Belongs to the sulfotransferase 1 family. NDST subfamily.
SEQUENCE CAUTION: Sequence=BAE41527.1; Type=Frameshift; Positions=185;

Grobe K, Inatani M, Pallerla SR, Castagnola J, Yamaguchi Y, Esko JD. **Cerebral hypoplasia and craniofacial defects in mice lacking heparan sulfate *Ndst1* gene function**. Development. 2005 Aug;132(16):3777-86. URL

Mutant mice bearing a targeted disruption of the heparan sulfate (HS) modifying enzyme GlcNAc N-deacetylase/N-sulfotransferase 1 (Ndst1) exhibit severe developmental defects of the forebrain and forebrain-derived structures, including cerebral hypoplasia, lack of olfactory bulbs, eye defects and axon guidance errors. Neural crest-derived facial structures are also severely affected. We show that properly synthesized heparan sulfate is required for the normal development of the brain and face, and that Ndst1 is a modifier of heparan sulfate-dependent growth factor/morphogen signalling in those tissues. Among the multiple heparan sulfate-binding factors potentially affected in Ndst1 mutant embryos, the facial phenotypes are consistent with impaired sonic hedgehog (Shh) and fibroblast growth factor (Fgf) interaction with mutant heparan sulfate. Most importantly, the data suggest the possibility that defects in heparan sulfate synthesis could give rise to or contribute to a number of developmental brain and facial defects in humans.

Pallerla SR, Pan Y, Zhang X, Esko JD, Grobe K. **Heparan sulfate *Ndst1* gene function variably regulates multiple signaling pathways during mouse development**. Dev Dyn. 2007 Feb;236(2):556-63. URL

Disruption of heparan sulfate (HS) synthesis in vertebrate development causes malformations that are composites of those caused by mutations of multiple HS binding growth factors and morphogens. We previously reported severe developmental defects of the forebrain and the skull in mutant mice bearing a targeted disruption of the heparan sulfate-generating enzyme GlcNAc N-deacetylase/GlcN N-sulfotransferase 1 (Ndst1). Here, we further characterize the molecular mechanisms leading to frontonasal dysplasia in Ndst1 mutant embryos and describe additional malformations, including impaired spinal and cranial neural tube fusion and skeletal abnormalities. Of the numerous proteins that bind HS, we show that impaired fibroblast growth factor, Hedgehog, and Wnt function may contribute to some of these phenotypes. Our findings, therefore, suggest that defects in HS synthesis may contribute to multifactor types of congenital developmental defects in humans, including neural tube defects.

MacArthur JM, Bishop JR, Stanford KI, Wang L, Bensadoun A, Witztum JL, Esko JD. **Liver heparan sulfate proteoglycans mediate clearance of triglyceride-rich lipoproteins independently of LDL receptor family members**. J Clin Invest. 2007 Jan;117(1):153-64. URL1 Comment in: Hepatology. 2007 Apr;45(4):1078-80. URL2. J Clin Invest. 2007 Jan;117(1):94-8. URL3

We examined the role of hepatic heparan sulfate in triglyceride-rich lipoprotein metabolism by inactivating the biosynthetic gene GlcNAc N-deacetylase/N-sulfotransferase 1 (Ndst1) in hepatocytes using the Cre-loxP system, which resulted in an approximately 50% reduction in sulfation of liver heparan sulfate. Mice were viable and healthy, but they accumulated triglyceride-rich lipoprotein particles containing apoB-100, apoB-48, apoE, and apoCI-IV. Compounding the mutation with LDL receptor deficiency caused enhanced accumulation of both cholesterol- and triglyceride-rich particles compared with mice lacking only LDL receptors, suggesting that heparan sulfate participates in the clearance of cholesterol-rich lipoproteins as well. Mutant mice synthesized VLDL normally but showed reduced plasma clearance of human VLDL and a corresponding reduction in hepatic VLDL uptake. Retinyl ester excursion studies revealed that clearance of intestinally derived lipoproteins also depended on hepatocyte heparan sulfate. These findings show that under normal physiological conditions, hepatic heparan sulfate proteoglycans play a crucial role in the clearance of both intestinally derived and hepatic lipoprotein particles.

Fuster MM, Wang L, Castagnola J, Sikora L, Reddi K, Lee PH, Radek KA, Schuksz M, Bishop JR, Gallo RL, Sriramarao P, Esko JD. **Genetic alteration of endothelial heparan sulfate selectively inhibits tumor angiogenesis**. J Cell Biol. 2007 May 7;177(3):539-49. URL

To examine the role of endothelial heparan sulfate during angiogenesis, we generated mice bearing an endothelial-targeted deletion in the biosynthetic enzyme N-acetylglucosamine N-deacetylase/N-sulfotransferase 1 (Ndst1). Physiological angiogenesis during cutaneous wound repair was unaffected, as was growth and reproductive capacity of the mice. In contrast, pathological angiogenesis in experimental tumors was altered, resulting in smaller tumors and reduced microvascular density and branching. To simulate the angiogenic environment of the tumor, endothelial cells were isolated and propagated in vitro with proangiogenic growth factors. Binding of FGF-2 and VEGF(164) to cells and to purified heparan sulfate was dramatically reduced. Mutant endothelial cells also exhibited altered sprouting responses to FGF-2 and VEGF(164), reduced Erk phosphorylation, and an increase in apoptosis in branching assays. Corresponding changes in growth factor binding to tumor endothelium and apoptosis were also observed in vivo. These findings demonstrate a cell-autonomous effect of heparan sulfate on endothelial cell growth in the context of tumor angiogenesis.

Locus 25

Significance (based on data with full allele set): CORRECT (under-estimated ?)

Top hit 1 : position chr 4:135'298'806
alleles (EMMA) # alleles 1 = 16; # alleles 2 = 5 (-> allele set is not complete)
condition / stat control, LRT
p-value: **$7.542x10^{-6}$**
alleles from the Broad1 SNP set (MPD): 15 vs 5; there is no matching SNP with a full allele set in the vicinity, but CGD1 imputed SNPs would support the association.

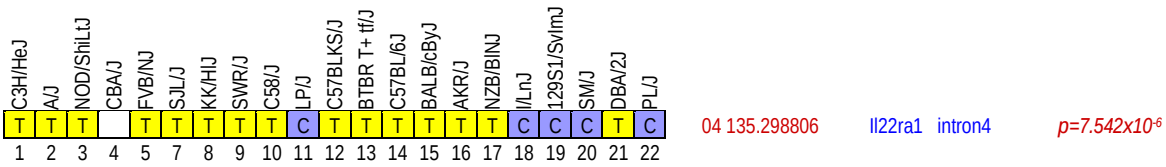

alleles from the CGD1 imputed SNP set (MPD): 17 vs 5

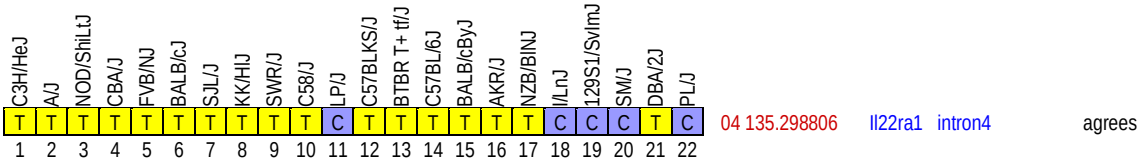

range : ca 135-136 Mb

Candidate gene(s) :

1. ***Il22ra1*** : interleukin 22 receptor, alpha 1. Link to UCSC gene information.

Notes and bibliography:

Comments and Description Text from UniProt (Swiss-Prot/TrEMBL) ID: I22R1_MOUSE
DESCRIPTION: Interleukin-22 receptor subunit alpha-1 precursor (IL-22R-alpha-1).
FUNCTION: Component of the receptor for IL20, IL22 and IL24. Component of IL22 receptor formed by IL22RA1 and IL10RB enabling IL22 signaling via JAK/STAT pathways. IL22 also induces activation of MAPK1/MAPK3 and Akt kinases pathways. Component of one of the receptor for IL20 and IL24 formed by IL22RA1 and IL20RB also signaling through STATs activation. Mediates IL24 antiangiogenic activity as well as IL24 inhibitory effect on endothelial cell tube formation and differentiation.
SUBUNIT: Heterodimer with IL10RB and with IL20RB (By similarity).
SUBCELLULAR LOCATION: Membrane; Single-pass type I membrane protein.
TISSUE SPECIFICITY: Expressed in kidney, liver and lung.
INDUCTION: By LPS stimulation in the liver.
SIMILARITY: Belongs to the type II cytokine receptor family.
SIMILARITY: Contains 2 fibronectin type-III domains.

Bleicher L, de Moura PR, Watanabe L, Colau D, Dumoutier L, Renauld JC, Polikarpov I. **Crystal structure of the IL-22/IL-22R1 complex and its implications for the IL-22 signaling mechanism**. FEBS Lett. 2008 Sep 3;582(20):2985-92. URL
Interleukin-22 (IL-22) is a member of the interleukin-10 cytokine family, which is involved in anti-microbial defenses, tissue damage protection and repair, and acute phase responses. Its signaling mechanism involves the sequential binding of IL-22 to interleukin-22 receptor 1 (IL-22R1), and of this dimer to interleukin-10 receptor 2 (IL-10R2) extracellular domain. We report a 1.9A crystal structure of the IL-22/IL-22R1 complex, revealing crucial interacting residues at the IL-22/IL-22R1 interface. Functional importance of key residues was confirmed by site-directed mutagenesis and functional studies. Based on the X-ray structure of the binary complex, we discuss a molecular basis of the IL-22/IL-22R1 recognition by IL-10R2.

Kebir H, Kreymborg K, Ifergan I, Dodelet-Devillers A, Cayrol R, Bernard M, Giuliani F, Arbour N, Becher B, Prat A. **Human TH17 lymphocytes promote blood-brain barrier disruption and central nervous system inflammation**. Nat Med. 2007 Oct;13(10):1173-5. URL
T(H)17 lymphocytes appear to be essential in the pathogenesis of numerous inflammatory diseases. We demonstrate here the expression of IL-17 and IL-22 receptors on blood-brain barrier endothelial cells (BBB-ECs) in multiple sclerosis lesions, and show that IL-17 and IL-22 disrupt BBB tight junctions in vitro and in vivo. Furthermore, T(H)17 lymphocytes transmigrate efficiently

across BBB-ECs, highly express granzyme B, kill human neurons and promote central nervous system inflammation through CD4+ lymphocyte recruitment.

Weiss B, Wolk K, Grünberg BH, Volk HD, Sterry W, Asadullah K, Sabat R. **Cloning of murine IL-22 receptor alpha 2 and comparison with its human counterpart**. Genes Immun. 2004 Aug;5(5):330-6. URL

We have identified the mouse and rat homologs of human interleukin-22 receptor alpha 2 (IL-22R alpha 2) and compared the localization, structure, and expression of the encoding murine and human genes. The mouse IL-22R alpha 2-encoding gene is located on chromosome 10A3 between, like in human, the genes for interferon-gamma R1 and IL-20R1. It spans a region of approximately 10 kb therefore being three times shorter than the human gene. Although the overall gene structure in both species is similar, the mouse gene lacks a counterpart to the third coding exon of the human gene known to be alternatively spliced. Like in human, mouse and rat IL-22R alpha 2 exist only as soluble receptors as deduced from the lack of transmembrane and intracellular domains encoding sequences. Quantitative expression analyses showed, analogically to the human system, a limited tissue distribution of mouse IL-22R alpha 2 mRNA. Differential modulation of IL-22R alpha 2 mRNA expression was observed upon systemic inflammation in mice in spleen, thymus, and lymph node.

Xu W, Presnell SR, Parrish-Novak J, Kindsvogel W, Jaspers S, Chen Z, Dillon SR, Gao Z, Gilbert T, Madden K, Schlutsmeyer S, Yao L, Whitmore TE, Chandrasekher Y, Grant FJ, Maurer M, Jelinek L, Storey H, Brender T, Hammond A, Topouzis S, Clegg CH, Foster DC. **A soluble class II cytokine receptor, IL-22RA2, is a naturally occurring IL-22 antagonist**. Proc Natl Acad Sci U S A. 2001 Aug 14;98(17):9511-6. URL

IL-22 is an IL-10 homologue that binds to and signals through the class II cytokine receptor heterodimer IL-22RA1/CRF2-4. IL-22 is produced by T cells and induces the production of acute-phase reactants in vitro and in vivo, suggesting its involvement in inflammation. Here we report the identification of a class II cytokine receptor designated IL-22RA2 (IL-22 receptor-alpha 2) that appears to be a naturally expressed soluble receptor. IL-22RA2 shares amino acid sequence homology with IL-22RA1 (also known as IL-22R, zcytor11, and CRF2-9) and is physically adjacent to IL-20Ralpha and IFN-gammaR1 on chromosome 6q23.3-24.2. We demonstrate that IL-22RA2 binds specifically to IL-22 and neutralizes IL-22-induced proliferation of BaF3 cells expressing IL-22 receptor subunits. IL-22RA2 mRNA is highly expressed in placenta and spleen by Northern blotting. PCR analysis using RNA from various tissues and cell lines showed that IL-22RA2 was expressed in a range of tissues, including those in the digestive, female reproductive, and immune systems. In situ hybridization revealed the dominant cell types expressing IL-22RA2 were mononuclear cells and epithelium. Because IL-22 induces the expression of acute phase reactants, IL-22RA2 may play an important role as an IL-22 antagonist in the regulation of inflammatory responses.

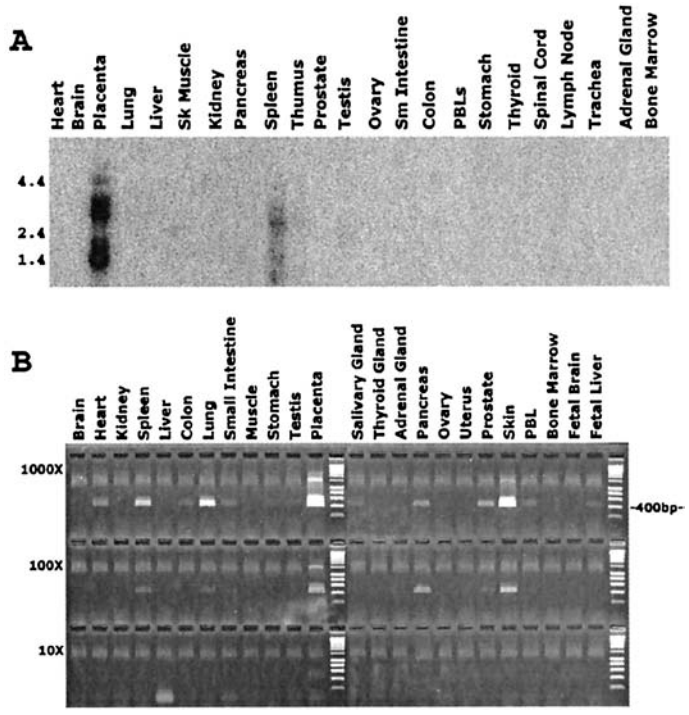

Figure 4
Tissue distribution of human IL-22RA2. (**A**) Northern blot of human multiple tissue mRNA hybridized to an IL-22RA2 probe. Tissue sources are given at the top and the positions of size markers (in kb) are indicated on the left. The predominant hybridizing species correspond to transcripts of about 1.6 and 3.0 kb. (**B**) PCR analysis of IL-22RA2 mRNA level in human tissues. The first-strand cDNAs from each human tissue were subject to normalization, such that they all contain an equivalent concentration of β-actin cDNA. Each cDNA was diluted in water to a series of three concentrations (labeled 1,000×, 100×, 10×), with the lowest concentration (10×) being ≈10pg. The 400-bp marker is labeled at the right.

Locus 26

Significance (based on data with full allele set): presumably CORRECT / false positive

Top hit 1 : position chr 5:45'736'224
alleles (EMMA) # alleles 1 = 10; # alleles 2 = 12
condition / stat iso 1, LRT
p-value: **$6.138x10^{-6}$**
alleles from the Broad1 SNP set (MPD): 11 vs 10. The association of these positions with iso 1, REMLt is far from significant.

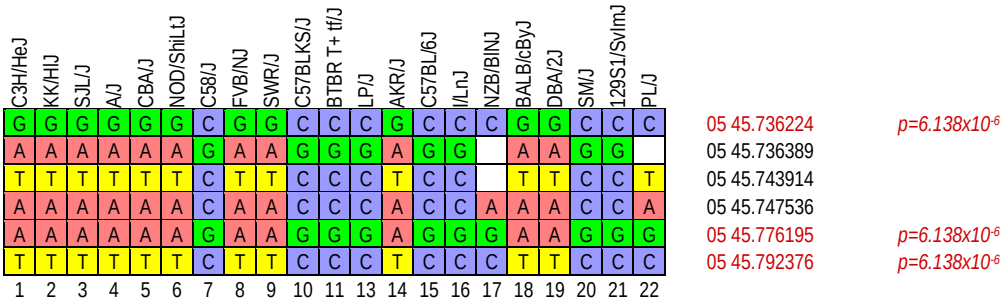

alleles from the CGD1 imputed SNP set (MPD): 12 vs 10

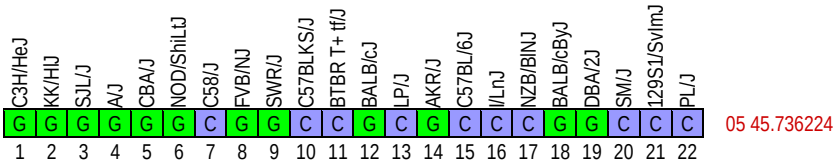

Top hit 2 : position chr 5:45'776'195
alleles (EMMA) # alleles 1 = 10; # alleles 2 = 12
condition / stat iso 1, LRT
p-value: $6.138x10^{-6}$
alleles from the Broad1 SNP set (MPD): 11 vs 10 (see above)
alleles from the CGD1 imputed SNP set (MPD): 12 vs 4

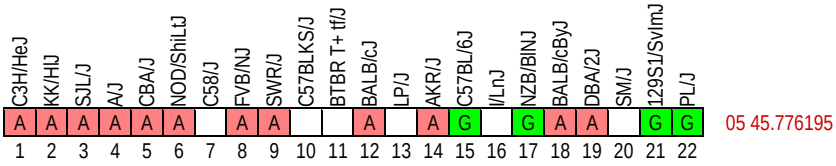

Top hit 3 : position chr 5:45'792'376
alleles (EMMA) # alleles 1 = 10; # alleles 2 = 12
condition / stat iso 1, LRT
p-value: $6.138x10^{-6}$
alleles from the Broad1 SNP set (MPD): 11 vs 10 (see above)
alleles from the CGD1 imputed SNP set (MPD): 12 vs 5

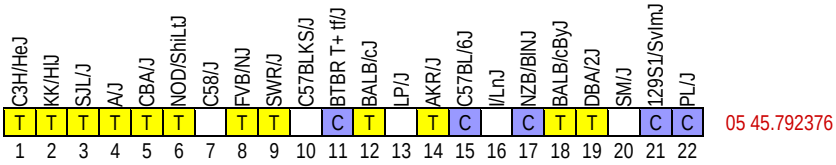

range : ca 45-47 Mb

Candidate gene(s) : **none**, at least based on SDPs in the surrounding genes, but several alleles are often missing.

Locus 27

Significance (based on data with full allele set): presumably CORRECT / false positive

Top hits 1-4: positions chr 5:47'619'864; chr5: 47'638'996; chr5:47'704'974; and chr5:47'729'042
alleles (EMMA) # alleles 1 = 10; # alleles 2 = 12
condition / stat iso 1, REMLt
p-value: **6.138×10^{-6}**
alleles from the Broad1 SNP set (MPD): 11 vs 10. The association of these positions with iso 1, REMLt is far from significant.

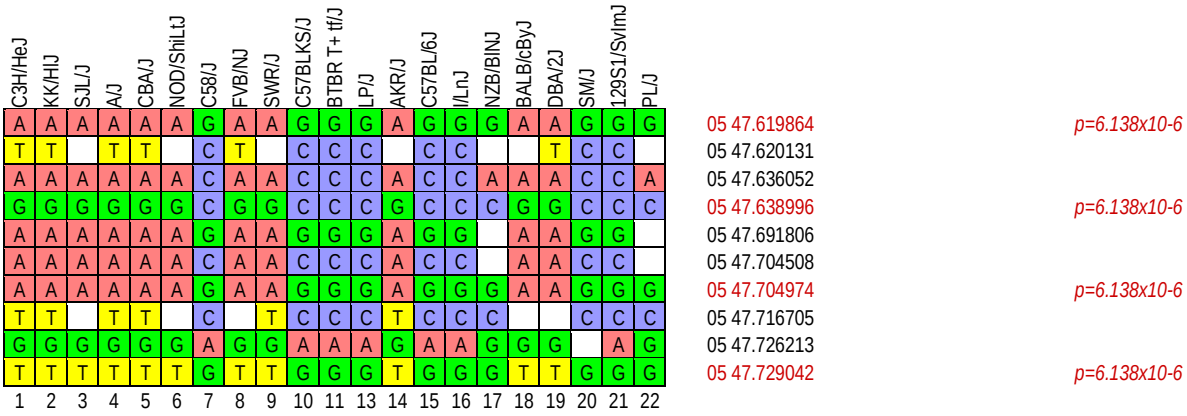

alleles from the CGD1 imputed SNP set (MPD): 12 vs 10

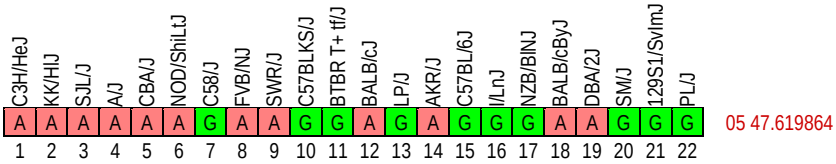

Top hit 2 : position chr5: 47'638'996
alleles (EMMA) # alleles 1 = 10; # alleles 2 = 12
condition / stat iso 1, REMLt
p-value: 6.138×10^{-6}
alleles from the Broad1 SNP set (MPD): 11 vs 10 (see above)
alleles from the CGD1 imputed SNP set (MPD): 12 vs 10

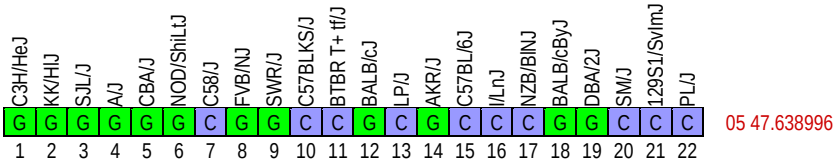

Top hit 3 : position chr5:47'704'974
alleles (EMMA) # alleles 1 = 10; # alleles 2 = 12
condition / stat iso 1, REMLt
p-value: 6.138×10^{-6}
alleles from the Broad1 SNP set (MPD): 11 vs 10 (see above)
alleles from the CGD1 imputed SNP set (MPD): 12 vs 10

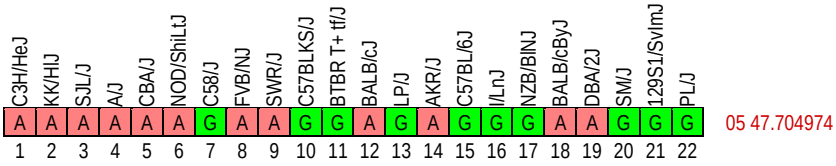

Top hit 4 : position chr5:47'729'042
alleles (EMMA) # alleles 1 = 10; # alleles 2 = 12
condition / stat iso 1, REMLt
p-value: 6.138×10^{-6}
alleles from the Broad1 SNP set (MPD): 11 vs 10 (see above)
alleles from the CGD1 imputed SNP set (MPD): 12 vs 9

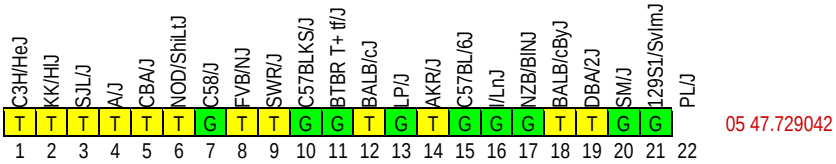

range : ca 47-49 Mb

Candidate gene(s) : **none**

Locus 28

Significance (based on data with full allele set): INFLATED

Top hit 1 : position chr 12:102'095'964
alleles (EMMA) # alleles 1 = 12; # alleles 2 = 8 (-> allele set is not complete)
condition / stat iso 10, LRT
p-value: $2.973x10^{-6}$
alleles from the Broad1 SNP set (MPD): 11 vs 8. The association of this position with iso 10, REMLt is far from significant.

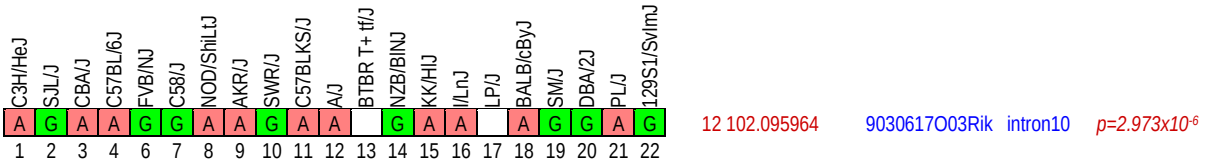

alleles from the CGD1 imputed SNP set (MPD): 12 vs 10; the segregation of SDP with the sorted pattern of VWI across strains is not obvious... That looks strange.

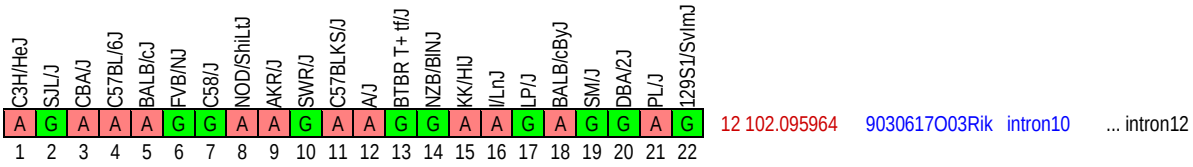

Matching SNP with full allele set in EMMAIII:

position chr 12: 102'085'056
alleles (EMMA) #alleles 1 =12; # alleles 2 = 10
condition / stat iso 10, REMLt
p-value: **$6.294x10^{-1}$**
alleles from the Broad1 SNP set (MPD): 11 vs 10

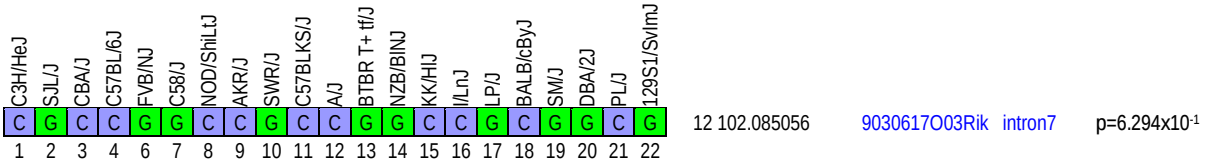

alleles from the CGD1 imputed SNP set (MPD): 12 vs 10

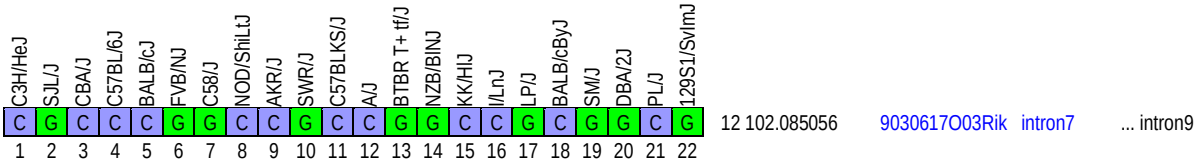

range : ca 101-103 Mb

Candidate gene(s) :

1. ***9030617O03Rik***: hypothetical protein LOC217830. Link to UCSC gene information. UPF0317 protein C14orf159 homolog, mitochondrial precursor.

Locus 29

Significance (based on data with full allele set): INFLATED

Top hit 1 : position chr 12:113'701'753 and chr12:113'701'290
alleles (EMMA) # alleles 1 = 12; # alleles 2 = 9 (-> allele set is incomplete)
condition / stat iso 10, LRT
p-value: 3.884×10^{-6}
alleles from the Broad1 SNP set (MPD): 9 vs 11; there is no matching SNP with a full allele set in the vicinity, but the association of these positions with iso 10, REMLt is far from significant.

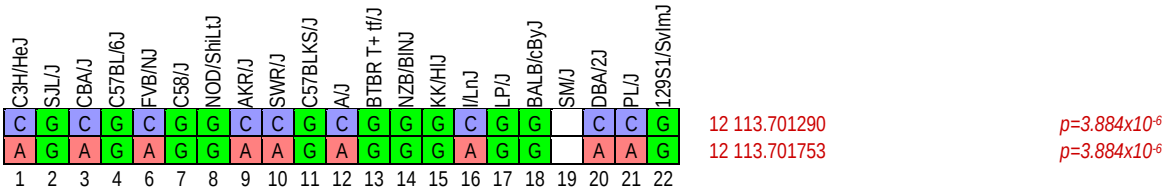

alleles from the CGD1 imputed SNP set (MPD): 5 vs 11

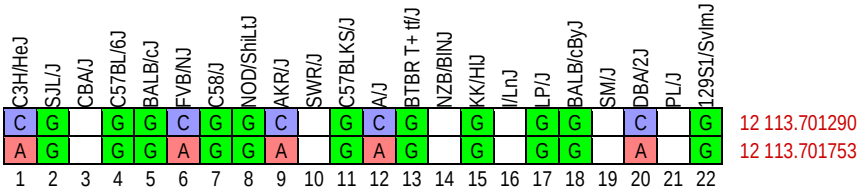

range : ca 113.5-114 Mb

Candidate gene(s) : **none** ? There are many missing alleles around these positions. Besides, the SNP and and VWI SDPs do not segregate well at these positions.

Locus 30

Significance (based on data with full allele set): presumably CORRECT / false positive

Top hit 1 : position chr 6:110'232'069
alleles (EMMA) # alleles 1 = 13; # alleles 2 = 9
condition / stat iso 10, LRT
p-value: **$6.407x10^{-6}$**
alleles from the Broad1 SNP set (MPD): 13 vs 8; there is no matching SNP with a full allele set in the vicinity, but the association of this position with iso 10, REMLt is far from significant.

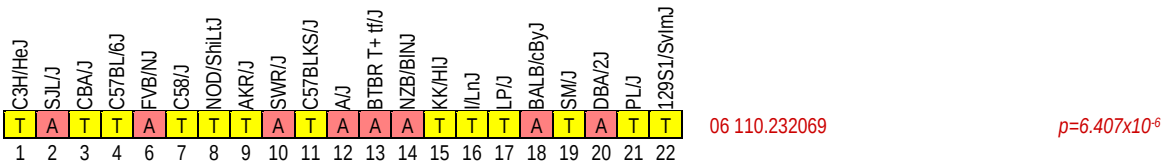

alleles from the CGD1 imputed SNP set (MPD): 12 vs 9

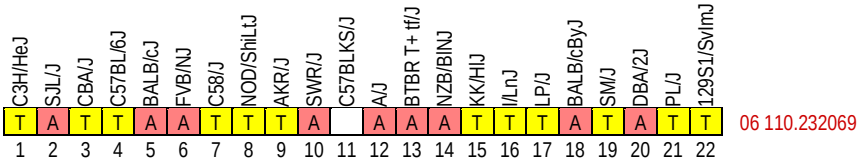

range : ca 109-111 Mb

Candidate gene(s) : **none**

Locus 31

Significance (based on data with full allele set): presumably CORRECT / false positive

Top hit 1 : position chr 1:3'125'499
alleles (EMMA) # alleles 1 = 8; # alleles 2 = 14
condition / stat iso 10, LRT
p-value: **7.007×10^{-6}**
alleles from the Broad1 SNP set (MPD): 14 vs 7; there is no additional matching SNP with the same allele set in the vicinity, but the association of this position with iso 10, REMLt is far from significant.

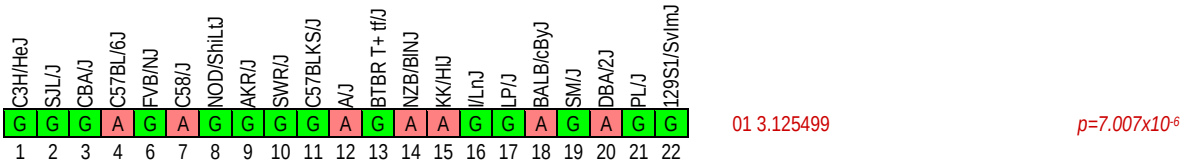

alleles from the CGD1 imputed SNP set (MPD): 5 vs 9

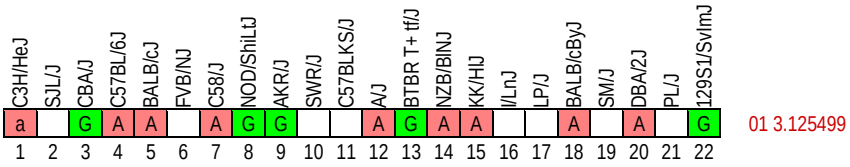

range : ca 2.5-3.5 Mb

Candidate gene(s) :

1. ***Xkr4 ?*** : X Kell blood group precursor related family. Link to UCSC gene information page.

Notes and bibliography: there is a single paper about *Xkr4* in PubMed.

Lavedan C, Licamele L, Volpi S, Hamilton J, Heaton C, Mack K, Lannan R, Thompson A, Wolfgang CD, Polymeropoulos MH. **Association of the *NPAS3* gene and five other loci with response to the antipsychotic iloperidone identified in a whole genome association study**. Mol Psychiatry. 2008 Jun 3. [Epub ahead of print]. URL

A whole genome association study was performed in a phase 3 clinical trial conducted to evaluate a novel antipsychotic, iloperidone, administered to treat patients with schizophrenia. Genotypes of 407 patients were analyzed for 334 563 single nucleotide polymorphisms (SNPs). SNPs associated with iloperidone efficacy were identified within the neuronal PAS domain protein 3 gene (NPAS3), close to a translocation breakpoint site previously observed in a family with schizophrenia. Five other loci were identified that include the XK, Kell blood group complex subunit-related family, member 4 gene (XKR4), the tenascin-R gene (TNR), the glutamate receptor, inotropic, AMPA 4 gene (GRIA4), the glial cell line-derived neurotrophic factor receptor-alpha2 gene (GFRA2), and the NUDT9P1 pseudogene located in the chromosomal region of the serotonin receptor 7 gene (HTR7). The study of these polymorphisms and genes may lead to a better understanding of the etiology of schizophrenia and of its treatment. These results provide new insight into response to iloperidone, developed with the ultimate goal of directing therapy to patients with the highest benefit-to-risk ratio.Molecular Psychiatry advance online publication, 3 June 2008; doi:10.1038/mp.2008.56.

Locus 32

Significance (based on data with full allele set): presumably CORRECT / false positive

Top hit 1 : position chr 17:12'465'938, 12'503'901, and 12'539'636
alleles (EMMA) # alleles 1 = 13; # alleles 2 = 9
condition / stat iso 10, LRT
p-value: **8.838×10^{-6}**
alleles from the Broad1 SNP set (MPD): 12 vs 9; there is no additional matching SNP with the same (and full) allele set in the vicinity, but the association of this position with iso 10, REMLt is far from significant.

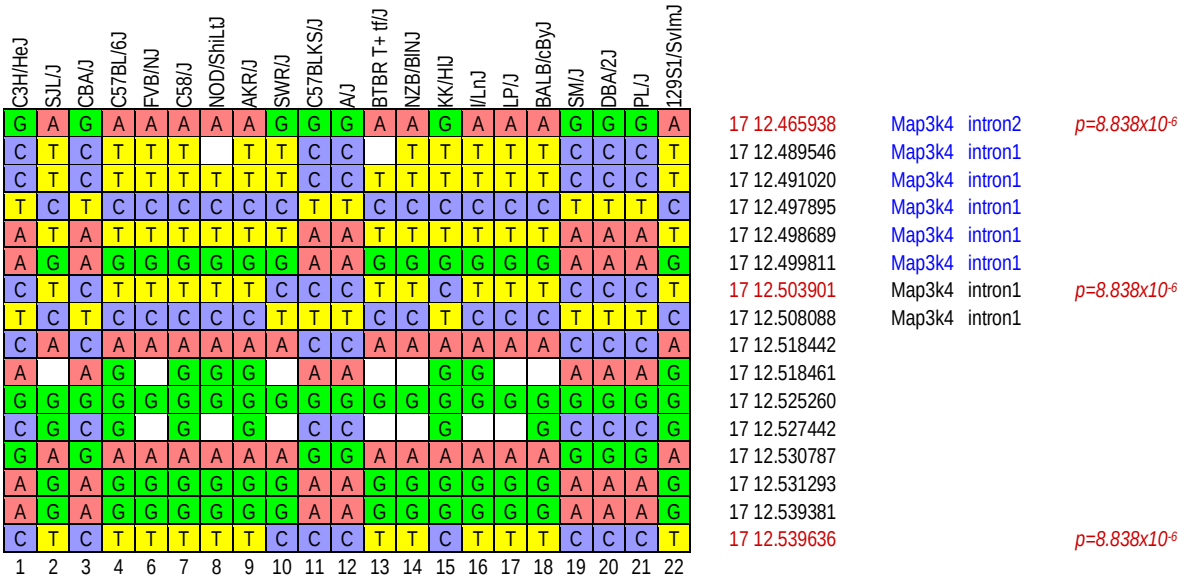

alleles from the CGD1 imputed SNP set (MPD): 8 vs 9

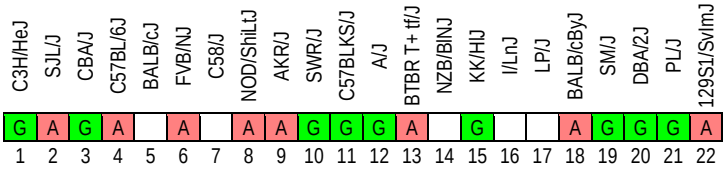

Top hit 2 : position chr 17:12'503'901
alleles (EMMA) # alleles 1 = 13; # alleles 2 = 9
condition / stat iso 10, LRT
p-value: 8.838×10^{-6}
alleles from the Broad1 SNP set (MPD): 12 vs 9 (see above)
alleles from the CGD1 imputed SNP set (MPD): 13 vs 5

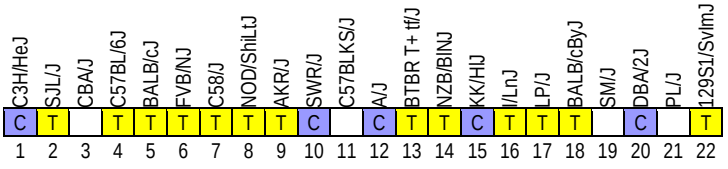

Top hit 3 : position 17:12'539'636
alleles (EMMA) # alleles 1 = 13; # alleles 2 = 9
condition / stat iso 10, LRT
p-value: 8.838×10^{-6}
alleles from the Broad1 SNP set (MPD): 12 vs 9 (see above)
alleles from the CGD1 imputed SNP set (MPD): 13 vs 9

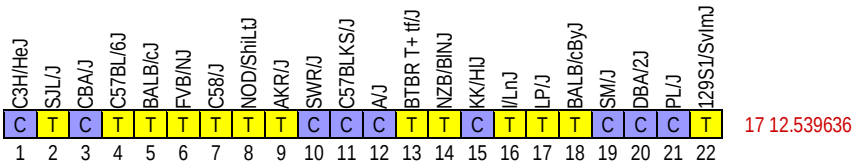

range : ca 12-13 Mb

Candidate gene(s) :

1. ***Map3k4*** : mitogen activated protein kinase kinase kinase (Mekk4; Mtk1). Link to UCSC gene information.

Notes and bibliography:

Stevens MV, Parker P, Vaillancourt RR, Camenisch TD. **MEKK4 regulates developmental EMT in the embryonic heart**. Dev Dyn. 2006 Oct;235(10):2761-70. URL

Congenital heart malformations occur at a rate of one per one hundred births and are considered the most frequent birth defects. This high incidence of cardiac defects underscores the complex developmental processes required to form the first functioning organ in mammals. The molecular cues which govern heart development are poorly defined and require an improved understanding in order to advance repair strategies for heart defects. The cytoplasmic MAP kinase kinase kinase, MEKK4, is a critical effector in cellular stress responses; however, the function of MEKK4 during embryonic development and cardiogenesis is not well understood. We have identified MEKK4 as a critical signaling molecule during cardiovascular development. We report the detection of MEKK4 transcripts to early myocardium, endocardium and to cardiac cushion cells that have executed epithelial to mesenchymal transformation (EMT). These observations suggest that MEKK4 may function during production of the cushion mesenchyme as required to create valves and the septated heart. We used a kinase inactive form of MEKK4(MEKK4(KI)) in an in vitro assay that recapitulates in vivo EMT, and show that MEKK4(KI) attenuates mesenchyme production. However, addition of a constitutively active MEKK4 into ventricular explants, a system that does not normally undergo EMT, is not able to cause mesenchymal cell outgrowth. Thus, the kinase activity of MEKK4 is essential, but not sufficient, to support developmental EMT. This knowledge provides a basis to understand how MEKK4 may integrate signaling cascades controlling heart development.

Arimoto K, Fukuda H, Imajoh-Ohmi S, Saito H and Takekawa M. **Formation of stress granules inhibits apoptosis by suppressing stress-responsive MAPK pathways**. Nature Cell Biology 10, 1324 - 1332 (2008). URL

When confronted with environmental stress, cells either activate defence mechanisms to survive, or initiate apoptosis, depending on the type of stress. Certain types of stress, such as hypoxia, heatshock and arsenite (type 1 stress), induce cells to assemble cytoplasmic stress granules (SGs), a major adaptive defence mechanism. SGs are multimolecular aggregates of stalled translation pre-initiation complexes that prevent the accumulation of mis-folded proteins1. Type 2 stress, which includes X-rays and genotoxic drugs, induce apoptosis through the stress-activated p38 and JNK MAPK (SAPK) pathways. A functional relationship between the SG and SAPK responses is unknown. Here, we report that SG formation negatively regulates the SAPK apoptotic response, and that the signalling scaffold protein RACK1 functions as a mediator between the two responses. RACK1 binds to the stress-responsive MTK1 MAPKKK and facilitates its activation by type 2 stress; however, under conditions of type 1 stress, RACK1 is sequestered into SGs. Thus, type 1 conditions suppress activation of the MTK1–SAPK pathway and apoptosis induced by type 2 stress. These findings may be relevant to the problem of hypoxia-induced resistance to cancer chemotherapy.

Sarkisian MR, Bartley CM, Chi H, Nakamura F, Hashimoto-Torii K, Torii M, Flavell RA, Rakic P. **MEKK4 signaling regulates filamin expression and neuronal migration.** Neuron. 2006 Dec 7;52(5):789-801. URL

Periventricular heterotopia (PVH) is a congenital malformation of human cerebral cortex frequently associated with Filamin-A (FLN-A) mutations but the pathogenetic mechanisms remain unclear. Here, we show that the MEKK4 (MAP3K4) pathway is involved in Fln-A regulation and PVH formation. MEKK4(-/-) mice developed PVH associated with breaches in the neuroependymal lining which were largely comprised of neurons that failed to reach the cortical plate. RNA interference (RNAi) targeting MEKK4 also impaired neuronal migration. Expression of Fln was elevated in MEKK4(-/-) forebrain, most notably near sites of failed neuronal migration. Importantly, recombinant MKK4 protein precipitated a complex containing MEKK4 and Fln-A, and MKK4 mediated signaling between MEKK4 and Fln-A, suggesting that MKK4 may bridge these molecules during development. Finally, we showed that wild-type FLN-A overexpression inhibited neuronal migration. Collectively, our results demonstrate a link between MEKK4 and Fln-A that impacts neuronal migration initiation and provides insight into the pathogenesis of human PVH.

Abell AN, Rivera-Perez JA, Cuevas BD, Uhlik MT, Sather S, Johnson NL, Minton SK, Lauder JM, Winter-Vann AM, Nakamura K, Magnuson T, Vaillancourt RR, Heasley LE, Johnson GL. **Ablation of MEKK4 kinase activity causes neurulation and skeletal patterning defects in the mouse embryo**. Mol Cell Biol. 2005 Oct;25(20):8948-59. URL

Skeletal disorders and neural tube closure defects represent clinically significant human malformations. The signaling networks regulating normal skeletal patterning and neurulation are largely unknown. Targeted mutation of the active site lysine of MEK kinase 4 (MEKK4) produces a kinase-inactive MEKK4 protein (MEKK4(K1361R)). Embryos homozygous for this mutation die at birth as a result of skeletal malformations and neural tube defects. Hindbrains of exencephalic MEKK4(K1361R) embryos show a striking increase in neuroepithelial cell apoptosis and a dramatic loss of phosphorylation of MKK3 and -6, mitogen-activated protein kinase kinases (MKKs) regulated by MEKK4 in the p38 pathway. Phosphorylation of MAPK-activated protein kinase 2, a p38 substrate, is also inhibited, demonstrating a loss of p38 activity in MEKK4(K1361R) embryos. In contrast, the MEK1/2-extracellular signal-regulated kinase 1 (ERK1)/ERK2 and MKK4-Jun N-terminal protein kinase pathways were unaffected. The p38

pathway has been shown to regulate the phosphorylation and expression of the small heat shock protein HSP27. Compared to the wild type, MEKK4(K1361R) fibroblasts showed significantly reduced phosphorylation of p38 and HSP27, with a corresponding heat shock-induced instability of the actin cytoskeleton. Together, these data demonstrate MEKK4 regulation of p38 and that substrates downstream of p38 control cellular homeostasis. The findings are the first demonstration that MEKK4-regulated p38 activity is critical for neurulation.

Derbyshire ZE, Halfter UM, Heimark RL, Sy TH, Vaillancourt RR. **Angiotensin II stimulated transcription of cyclooxygenase II is regulated by a novel kinase cascade involving Pyk2, MEKK4 and annexin II**. Mol Cell Biochem. 2005 Mar;271(1-2):77-90. URL

Although it is known that MEKK4 regulates MKK6, and p38 MAP kinase, extracellular stimuli that activate the serine/threonine kinase, MEKK4, are unknown. The aim of this study was then to identify stimuli that regulate MEKK4. By using recombinant MEKK4, as bait to attract interacting proteins, the calcium binding protein, annexin II, was identified by mass spectrometry as interacting with MEKK4, suggesting that MEKK4 might be regulated by calcium. A calcium-dependent interaction between MEKK4 and annexin II was observed when MEKK4 was immunoprecipitated from rat aortic smooth muscle cells that were treated with angiotensin II. Additional studies using recombinant MEKK4 in a Far-Western immunoblot identified a protein of 120 kDa as interacting directly with MEKK4. Prior studies indicated that MEKK4 was phosphorylated on tyrosine in vivo, and in fact, Pyk2 interacts with MEKK4 in an angiotensin II dependent manner in rat aortic smooth muscle cells. Pyk2 phosphorylates MEKK4 in vitro and Pyk2-dependent phosphorylation further regulates MEKK4-dependent phosphorylation of MKK6. Finally, dominant-negative MEKK4 inhibits angiotensin II mediated transcription of a luciferase reporter construct containing the cyclooxygenase II promoter, demonstrating that MEKK4 functions in a calcium-dependent manner as a substrate for Pyk2 and regulates transcription of cyclooxygenase II.

Chi H, Sarkisian MR, Rakic P, Flavell RA. **Loss of mitogen-activated protein kinase kinase kinase 4 (MEKK4) results in enhanced apoptosis and defective neural tube development**. Proc Natl Acad Sci U S A. 2005 Mar 8;102(10):3846-51. URL

Neural tube defects (NTDs) are prevalent human birth defects. Mitogen-activated protein kinases (MAPKs), such as c-Jun N-terminal kinase (JNK), are implicated in facilitating neural tube closure, yet upstream regulators remain to be identified. Here, we show that MAP kinase kinase kinase 4 (MEKK4) is strongly expressed in the developing neuroepithelium. Mice deficient in MEKK4 develop highly penetrant NTDs that cannot be rescued by supplementation with folic acid or inositol. Unlike most mouse models of NTDs, MEKK4 mutant embryos display genetically co-segregated exencephaly and spina bifida, recapitulating the phenotypes observed in human patients. To identify downstream targets of MEKK4 during neural tube development, we examined the activity of MAP kinase kinase 4 (MKK4), a signaling intermediate between MAP kinase kinase kinase and JNK/p38. We found a significant reduction in MKK4 activity in MEKK4-deficient neuroepithelium at sites of neural tube closure. MAPK pathways are key regulators of cell apoptosis and proliferation. Analyses of the neuroepithelium in MEKK4-deficient embryos showed massively elevated apoptosis before and during neural tube closure, suggesting an antiapoptotic role for MEKK4 during development. In contrast, proliferation of MEKK4-deficient neuroepithelial cells appeared to be largely unaffected. MEKK4 therefore plays a critical role in regulating MKK4 activity and apoptotic cell death during neural tube development. Disruption of this signaling pathway may be clinically relevant to folate-resistant human NTDs.

Chi H, Lu B, Takekawa M, Davis RJ, Flavell RA. **GADD45beta/GADD45gamma and MEKK4 comprise a genetic pathway mediating STAT4-independent IFNgamma production in T cells**. EMBO J. 2004 Apr 7;23(7):1576-86. URL

The stress-inducible molecules GADD45beta and GADD45gamma have been implicated in regulating IFNgamma production in CD4 T cells. However, how GADD45 proteins function has been controversial. MEKK4 is a MAP kinase kinase kinase that interacts with GADD45 in vitro. Here we generated MEKK4-deficient mice to define the function and regulation of this pathway. CD4 T cells from MEKK4-/- mice have reduced p38 activity and defective IFNgamma synthesis. Expression of GADD45beta or GADD45gamma promotes IFNgamma production in MEKK4+/+ T cells, but not in MEKK4-/- cells or in cells treated with a p38 inhibitor. Thus, MEKK4 mediates the action of GADD45beta and GADD45gamma on p38 activation and IFNgamma production. During Th1 differentiation, the GADD45beta/GADD45gamma/MEKK4 pathway appears to integrate upstream signals transduced by both T cell receptor and IL12/STAT4, leading to augmented IFNgamma production in a process independent of STAT4.

Takekawa M, Saito H. **A family of stress-inducible GADD45-like proteins mediate activation of the stress-responsive MTK1/MEKK4 MAPKKK.** Cell. 1998 Nov 13;95(4):521-30. URL

The stress-responsive p38 and JNK MAPK pathways regulate cell cycle and apoptosis. A human MAPKKK, MTK1 (= MEKK4), mediates activation of both p38 and JNK in response to environmental stresses. Using a yeast two-hybrid method, three related proteins, GADD45alpha (= GADD45), GADD45, (= MyD118), and GADD45gamma, were identified that bound to an N-terminal domain of MTK1. These proteins activated MTK1 kinase activity, both in vivo and in vitro. The GADD45-like genes are induced by environmental stresses, including MMS, UV, and gamma irradiation. Expression of the GADD45-like genes induces p38/JNK activation and apoptosis, which can be partially suppressed by coexpression of a dominant inhibitory MTK1 mutant protein. We propose that the GADD45-like proteins mediate activation of the p38/JNK pathway, via MTK1/ MEKK4, in response to environmental stresses.

Gerwins P, Blank JL, Johnson GL. **Cloning of a novel mitogen-activated protein kinase kinase kinase, MEKK4, that selectively regulates the c-Jun amino terminal kinase pathway.** J Biol Chem. 1997 Mar 28;272(13):8288-95. URL

Mitogen-activated protein kinases (MAPKs) are components of sequential kinase cascades that are activated in response to a variety of extracellular signals. Members of the MAPK family include the extracellular response kinases (ERKs or p42/44(MAPK)), the c-Jun amino-terminal kinases (JNKs), and the p38/Hog 1 protein kinases. MAPKs are phosphorylated and activated by MAPK kinases (MKKs or MEKs), which in turn are phosphorylated and activated by MKK/MEK kinases (Raf and MKKK/MEKKs). We have isolated two cDNAs encoding splice variants of a novel MEK kinase, MEKK4. The MEKK4 mRNA is widely expressed in mouse tissues and encodes for a protein of approximately 180 kDa. The MEKK4 carboxyl-terminal catalytic domain is approximately 55% homologous to the catalytic domains of MEKKs 1, 2, and 3. The amino-terminal region of MEKK4 has little sequence homology to

the previously cloned MEKK proteins. MEKK4 specifically activates the JNK pathway but not ERKs or p38, distinguishing it from MEKKs 1, 2 and 3, which are capable of activating the ERK pathway. MEKK4 is localized in a perinuclear, vesicular compartment similar to the Golgi. MEKK4 binds to Cdc42 and Rac; kinase-inactive mutants of MEKK4 block Cdc42/Rac stimulation of the JNK pathway. MEKK4 has a putative pleckstrin homology domain and a proline-rich motif, suggesting specific regulatory functions different from those of the previously characterized MEKKs.

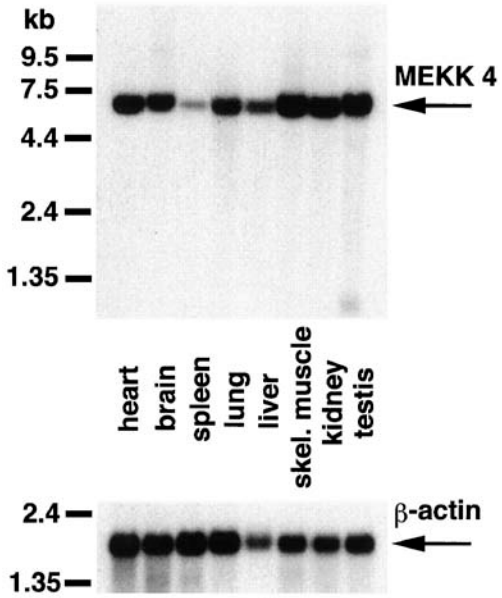

Figure 2

Northern blot analysis of MEKK4 expression. Messenger RNA from different mouse tissues (mouse multiple Northern blot, Clontech) were hybridized with either a 300-bp cDNA fragment derived from the catalytic domain of MEKK4 (recognizes both splice forms of MEKK4) or a β-actin control probe. Positively hybridizing mRNAs were visualized by autoradiography.

Takekawa M, Posas F, Saito H. **A human homolog of the yeast Ssk2/Ssk22 MAP kinase kinase kinases, MTK1, mediates stress-induced activation of the p38 and JNK pathways.** EMBO J. 1997 Aug 15;16(16):4973-82. URL

A human homolog of the yeast Ssk2 and Ssk22 mitogen-activated protein kinase kinase kinases (MAPKKK) was cloned by functional complementation of the osmosensitivity of the yeast ssk2delta ssk22delta sho1delta triple mutant. This kinase, termed MTK1 (MAP Three Kinase 1), is 1607 amino acids long and is structurally highly similar to the yeast Ssk2 and Ssk22 MAPKKKs. In mammalian cells (COS-7 and HeLa), MTK1 overexpression stimulated both the p38 and JNK MAP kinase pathways, but not the ERK pathway. MTK1 overexpression also activated the MKK3, MKK6 and SEK1 MAPKKs, but not the MEK1 MAPKK. Furthermore, MTK1 phosphorylated and activated MKK6 and SEK1 in vitro. Overexpression of a dominant-negative MTK1 mutant [MTK1(K/R)] strongly inhibited the activation of the p38 pathway by environmental stresses (osmotic shock, UV and anisomycin), but not the p38 activation by the cytokine TNF-alpha. The dominant-negative MTK1(K/R) had no effect on the activation of the JNK pathway or the ERK pathway. These results indicate that MTK1 is a major mediator of environmental stresses that activate the p38 MAPK pathway, and is also a minor mediator of the JNK pathway.

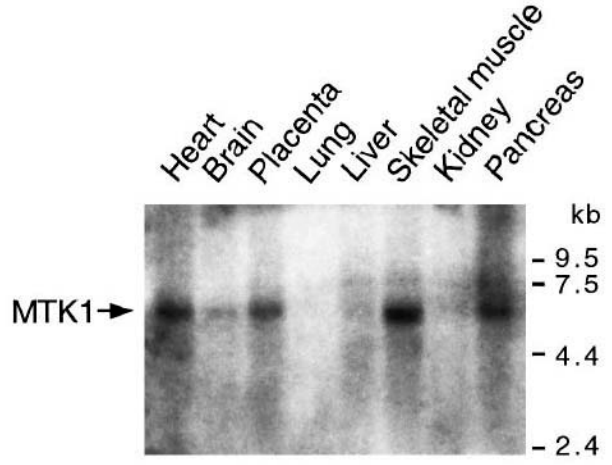

Figure 3

Distribution of MTK1 mRNA in various human tissues. A membrane with 2 μg of poly(A)+ RNA from various human tissues (Clontech) was probed with a ^{32}P-labeled MTK1 cDNA corresponding to nucleotides 1557–3605. Positions of molecular size standards are indicated on the right in kilobases (kb).